INFLUENCE OF BLENDED CEMENTS ON RATE OF STEEL CORROSION IN REINFORCED CONCRETE STRUCTURES IN A MARINE TIDAL ZONE

LUTHANDO NGCOTWANA

Dissertation submitted in fulfilment of the requirements for the Degree

MASTER OF ENGINEERING IN CIVIL ENGINEERING

Department of Civil Engineering
Faculty of Engineering, Built Environment and Information Technology
Central University of Technology, Free State, South Africa

Supervisor: Dr R. Gopinath, PhD.
Co-supervisor: Prof. M. Otieno, PhD.

BLOEMFONTEIN
October 2022

DECLARATION OF INDEPENDENT WORK

DECLARATION WITH REGARD TO INDEPENDENT WORK

I, LUTHANDO NGCOTWANA, identity number _____ and student number _____, do hereby declare that this research project submitted to the Central University of Technology, Free State, for the degree Master of Engineering in Civil Engineering, is my own independent work; it complies with the Code of Academic Integrity, as well as other relevant policies, procedures, rules and regulations of the Central University of Technology, Free State, and has not been submitted before to any institution by myself or any other person in fulfilment (or partial fulfilment) of the requirements for the attainment of any qualification.

_____ **October 2022**

SIGNATURE OF STUDENT **DATE**

ABSTRACT

To minimise the impact of early deterioration of reinforced concrete (RC) structures in the marine environment, blended cements made using supplementary cementitious materials (SCMs) are used. However, the physical, chemical, and mineralogical composition of these materials varies, hence, there is variation in their performance. This study therefore investigated the influence of selected SCMs on the corrosion rate of RC structures in a marine tidal zone, in correlation with some influencing parameters of reinforcement corrosion such as cover depth, oxygen availability, and concrete resistivity. This was achieved through an automated cycle change system, simulating the natural tide change in the marine tidal zone. Accordingly, three binders (100%PC, 70%PC/30%FA, and 50%PC/50%SL), 2 water to binder ratios (w/b) (0.45 and 0.65), and 2 cover depths (20 mm and 40 mm) were used to manufacture corrosion specimens.

A total of 12 specimens were cast, each reinforced with one high tensile mild steel to act as an anode and 2 stainless steels (316 grade) which served the function of cathode. The corrosion specimens were exposed to a simulated marine tidal zone in the laboratory, which consisted of 6 hours of cyclic wetting with 5% NaCl solution and 6 hours of air-drying for a period of 3 months. All corrosion specimens were connected to a data logger which measured the voltage across a 100-ohm resistor between the working and counter electrodes on a weekly basis. The resulting current was calculated as the corrosion rate indicator.

The results of this experimental study indicate that, at the early age of RC structures in the marine tidal zone, the rate of reinforcement corrosion is mostly influenced by the concrete quality and concrete cover depth. The increase in concrete cover depth reduced the corrosion rate of all the specimens, irrespective of the w/b. This was because of the increased travel path for chlorides and oxygen. In addition, higher cover depth prolongs the drying rate of the concrete pore structure, causing low oxygen availability, especially at low w/b, and thus low corrosion risk. Furthermore, a higher w/b 0.65 was found to increase the corrosion risk of the specimens, especially at lower cover depth. Nevertheless, due to the denser microstructure of blended cement concretes, Portland cement (PC) exhibited the highest corrosion

rate. Hence, it can be inferred that high w/b can be used in the application of blended cements, provided relatively higher cover depth is used.

Blended cement concretes, overall, showed relatively high concrete resistivity compared to PC concretes. In relation to the refinement of the exposure classification used in SANS guidelines, the findings of this study support the notion of adopting the classification of RC structures with a concrete cover depth ≥ 30 mm in the same category as the submerged zone. However, a further laboratory investigation over a longer period of exposure is required to further clarify the corrosion performance of blended cement concretes in a marine tidal zone.

ACKNOWLEDGEMENT

I would like to express my sincere gratitude to my supervisor, Dr Rakesh Gopinath, and co-supervisor, Prof. Mike Otieno, for their support, encouragement, and guidance. The success of this project would not have come to light without you. Also, further appreciation to Prof. Mike Otieno for granting me the opportunity to use the facilities at the University of the Witwatersrand (Wits), Johannesburg.

Also, I would like to thank all the Wits laboratory and workshop personnel, especially Mr Ronald Manameni, and the following postgraduate students: Mr Williams Dunu and Mr Victor Gilayeneh for their assistance throughout my experimental programme.

Special thanks to the National Research Foundation (NRF), the Central University of Technology (CUT grant), merSETA for providing financial support for this project, and also to PPC, Afrisam, and Ulula ash for donating the materials used for this project.

Lastly, I would like to thank my family for their prayers and continued support. A special thanks to my late Father for his support and words of wisdom throughout my academic career.

TABLE OF CONTENTS

LIST OF TABLES

LIST OF FIGURES

1 INTRODUCTION

1.1 Background

Reinforced concrete (RC) structures in the marine environment are most likely to experience premature deterioration problems. The high chloride concentrations available in their exposure environment makes the reinforcing steel vulnerable to chloride-induced corrosion (Mackechnie, 2001). However, the rate of corrosion of reinforcement in the marine environment is mostly influenced by various factors such as oxygen, moisture, exposure zone, etc. (Moore, 2019).

Chloride-induced corrosion of steel is an electrochemical process in which iron dissolves at the anode while oxygen is reduced at the cathode. Figure 1-1 shows a short-circuit corrosion cell, where the flow of electrons around the steel is from the anode to the cathode and the flow of ions, from the cathode, through the concrete pore structure to the anode. For this process to occur, the following 4 components are required (Otieno *et al*., 2010):

a) Anode – the surface of the steel, where corrosion takes place and from which current flows.
b) Cathode – where there is no occurrence of corrosion but the corrosion current flows.
c) Electrolyte – concrete pore solution.
d) Metallic connection – this connects the anode and cathode. It also permits the flow of current and completes the circuit (reinforcing steel serves this purpose).

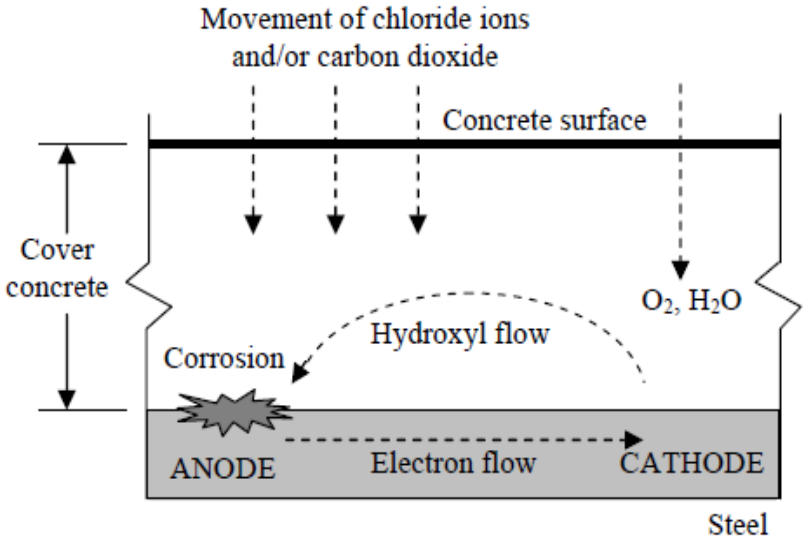

Figure 1-1: A schematic illustration of the corrosion process in concrete (Otieno *et al*., 2010)

In order to design concrete structures that can withstand the harsh environmental conditions in the marine environment, modern concrete design strategies consider durability rather than strength-based designs (Alexander & Beushausen, 2019). According to ACI (2005), the durability of concrete structures is defined by its ability to resist weathering action, chemical attack, abrasion, and other degradation processes. Therefore, the penetrability of concrete becomes crucial when designing concrete mixes for structures that are exposed to a marine environment.

The use of blended cements in modern concrete production is notably increasing. This is because blended cements produce dense and less permeable concretes (Zhang *et al*., 2017; Wu *et al*., 2019), which improves the pore structure of the steel-concrete interface (Broomfield, 2007; Xu *et al.*, 2012) and increases the service life of reinforced concrete structures, as well as reducing the level of carbon dioxide emission into the atmosphere. Additionally, the incorporation of blended cements in concrete increases concrete resistivity and reduces oxygen availability to the level of reinforcement, which results in the reduction of corrosion rate of steel in reinforced concrete structures (Otieno, 2014). Blended cement is manufactured using supplementary cementitious materials (SCMs), such as ground granulated blast furnace slag (GGBS), fly ash (FA), and silica fume (SF), as a partial replacement for Portland cement (PC).

To address the problem of early deterioration of structures exposed to marine environmental conditions, design guidelines have been developed. South Africa adopted European standards (EN 206-1, 2013) in an attempt to address the issue of premature deterioration (Ballim *et al*., 2009). According to the European standards for concrete structures (EN 206-1, 2013), reinforced concrete subjected to chlorides from the seawater or air containing salts from the seawater, the exposure conditions are classified as shown in Table 1-1. RC structures in the marine environment are subjected to 4 main exposure conditions/zones i.e., atmospheric, submerged, and tidal, as well as splash and spray. The classification is made with regard to the potential for corrosion severity. Accordingly, the structures from the tidal, splash and spray zones (XS3) have a higher probability of corrosion-induced damage compared to the structures permanently submerged (XS2) or in the atmospheric zone (XS1).

Table 1-1: Environmental exposure classes for risks of corrosion induced by chlorides from seawater (EN 206-1, 2013)

Class designation	Description of the environment	Informative examples where exposure classes may occur
XS1	Exposed to airborne salt but not in direct contact with seawater	Structures near to or on the coast
XS2	Permanently submerged	Parts of marine structures
XS3	Tidal, splash and spray zones	Parts of marine structures

The RC structures in the XS3 class experience cyclic wetting and drying during low and high tides (Ghods *et al*., 2005). This results in intermediate moisture contents (relative humidity), allowing oxygen diffusion for corrosion initiation (DuraCrete, 1998). Hence, the corrosion rate is initially slow. However, during the propagation phase, the availability of oxygen and moisture may accelerate the rate of corrosion (Hunkeler, 2005).

Recent studies (Moore, 2019) show that the rate of corrosion for RC structures in the marine tidal zone was indicated to be lower at higher cover depths and that this was due to short cycle durations. As a result of higher cover depth, exceeding

30 mm, the steel was deprived of oxygen for concrete in the tidal zone, hence the stifled corrosion. The study further concludes that with adequate cover depth (at least 30 mm), concrete in the tidal zone will theoretically perform as if it were continuously submerged. Hence, this suggests that the exposure zone classifications should be adjusted for the tidal zone by classifying concrete with 30 mm cover depth to the submerged zone category. However, the study was based on the application of Portland cement (PC, also referred to as CEM I). Therefore, due to the difference in concrete resistivity when using blended cements, the results may vary, necessitating additional research in this area.

1.2 Problem statement

Modern strategies of reinforced concrete design have been aimed at designing durable concrete structures which can withstand reinforcement corrosion when exposed to the harsh environment (e.g., marine environment) (Alexander & Beushausen, 2019). This is because the service life of a reinforced concrete structure is not only dependent on the concrete strength but also on its ability to withstand the impact of the aggressive environment to which it is exposed.

Cement is one of the most important constituents of concrete, which binds together other ingredients of concrete (coarse and fine aggregates). Cementitious materials are also responsible for the development of the pore structure of concrete, which influences the transport mechanism of moisture, oxygen, and other aggressive agents from the external environment to the level of steel inside the reinforced concrete structures. During the 19th century, CEM I cement (which consists of about 95–100% clinker) was the only type of binder used in the construction of concrete structures (McNally & Sheils, 2012; Sanjuan *et al*., 2020). However, the manufacture of CEM I cement is associated with high levels of carbon dioxide emission. To curb the environmental impact caused by the cement industry in the production of CEM I, blended cements were developed by partially replacing clinker content in cement with cement additions such as fly ash, ground granulated blast furnace slag, silica fume, etc. (McNally & Sheils, 2012).

The inclusion of SCMs also influences the reinforcement corrosion resistance of RC structures due to their improved durability performance, which is susceptible to the ease of movement of corrosion agents such as chlorides, carbon dioxide, oxygen, and moisture (Yang *et al*., 2013). The severity of corrosion of reinforced concrete structures in the marine environment is highly dependent on the exposure zone of the RC structure. The exposure zones largely influence the rate of corrosion propagation and transportation of corrosion-promoting agents like oxygen, moisture, and chlorides (Zuquan *et al*., 2018; Moore, 2019). Based on EN 206-1 (2013), the tidal, splash and spray zones are classified to have a higher probability of corrosion-induced damage compared to the structures permanently submerged or in the atmospheric zone. However, studies on PC by Moore (2019) show that the corrosion damage in the tidal zone is relatively low when compared to the splash and spray zone, even though they are classified under the same category.

Therefore, it is important to understand the influence of blended cements on the corrosion mechanism and rate of corrosion in a marine tidal environment. This will enable knowledgeable engineers to enhance the service life of reinforced concrete structures. Furthermore, it is necessary to improve the classification of exposure classes that reflect the severity of corrosion damage, taking into account the type of binders used and the cover depth adopted. This will allow for more exact durability design parameters based on exposure classes, resulting in a more sustainable design approach.

1.3 Research Aim and Objectives

1.3.1 Aim

The aim of this study is to investigate the influence of blended cements on the rate of steel corrosion in reinforced concrete structures in a marine tidal zone.

1.3.2 Objectives

a) To investigate the influence of variation in cover depth on the rate of steel corrosion in reinforced concrete structures made with blended cements.

b) To investigate the influence of blended cements in limiting the availability of oxygen to the surface of reinforcement due to the effect of cyclic wetting and drying in the marine tidal zone.
c) To assess the impact of the resistivity of concrete made with blended cements on the rate of corrosion of steel.
d) To refine the exposure classes (tidal, splash, and spray zones) of the marine environment based on parameters such as the cover depth and binder type.

1.4 Scope of work and limitations of the study

- Blended cements used in this study were limited to the cement classes CEM II, and CEM III.
- Although there are 2 main mechanisms inducing steel corrosion in reinforced concrete structures (i.e., chloride-induced and carbonation-induced corrosion), this study only focuses on chloride-induced corrosion of reinforcement.
- The study is based only on laboratory experimental work. Due to the limited time constraints for this study, an accelerated corrosion process and simulation of the marine tidal zone were adopted. Moreover, only the marine tidal zone was investigated in this study. The experiments were conducted on uncracked specimens. The influence of cracks was therefore not investigated in this study.

1.5 Dissertation outline

Chapter 1 introduces the research topic by outlining a brief background, problem statement, scope, and limitations of the study, as well as the aim and objectives to be achieved. The chapter provides a brief overview of the corrosion process in the marine environment and a general understanding of the influence of blended cements on corrosion.

Chapter 2 is a critical review of the recent literature. This chapter explains the fundamental concepts of chloride-induced corrosion of RC structures in the marine environment.

Chapter 3 outlines the methodology that was followed in conducting the study. For example, the techniques that were used, such as the corrosion activation, corrosion monitoring, durability index tests (OPI, WSI, and CCI), compressive strength test, and resistivity measurements, as well as specimen details. Furthermore, detailed descriptions of the materials such as sand, stone, binder types, and mix proportions, as well as the method of curing used for this study are provided.

Chapter 4 presents key experimental results of this study. The chapter discusses the key findings and significance of the trends obtained from the results analysis of the compressive strength test, corrosion rate measurements, durability index tests, and resistivity measurements.

Chapter 5 concludes the research by summarising the key findings presented in the preceding chapters. Furthermore, the chapter provides recommendations for future studies based on the findings of this study.

2 LITERATURE REVIEW

2.1 Introduction

In this chapter, a critical review of the fundamentals of reinforcing steel corrosion in concrete is presented, with focus given to chloride-induced corrosion in a marine tidal zone. The transport mechanism of corrosion-inducing species is discussed. This will provide a general understanding of the process of corrosion of steel in reinforced concrete (RC) structures. Also, the role of blended cements as well as the depth of the cover to reinforcing steel required to mitigate the mechanism of corrosion of steel in RC structures that are exposed to cyclic wetting and drying in a marine tidal zone are explored. The chapter also gives an overview of the accelerated techniques used for measuring the rate of steel corrosion.

2.2 Reinforcing steel corrosion process in concrete structures

Concrete is known to have a very alkaline environment with pH values ranging from 12 – 13 (Broomfield, 2007). As a result of the high pH conditions in concrete pore solution, the formation of a protective film of gamma ferric oxide (passive layer formation) on the surface of the steel is promoted, which protects the steel from corrosion (Ballim *et al*., 2009). This process is known as passivation.

In chloride-induced corrosion, the ingress of chloride ions (Cl^-) from the seawater in sufficient quantities results in the disruption of the passive layer on the reinforcing steel surface, leading to the initiation of corrosion (Alonso *et al*., 2002; Hunkeler, 2005; Broomfield, 2007; Otieno, 2008; Babaee & Castel, 2018). This process is known as de-passivation. Chloride-induced corrosion develops slowly from pits that are randomly distributed on the surface of the reinforcement and expand over time; it is commonly referred to as localised corrosion process (Hunkeler, 2005; Bertolini *et al*., 2016). It is arbitrated by the formation of small anodic and large cathodic areas (Raupach, 1996; Ballim *et al*., 2009). In addition, the chloride-induced corrosion process may further be exacerbated by the presence of oxygen and moisture at reinforcement level (Bertolini *et al*., 2016).

The corrosion process is shown in Figure 1-1 which leads to the formation of rust – see equation (3) – based on the following electrochemical reactions (equation (1 (2):

$$\text{Anodic reaction: } Fe \rightarrow Fe^{2+} + 2e^{-} \quad (1)$$

$$\text{Cathodic reaction: } 2e^{-} + H_2O + \frac{1}{2}O_2 \rightarrow 2OH^{-} \quad (2)$$

$$\text{Rust formation reaction: } 2Fe^{2+} + 4OH^{-} \rightarrow 2Fe(OH)_2 \quad (3)$$

As a result of de-passivation of the embedded steel due to chloride attack, dissolution of steel occurs, and electrons are released. The released electrons from the anode (equation (1) are consumed at the cathode where there is availability of water and oxygen to form hydroxyl ions (OH^{-}) (equation (2). Furthermore, the reduction of oxygen due to hydroxyl ion (OH^{-}) formation results in a high alkaline environment at the cathode, strengthening the passive layer and stifling corrosion at the cathode. As it can be observed from Figure 1-1, the formed hydroxyl ions (OH^{-}) are transported back to the anode to form corrosion products (rust). The formation of corrosion products results in volume expansion of steel, limiting the surface area within the concrete to accommodate the formed rust, which leads to cracking of the concrete cover (Broomfield, 2007; Moore, 2019). The relative volume expansion of iron oxides is shown in Figure 2-1, where the volume expansion of steel increases by more than 6 times (Broomfield, 2007).

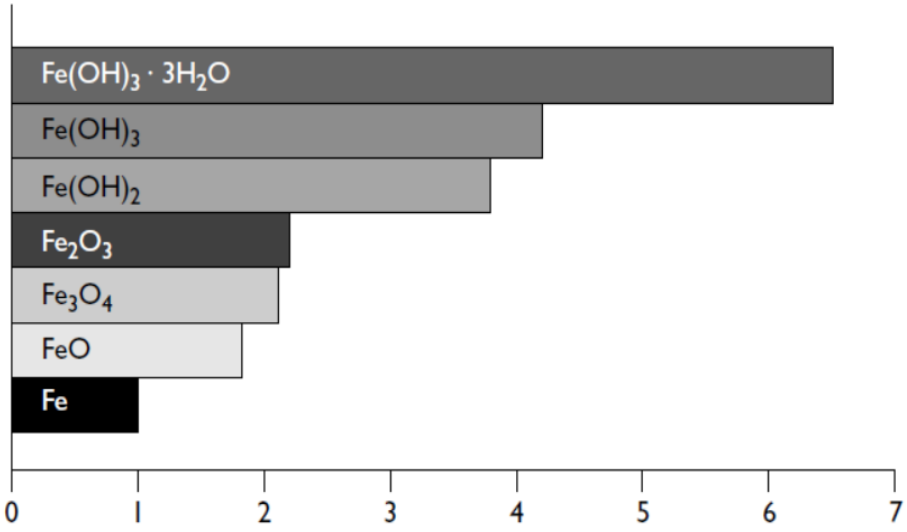

Figure 2-1: Relative volume of iron and its oxides (Broomfield, 2007)

2.3 Types of corrosion

There are 2 types of reinforcement corrosion, namely macrocell and microcell corrosion, occurring in the form of localised and uniform corrosion, respectively (Raupach, 1996; Elsener, 2002; Hansson *et al*., 2006). They are further discussed in the sections to follow.

2.3.1 Macrocell corrosion

For structures exposed to the marine environment, where localised corrosion (pitting) occurs, macrocell corrosion is frequently found (Broomfield, 2007; Moore, 2019). It presents a scenario where the anode and cathode are located on 2 distinct but electrically connected steel bars (Miyazato & Otsuki, 2010; Thomas, 2013), as shown in Figure 2-2(a). Hansson *et al*. (2006) also pointed out that, notwithstanding the general understanding that macrocell corrosion occurs in the presence of 2 distinct reinforcements, macrocell corrosion can also take place on a single reinforcing steel, provided that different environments within the concrete exist or a part of the reinforcement is exposed to the external environment. Macrocell corrosion predominantly manifests itself in chloride-contaminated RC structures, leading to chloride-induced reinforcement corrosion, especially when the structure is reinforced with multiple layers of steel (Raupach, 1996; Elsener, 2002; Arito, 2012).

2.3.2 Microcell corrosion

In contrast with the macrocell corrosion, for microcell corrosion, the anode and cathode are located adjacent to one another on the same reinforcing steel, leading to uniform steel dissolution (Broomfield, 2007; Hansson *et al*., 2006; Thomas, 2013), as shown in Figure 2-2(b). Microcell corrosion frequently occurs in structures damaged due to carbonation and high chloride content (Elsener, 2002; Moore, 2019).

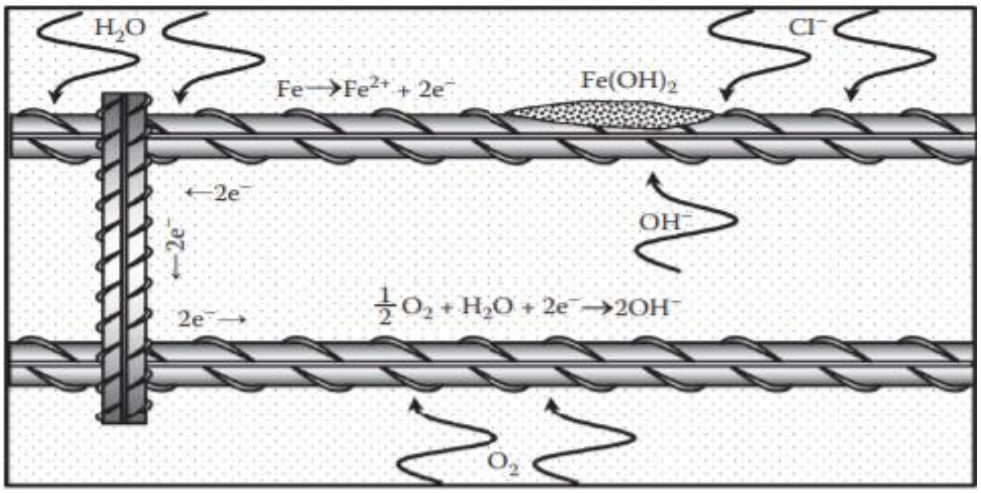

(a) Macrocell corrosion

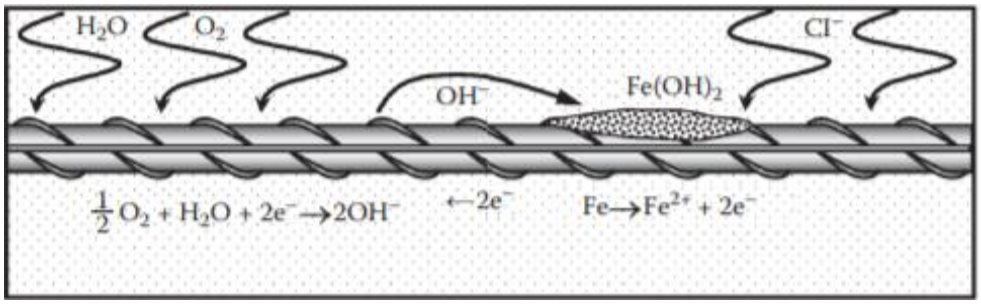

(b) Microcell corrosion

Figure 2-2: Schematics illustrating (a) macrocell corrosion and (b) microcell corrosion (Thomas, 2013)

Aside from the general understanding of the occurrence of macrocell and microcell corrosion, both mechanisms coexist in RC structures (Ji *et al*., 2013; Hansson *et al*., 2006). Therefore, it is important to incorporate the total corrosion rate measurements to avoid underestimation if one mechanism is neglected. Furthermore, the macrocell and microcell corrosion are largely influenced by the ionic movement in the concrete pore structure, with the latter requiring shorter travel via ionic paths (Hansson *et al*., 2006). Hence, it is important for engineers to be mindful of the influence of SCMs and cover depth in the interpretation of both mechanisms, as these play a significant role in limiting the influx of chlorides available to the reinforcing steel.

2.4 Service life of RC structures

The service life of a structure is defined as the period for which a structure's performance is expected to meet its durability requirements with minimal or no maintenance needed (Alexander & Beushausen, 2019). To build durable and long-lasting RC structures, Alexander and Beushausen (2019) suggest that engineers and designers should not only consider the economic representation of the structure, but also its societal representation. This is because a built structure has a meaningful role to play in society, particularly public facilities, and they form part of the community's heritage. Thus, this suggests that the service life of structures should be designed for a period of at least 100 years or more instead of 50 years.

Figure 2-3 shows a schematic representation of the service life of 2 reinforced concrete structures with progressive time. From Figure 2-3, it can be observed that structure A shows better resistance to deterioration, as it is able to sustain acceptable quality until the expected service life period, whereas structure B shows the inability to resist deterioration. Consequently, there will be a need for repair of damage before the anticipated service life period is reached. This highlights the need for engineers and designers to be able to predict the service life of RC structures through an understanding of the different phases of deterioration of these structures, especially for structures exposed to aggressive environments such as the marine environment.

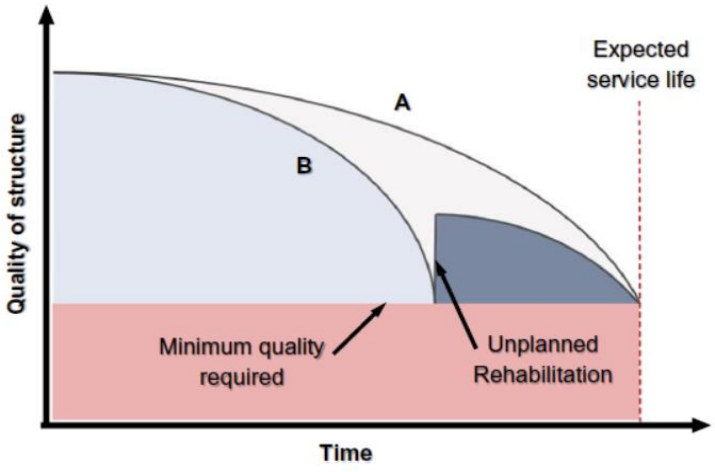

Figure 2-3: A schematic illustration of service life of a structure (Alexander & Beushausen, 2019)

2.5 Phases of chloride-induced corrosion damage

The process of corrosion of steel in reinforced concrete structures, as described in section 2.2, takes place in 2 different phases, namely the corrosion initiation phase and the corrosion propagation phase (Tuutti, 1982).

2.5.1 Corrosion initiation

During the initiation phase, the chloride ions present in seawater are transported into the concrete pore structure through diffusion, convection, permeation, and wick action, depending on the exposure conditions (Moore, 2019). These chloride ions in sufficient concentrations (chloride threshold) at the level of steel act as a catalyst for corrosion initiation of steel reinforcement (see Figure 2-4) (Alonso *et al*., 2002; Otieno, 2008; Otieno *et al*., 2010; Babaee & Castel, 2018).

The chloride threshold refers to the concentration of chlorides required for steel de-passivation (Angst *et al*., 2009). Thus far, no unique chloride threshold value has been established due to a number of factors influencing the ingress of chlorides to the level of steel reinforcement, such as the difference in concrete microstructure, binder type, steel surface, etc. (Alonso *et al*., 2002; Angst *et al*., 2009).

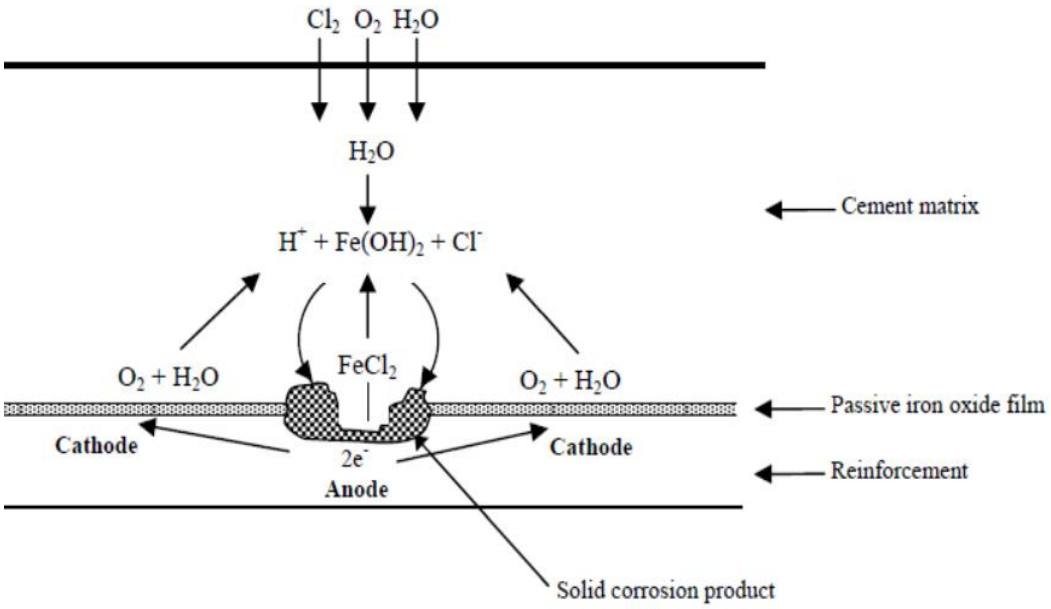

Figure 2-4: Corrosion of reinforcement in concrete exposed to chloride ions (Otieno *et al*., 2010)

The passive protective oxide layer of steel reinforcement is disturbed when the chloride threshold is reached, leading to the de-passivation of the reinforcing steel. As a result of breaking down the passive layer, corrosion is initiated (Broomfield, 2007; Angst *et al*., 2009). Chloride binding capacity (which refers to the ability of the concrete to chemically bind or absorb some of the chlorides during the hydration process, thus inhibiting these chlorides from participating in corrosion initiation) (Tuutti, 1982), cover depth (the distance between the reinforcing steel and the concrete surface), and concrete quality have been identified as the most influential factors affecting time to corrosion initiation in concrete (Otieno, 2008) (refer to section 2.7 for more details on these factors).

It should be noted that the initiation of corrosion merely indicates the activeness of corrosion. However, for the process to further proceed, corrosion influencing factors, such as oxygen, moisture content, increase in chloride content, etc., must be available (Tuutti, 1982; Otieno *et al*., 2010). Consequently, the availability of these factors increases the formation of the corrosion product, leading to tensile stress in the concrete due to the expansion of the formed corrosion product. Thus, crack formation, delamination, and spalling of the concrete cover during the propagation phase (Tuutti, 1982).

2.5.2 Corrosion propagation

Once the corrosion has been initiated, the propagation phase starts if enough oxygen and high chloride content are available at the reinforcement level. During the propagation phase, evidence of corrosion-induced damage can be observed and high penetration of oxygen, moisture, and chlorides through concrete cover due to visible cracks and spalling, which leads to loss of structural integrity and durability performance of the RC structure (Scott, 2004; Otieno, 2008).

The availability of moisture and oxygen propagation phase primarily influences the rate of corrosion, which helps to increase, leading to large cracks and spalling of the concrete cover (Broomfield, 2007; Moore, 2019). This means that without sufficient oxygen content present at the level of steel, the corrosion process is inhibited, and

if there is not enough moisture content, the transportation of ions to the level of reinforcement would be poor (Moore, 2019).

A conceptual model showing the phases of corrosion-induced damage during the service life of RC structures is presented in Figure 2-5. The propagation phase is comprised of different sub-phases (time to corrosion-induced cracking, spalling, and structural failure), and these sub-phases are dependent on the rate of corrosion due to the influence of factors such as the water to binder ratio (w/b), binder type, etc. (Otieno *et al*., 2011).

Overall, corrosion propagation is highly dependent on the penetrability of the concrete cover, which is influenced by the selection of materials and proportions of the concrete mix design (binder type, w/b, etc.). The influencing factors of the rate of corrosion propagation, as mentioned above, are discussed in more detail in section 2.7.

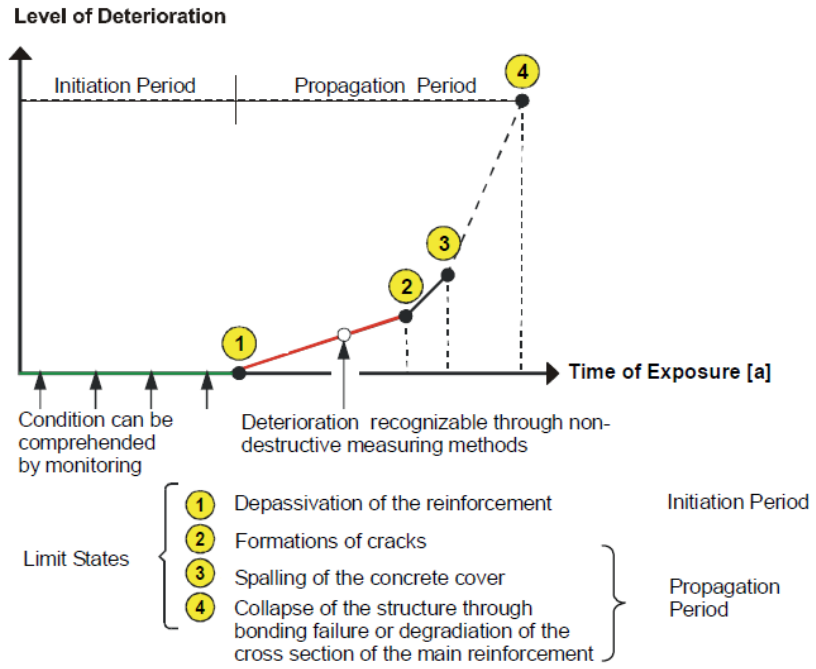

Figure 2-5: Phases and sub-phases in the service life of corrosion affected reinforced structures (Fib model code for service-life design, 2006)

2.6 Transport mechanism of corrosion agents

The ingress of corrosion agents into concrete is as a result of the movement of gases, liquids, ions, etc., through the concrete pores. The transport properties of cementitious materials are crucial parameters for predicting the RC structure's service life. This is because the ingress of chlorides, oxygen, and moisture through the concrete cover is mostly influenced by the penetrability of the concrete microstructure (Ballim *et al*., 2009; Otieno *et al*., 2010). Penetrability is defined as the ease with which concrete allows gases, liquids, or ionic species to move through the concrete pore structure (Ballim *et al*., 2009).

The transport mechanism occurring in different marine exposure zones is demonstrated in Figure 2-6, showing the movement and how corrosion agents are transported to the level of reinforcement. From Figure 2-6, it can be observed that different exposure conditions in the marine environment undergo different transport mechanisms of corrosion agents.

Depending on the exposure conditions, corrosion agents may be transported to the level of the reinforcing steel through a variety of transport mechanisms, including diffusion, convection, permeation, absorption, migration, and wick action. For example, in the submerged zone of the marine environment, the ingress of chlorides is mainly through diffusion. While in the tidal and splash and spray zones, chlorides travel to the reinforcing steel by means of a combination of absorption, diffusion, and convection. Sub-sections 2.6.1 to 2.6.7 cover the transport mechanism of corrosion agents in concrete.

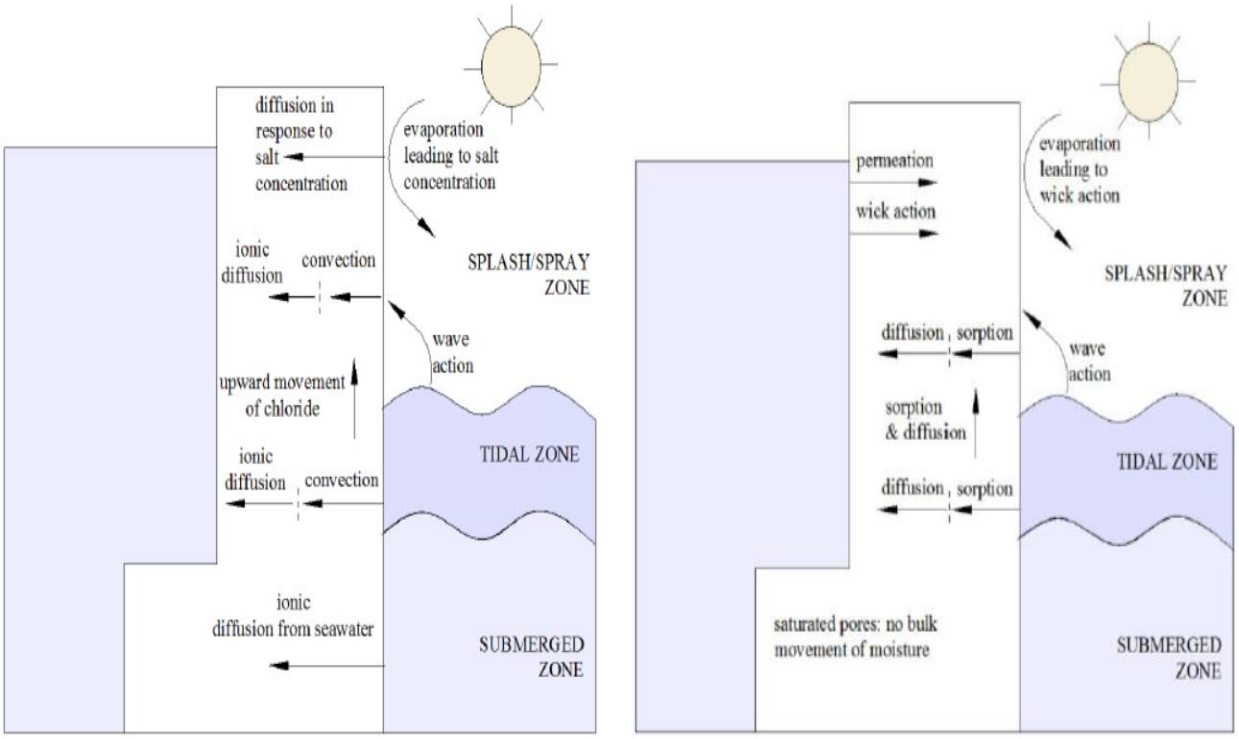

(a) (b)

Figure 2-6: Schematic representation of (a) chloride transport mechanisms and (b) moisture transport mechanisms (Alexander, 2016; cited by Moore, 2019)

2.6.1 Diffusion

Diffusion in concrete is defined as the movement of gases, liquids, or ions under the influence of a concentration gradient (Ballim *et al*., 2009). This phenomenon occurs in 2 forms, namely gaseous diffusion in unsaturated concrete, and ionic diffusion, experienced in saturated and partially saturated concrete structures in seawater (Otieno *et al*., 2010). In a marine submerged and tidal zone, the latter form is the governing form of the diffusion mechanism. Prediction models based on ionic diffusion, such as DuraCrete, have been developed and applied by most researchers to predict the service life of RC structures as a result of the ingress of corrosion agents. This model has been recognised by many researchers (Safehian & Ramezanianpour, 2013; Yu *et al*., 2015; Wu *et al*., 2017; Wang *et al*., 2019) and it is based on Fick's second law of diffusion:

$$\frac{\partial C}{\partial t} = \frac{\partial}{\partial x}\left(D \cdot \frac{\partial C}{\partial x}\right) \quad (4)$$

Where: D denotes the diffusion coefficient in (m^2/s); C is the concentration of fluid in (kg/m^3); and x is the distance in (m).

The analytical solution to the above equation is expressed by Crank's error function. The diffusion coefficient is also dependent on test conditions (Ballim *et al*., 2009; Otieno *et al*., 2010; Wang *et al*., 2019). As presented by Kim *et al*. (2016), the following assumptions are made about the duration of exposure:

$$C_x = 0 \text{ at } t = 0 \text{ and } 0 < x < \infty \quad (5)$$

$$C_x = C_s \text{ at } x = 0 \text{ and } 0 < t < \infty \quad (6)$$

$$C_{x,t} = C_s \left[1\text{-}erf\left(\frac{x}{2\sqrt{D_\alpha t}}\right)\right] \quad (7)$$

Where: $C_{x,t}$ is the concentration of chlorides at a depth x and time t in $(\%/m^3)$; C_s is the surface chloride concentration in $(\%/m^3)$; *erf* is the error function; D_α is the apparent diffusion coefficient in (m^2/s); x is the distance in (m); and t is the time in (s).

2.6.2 Convection

Convection is the process by which solutes are transported into concrete as a result of the bulk movement of water (Otieno *et al*., 2010; Golden, 2015). As indicated in the preceding sub-section 2.6.1, the penetration of solutes to the level of steel reinforcement is because of diffusion. In a marine tidal zone, the transportation of chlorides is a very complex mechanism. The effect of intermediate wetting and drying causes the inward and outward movement of water containing chlorides, hence a clear diffusion mechanism is inhibited (Ballim *et al*., 2009).

The depth (Δx) where the convection process happens is known as the convection zone (Gao *et al*., 2017). In addition, the depth of the convection zone is mainly influenced by (i) penetrability of the concrete surface; (ii) water pressure gradient;

(iii) drying and wetting period, and (iv) capillary suction during the wetting period (Golden, 2015).

Beyond the convection zone, diffusion of chloride ions occurs due to a concentration gradient (see Figure 2-7), thus Fick's second law of diffusion is not suitable to be applied in modelling the convection process.

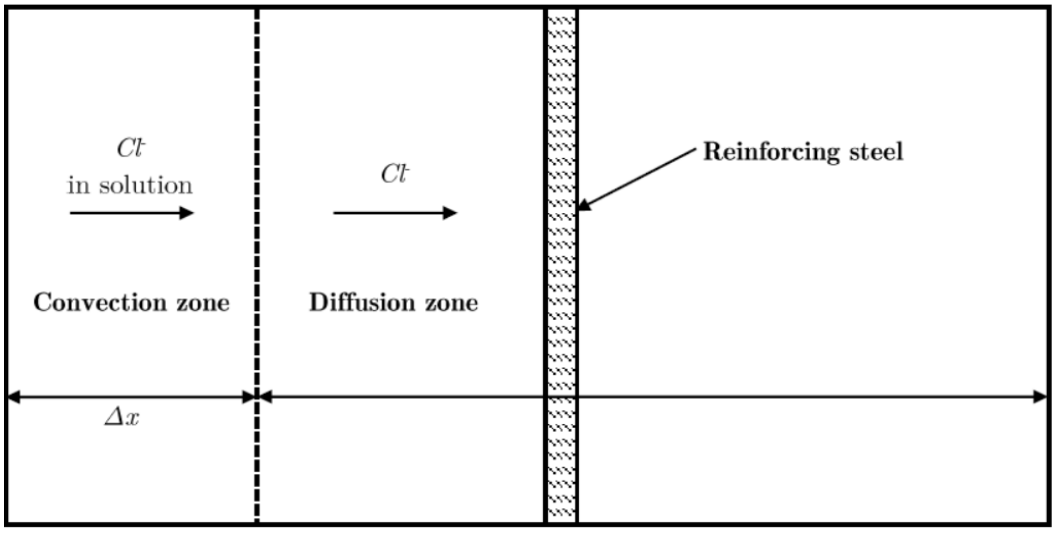

Figure 2-7: An illustration of the convection and diffusion zone controlling the ingress of chlorides under cycles of wetting and drying (Golden, 2015)

The convection process is described as per equation (8):

$$\frac{\partial C}{\partial t} = -v\left(\frac{\partial^2 C}{\partial x^2}\right) \tag{8}$$

Where: C is the concentration of solute at a depth x after time t; v is the average velocity of fluid flow.

Furthermore, beyond the convection zone, the ingress of chlorides can be described using Crank's error function complement, provided the diffusion coefficient is kept constant and also, considering the depth of the convection zone as shown in equation (9) below.

$$C_{x,t} = C_i + (C_{\Delta x} - C_i) \cdot erf\left[1 - \frac{x - \Delta x}{2\sqrt{(t - t_{exp})D_{\alpha}(t)}}\right] \quad (9)$$

Where: $C_{x,t}$ is the concentration of chlorides at a depth x and time t in $(\%/m^3)$; C_i is the initial chloride background level in $(\%/m^3)$; $C_{\Delta x}$ is the chloride content in depth Δx in $(\%/m^3)$; *erf* is the error function; t is the concrete age in (s); t_{exp} is the time until to first exposure to chlorides in (s); $D_{\alpha}(t)$ is the time dependent apparent diffusion in (m^2/s).

2.6.3 Permeability

Permeation is defined as the transfer of fluids through the concrete pore solution under an externally applied pressure, while the pores are still saturated with the fluid. It is also related to the concentration gradient of the permeating fluid. Permeability, therefore, is a measure of the capacity for concrete to transfer fluids by permeation, which is dependent on the concrete microstructure, moisture conditions, as well as the nature of the permeating fluid (Ballim *et al.*, 2009). Additionally, the significance of this process is experienced in water retaining structures.

Darcy's law is used to measure the rate of penetration of fluids (average velocity):

$$v = \left(\frac{k}{n}\right)\left(-\frac{\partial h}{\partial x}\right) \quad (10)$$

Where: v is the average velocity of flow of the fluid in (m/s); k is the permeability coefficient in (m/s); n denotes the porosity of the concrete in (%); h is the hydraulic head in (m); and x denotes the distance covered in (m).

2.6.4 Absorption

Absorption, also referred to as sorption, refers to the transfer of fluids into a partially saturated or completely dry concrete surface as a result of capillary suction (Otieno *et al*., 2010; Wang *et al*., 2020). The measure of the rate of transfer of fluids under capillary action is described as sorptivity. Sorptivity is influenced by hydration, larger capillaries, and their degree of interconnectivity, and concrete mix, thus curing of concrete is a necessity to improve the concrete pore structure (Ballim *et al*., 2009; Otieno *et al*., 2010). The following equation is used to determine sorptivity:

$$S = \frac{Fd}{M_{sv} - M_{s0}} \tag{11}$$

Where: F is the slope of the straight line when the mass loss is plotted against the square root of time in $\left(\mathrm{g/h^{1/2}}\right)$; d is the concrete specimen thickness in (mm); M_{sv} is the saturated mass of concrete specimen in (g); M_{s0} is the dry mass of concrete specimen in (g) at the initial time of 0 seconds.

2.6.5 Migration

Migration, also referred to as accelerated diffusion, electro diffusion, or conduction, is the movement of ions in a solution under an electrical field (Ballim *et al*., 2009). It is mostly applied in accelerated chloride laboratory tests, expressed by the Nersnt-Planck equation (Andrade, 1993):

$$J = \frac{D\, z\, F\, C_{Cl}\, E}{R\, T} \tag{12}$$

Where: J denotes the unidirectional flux of species in $\left(\mathrm{mol/m^2/s}\right)$; D is the diffusion coefficient in $\left(\mathrm{m^2/s}\right)$; z is the electrical charge (valence) of the ionic species; F denotes the Faraday's number in $\left(9.65\times10^4\ \mathrm{C/mol^{-1}}\right)$; C is the bulk concentration of the ionic species in $\left(\mathrm{mol/m^3}\right)$; E is the electrical field potential in (V); R is the gas constant in 8.314 $\mathrm{J/mol/K}$; and T is the absolute temperature in(°K).

Also, Andrade (1993) indicates that the unidirectional flux of a particular ion (J) is a result of the sum of diffusion, migration, and convection (flux = diffusion + migration + convection). Hence, the equation takes into account that corrosion agents can move through the concrete structure in different transport mechanisms simultaneously, even though the migration process is the main transport mechanism (Otieno *et al*., 2010).

2.6.6 Wick action

Wick action is the ingress of water through the concrete surface from the concrete saturated face to the dry face (Aldred *et al*., 2004; Otieno *et al*., 2010). This mechanism may also happen in concrete structures in the marine tidal zone. The manner in which this mechanism occurs is illustrated in Figure 2-8.

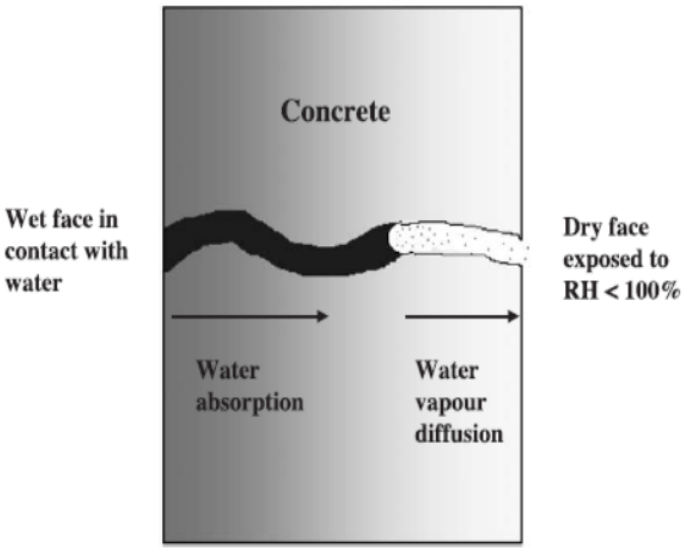

Figure 2-8: Wick action in concrete (Aldred *et al*., 2004)

2.6.7 Combined transport mechanisms

In general, the transport mechanism of corrosion agents in a marine exposure environment is not solely dependent on one mechanism to occur in a particular zone. Rather, a combination of several the aforementioned mechanisms can take place simultaneously in any direction (Otieno *et al*., 2010). For example, in a marine

tidal zone, a combination of sorption, diffusion, and convection can take place in transporting corrosion agents (Figure 2-6).

2.7 Influencing parameters of corrosion rate in RC structures

Numerous factors influence the rate of corrosion of RC structures in marine environments. For example, the type of materials, mix proportions, etc., used to produce concrete influences the penetrability of the concrete pore structure, thus allowing the ingress of aggressive fluids and gases (water and oxygen) to permeate through the concrete. As a result, the rate of corrosion propagation is expedited because it depends on the adequate supply of aggressive corrosion species. Hereunder, the following influencing parameters will be discussed in more detail: influence of exposure zone, blended cements, cover depth, concrete resistivity, oxygen and moisture availability, chloride ingress, water to binder ratio, and temperature.

2.7.1 Exposure zones

In the marine environment, structures are exposed to mainly 4 conditions, namely the atmospheric, splash and spray, tidal, and submerged zones, as demonstrated in Figure 2-9. The atmospheric zone refers to the part of the structure that is not in direct contact with seawater. The splash zone describes the area where seawater particles periodically wash out the concrete structure. The tidal zone is the area between the submerged and the splash zone (between high and low tide). The submerged zone is the part of a structure that is completely immersed in seawater (Ghods *et al.*, 2005).

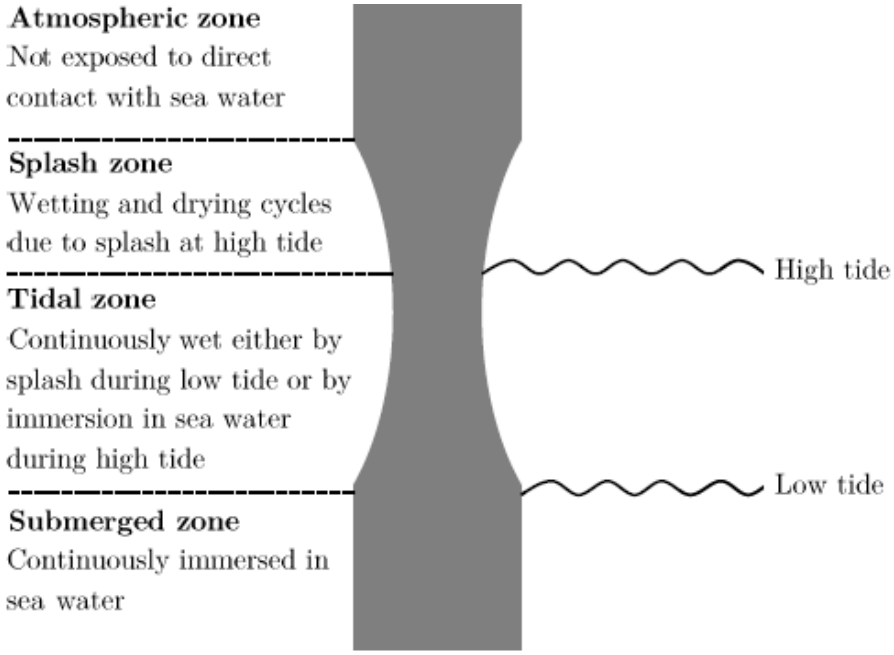

Figure 2-9: Schematic demonstration of exposure zones in the marine environment (Ghods *et al*., 2005)

2.7.1.1 Submerged zone

The submerged zone is characterised as the zone in which a concrete structure is continuously submerged and saturated to the level of reinforcing steel. It is generally considered to have low corrosion risk. This is due to the constant saturation of the concrete pore structure within the concrete cover, which allows chloride ions to diffuse to the level of reinforcement and cause de-passivation of the embedded steel (Polder & de Rooij, 2005; Moore, 2019). In addition, the oxygen concentrations at the level of reinforcement are very low, hence there is minimal corrosion potential (Otieno *et al*., 2010). Furthermore, chlorides are available in large quantities for structures completely submerged in seawater. Nonetheless, limited oxygen concentrations result in a reduced corrosion rate (Moore, 2019).

2.7.1.2 Splash and spray zone

The splash and spray zone is located just above the tidal zone (see Figure 2-9). Chloride penetration and the rate of corrosion is relatively higher in this zone because of moisture splashing on the concrete surface caused by wave action and the movement of chloride ions through capillary suction from the bottom to the top

(tidal zone) (Moore, 2019). This indicates the complexity of the effects of the marine environment and that the mechanism of corrosion in this environment may vary depending on factors affecting reinforced concrete structures, such as the exposure zone. The partial drying in the splash and spray zone results in high chloride penetration as well as oxygen and moisture availability in concrete. Since oxygen, moisture, and chloride ions are readily available in adequate quantities at the level of reinforcing steel, they catalyse the rate of corrosion in RC structures in the splash and spray zone; hence, the rapid deterioration of structures in this region (Golden, 2015).

2.7.1.3 Tidal zone

In the tidal zone, cycles of wetting and drying during low and high tides occur, which causes a heating and cooling effect on the concrete surface (Mehta, 1991; Ghods *et al*., 2005; Golden, 2015). According to Mehta (1991), wetting and drying occurs twice a day when seawater gradually rises (high tide) and falls (low tide). Generally, this happens at an interval of 12 hours and 25 minutes. For 6 hours and 13 minutes, the water rises gradually to the level of the high tide mark and vice versa until it reaches the low tide mark (Mehta, 1991). Depending on the depth and size of the ocean, the tide range (the distance from a high to a low tide mark) differs from one location to another (Mehta, 1991).

The high and low tide marks are dependent on the position of the moon, and the tide change is as a result of the gravitational pull of the moon in relation to the earth (Mehta, 1991) (see Figure 2-10). Figure 2-10 depicts an illustration of the spring and neap tide development as a result of the moon's gravitational pull. The spring tide occurs when the moon, sun, and earth are on the same linear axis, which results in higher high tides and lower low tides. The neap tide, on the other hand, occurs when the sun and moon are positioned perpendicular to the earth's surface, creating an opposing gravitational force on it, thus lower high tides and higher low tides.

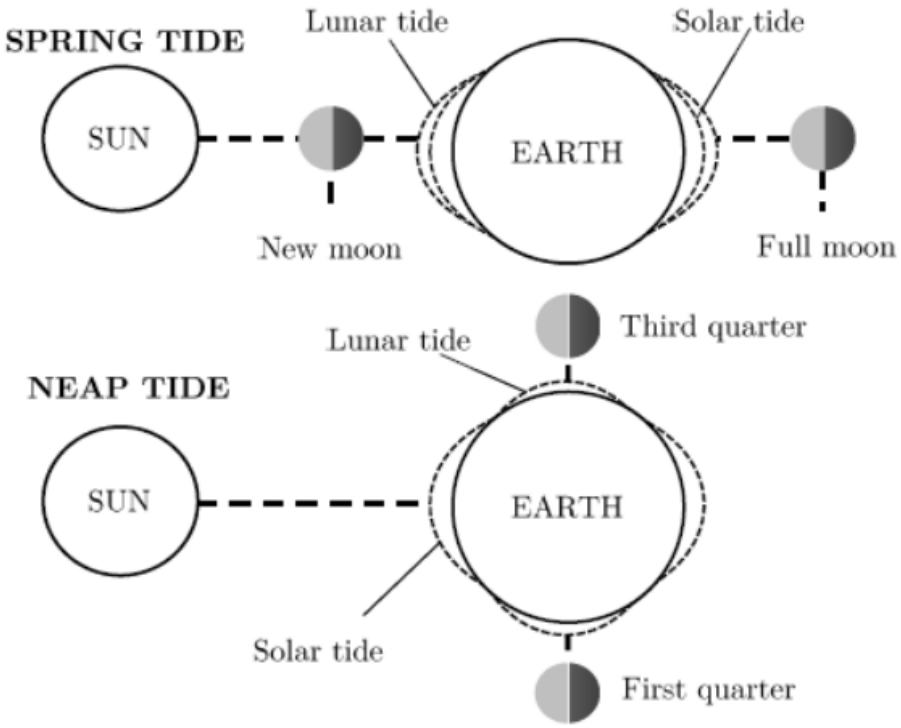

Figure 2-10: Schematic illustration of the effect of Spring tide and Neap tide on the range of high and low tide mark (Golden, 2015)

The heating and cooling effects (during the low and high tides) in the marine tidal zone result in intermediate moisture content, allowing oxygen diffusion for corrosion initiation (DuraCrete, 1998). Hence, the corrosion rate is initially slow. However, once de-passivation of steel occurs, the availability of oxygen and moisture may lead to a higher acceleration of the rate of corrosion (Hunkeler, 2005). The diffusivity of oxygen is in turn affected by w/b ratio, relative humidity, and cover depth to reinforcement (Otieno 2008; Moore, 2019). Moreover, the alternate wetting and drying may create the added problem of salt crystallisation with associated expansive cracking of the concrete (Ballim *et al*., 2009).

Corrosion rates for RC structures in the marine tidal zone vary depending on the location within the tidal zone, i.e., high-tide, mid-tide, and low-tide marks (Polder & de Rooij, 2005). For example, corrosion rates may be lower at low-tide and mid-tide mark (the central point between high and low tide marks) than the high-tide mark area. This can be attributed to short cyclic wetting and drying periods in the tidal zone that retard the availability of oxygen as the concrete in the mid and low-tide areas may not fully dry (Moore, 2019). This is evident on some of the concrete

structures in the Southern parts of Africa, where structures in the marine tidal zone showed a variation in the corrosion rate (Figure 2-11) (Moore, 2019).

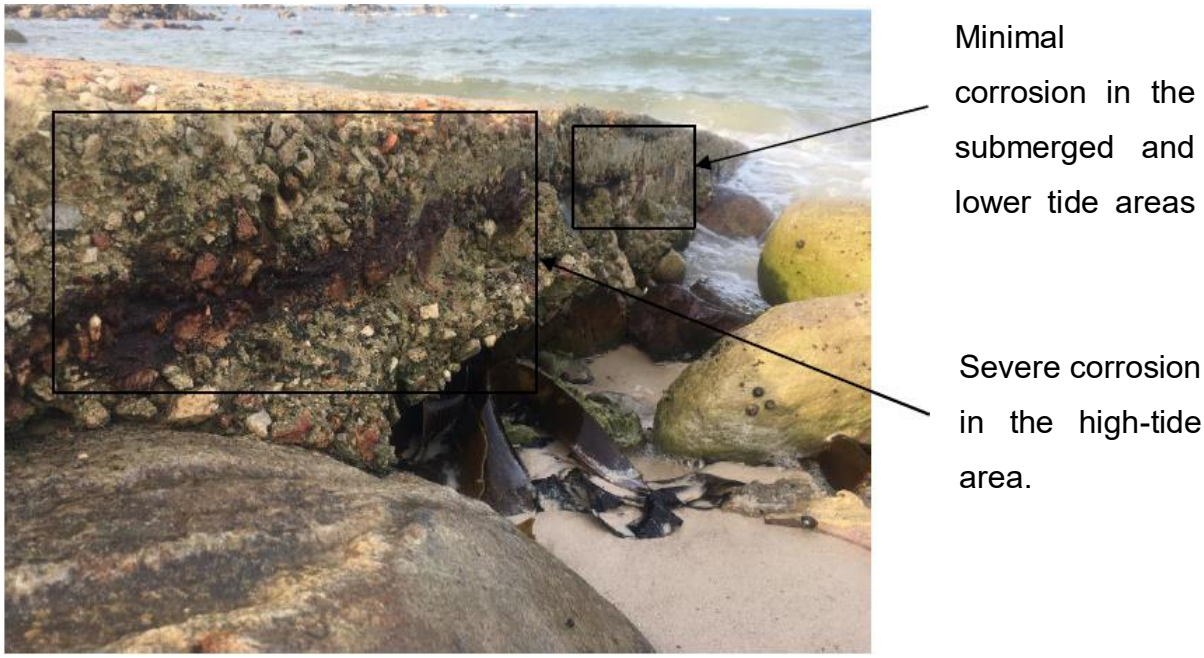

Figure 2-11: Varying corrosion rates in the marine tidal zone (Moore, 2019)

Furthermore, even though standards (for example, EN 206-1, 2013; SANS 10100-2, 2013) classify the marine tidal and splash and spray zones in the same category as the most severe exposure conditions, studies have shown that the corrosion rates of these regions differ considerably (Valipour *et al*., 2013; Valipour *et al*., 2014, Moore, 2019). In addition, results from a study comparing the experimental and modelling measurements of the corrosion rate of reinforced concrete in the tidal and splash and spray zones showed that the corrosion rate in the tidal zone was lower compared to the splash and spray zone (Valipour *et al*., 2014).

Other studies (Otieno *et al*., 2016) found no correlation in terms of corrosion rates of concrete specimens exposed in simulated conditions in the laboratory and in the natural tidal zone. However, the concrete specimens in the natural tidal zone showed minimal corrosion after over 2 years of exposure. From the studies reviewed in this section, it can be inferred that more research is still required, as well as correlation of the results of laboratory-based experiments (that closely simulate the

natural conditions of the marine tidal zone) and field investigations need to be established in order to understand the corrosion in the marine tidal zone.

2.7.2 Blended cements

The production of concrete using only Portland cement (PC) (CEM I) is degrading worldwide, resulting in more use of blended cements made with supplementary cementitious materials (SCMs) (Juenger *et al.*, 2011; Lothenbach *et al*., 2011; Snellings *et al*., 2012; Juenger *et al*., 2019). This is because of the amount of carbon dioxide produced during the manufacturing of CEM I, which accounts for over 5% of the emission into the atmosphere (Bouzoubaa *et al*., 1998; Damtoft *et al*., 2008; Snellings *et al*., 2012; Moore, 2019). Furthermore, blended cements produce dense and less permeable concrete, lowering the risk of reinforcement corrosion and thus increasing the service life of reinforced concrete structures (Guneyisi *et al*., 2005; Xu *et al.*, 2012; Zhang *et al*., 2017).

Blended cement is the type of binder that is produced by replacing a portion of the PC with SCMs. Blended cement includes SCMs, such as ground granulated blast furnace slag (GGBS), fly ash (FA), and silica fume (SF), as well as natural pozzolans, such as calcined clay (also referred to as metakaolin), volcanic ash, and calcined shale. Therefore, a blended cement can be made by replacing the PC with either one or a dual combination of the aforementioned SCMs (i.e., a ternary blend). A brief background about the origin of SCMs and their use as a partial replacement of PC to produce blended cement in concrete is presented in subsection 2.7.2.1. Also, the influence of blended cements on the rate of corrosion of RC structures in the marine environment is discussed in subsection 2.7.2.2.

2.7.2.1 Origin of SCMs

The term supplementary cementitious materials (SCMs) describes the different types of materials that are used in concrete as partial or complete replacement of PC cement. In South African engineering practise, fly ash, ground granulated blast furnace slag, and silica fume are the most widely used SCMs. These SCMs are classified as pozzolans and hydraulic materials (Thomas, 2013). Through

pozzolanic or hydraulic activity, or a combination thereof, the incorporation of SCMs into concrete improves the fresh, hardened, and durability properties of concrete (Thomas, 2013).

The term pozzolan is defined as “a siliceous or siliceous and aluminous material that in itself possesses little or no cementitious value but will, in finely divided form and in the presence of water, chemically react with calcium hydroxide at ordinary temperatures to form compounds shows or possessing cementitious properties” (ASTM C125-15b, 2016, p. 6). Accordingly, on the one hand, low calcium fly ash, silica fume, volcanic ash, calcined clay, and shale have pozzolanic behaviour when used in concrete, while high calcium fly ash shows both pozzolanic and hydraulic reactions. On the other hand, GGBS has hydraulic behaviour because of its ability to produce cement hydration products when in reaction with water. Consequently, GGBS can, independently of PC, harden or gain strength. However, when combined with PC, chemical reactions are accelerated (Thomas, 2013). The characteristics of the most commonly used SCMs are demonstrated in Table 2-1.

It is generally understood that, even though SCMs improve the mechanical and durability properties of concrete, their durability performance considerably varies (Guneyisi *et al*., 2005). The physical, chemical, and mineralogical composition of SCMs vary as a result of their production and the properties of the raw material used to make cementitious materials, such as concrete, resulting in varying durability performance (Guneyisi *et al*., 2005; Thomas, 2018).

Also, other studies have shown that SCMs reduce the amount of calcium hydroxide in concrete due to the dilution effect and pozzolanic reaction, resulting in a decrease in the concrete pH (Zhang *et al*., 2000; Detwiler, 2002). As a result of pH reduction, the passive layer of concrete becomes less protected from corrosion agents (Poursaee, 2010). Therefore, due to the varying effects of SCMs on concrete properties, which in turn influences their durability performance, careful consideration of the type and content of the SCM to be used in the preparation of the concrete mixture is essential.

Table 2-1: Characteristics of SCMs (Mehta, 1983; cited by Thomas, 2013)

Property	**Low-Calcium Oxide fly ash**	**High-Calcium Oxide fly ash**	**Slag**	**Silica Fume**
Mineralogy	Al-Si glass, inert crystalline phases	Ca-Al-Si glass, some Ca-Al glass, crystalline C_2S, C_3S, $C\hat{S}$, MgO and lime	Ca-Al-Si-Mg glass	Silicate glass
Shape	Spherical	Spherical	Angular crushed particles	Spherical
Median size (μm)	5 - 20	2 - 20	5 - 20	0.1 - 0.2
Surface area (m^2/kg)	300 - 500	300 - 500	400 - 650	15 000 - 25 000
Specific gravity	1.9 - 2.8	1.9 - 2.8	2.85 - 2.95	2.2 - 2.3
Bulk density (kg/m^3)			1 200	130 - 430
Nature of reactions	Pozzolanic	Pozzolanic and hydraulic	Hydraulic	Pozzolanic
Colour	Gray	Gray to buff white	White	Dark grey to black

Figure 2-12 demonstrates a variation in chemical composition [silicon dioxide (SiO_2), calcium oxide (CaO) and aluminium oxide (Al_2O_3)] for different SCMs. For example, from Figure 2-12, it can be observed that silica fume mainly contains silicon dioxide compounds, whereas slag and PC exhibit more calcium oxide compounds.

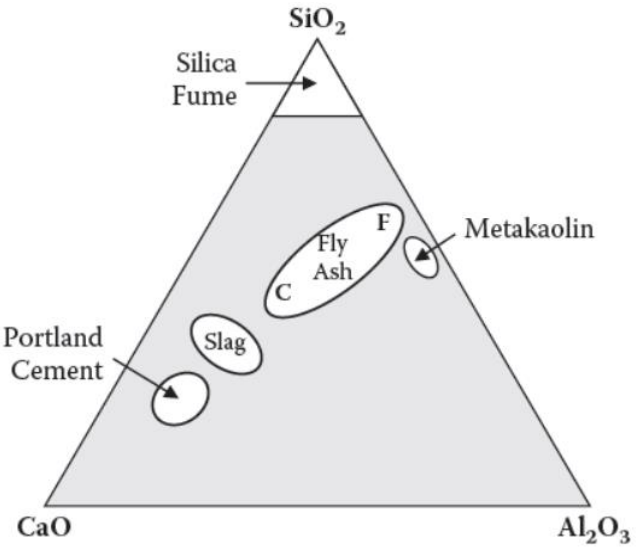

Figure 2-12: Chemical composition of some commonly used SCMs (Thomas, 2013)

In summary, the use of blended cements in modern concrete production is notably increasing. Their introduction to concrete influences the mechanical and transport properties of concrete, which consequentially has an impact on the durability and service life of the structure. Blended cement improves the homogeneity of concrete mixes, the paste-aggregate interface, etc., and consequentially reduces the permeability of the structure. Hence, the use of blended cements in concrete improves the durability of reinforced concrete structures (Kwon *et al*., 2017).

2.7.2.2 Influence of blended cements on corrosion rate

The use of blended cement concrete is beneficial for RC structures exposed to aggressive environments due to the widely known durability performance of the constituting materials (SCMs) (Kwon *et al*., 2017). Kwon *et al*. (2017) reported that blended cement concretes showed a decrease in strength even though the corrosion rate in blended cement concretes was lower than in PC concrete.

The decrease in strength was due to the chemical reaction of sulphate (SO_4) in sea water and aluminium oxide (Al_2O_3) in SCMs, and the formation of calcium sulphate ($CaSO_4$) in the concrete pore structure (Kwon *et al*., 2017). However, this proved to be advantageous in reducing the rate of corrosion of reinforcement as the formation of the calcareous deposits inhibited the ease of movement of corrosion species in the concrete pores (Kwon *et al*., 2017). This observation is an indicator that the

compressive strength of concrete should not be considered as an indicator of the service life of a structure, but instead as a basic property of concrete (Ballim & Alexander, 2018).

Even though SCMs are recommended, they show different characteristics and performance under different exposure conditions. On the one hand, depending on the replacement levels, SCMs result in a reduction in alkaline concentrations and hydroxyl ion concentrations in the concrete pore structure, which in turn influences the time to corrosion initiation (Tuutti, 1982; Byfors, 1987; Ozkul *et al*., 2008; Vollpracht *et al*., 2016). On the other hand, studies (Ozkul *et al*., 2008; Angst *et al*., 2009; Al-Ayish *et al*., 2018) have shown that the use of supplementary cementitious materials increases the chloride binding capacity of the concrete due to the high alumina content in these materials, thus prolonging the corrosion impact of RC structures when blended cement concrete is used.

For the purpose of this study, only the influence of GGBS and FA will be reviewed. Concrete made with GGBS has been found to exhibit the lowest corrosion rates compared to other binders (PC and FA) (Scott, 2004; Otieno, 2008; Otieno, 2014; Golden, 2015; Yi *et al*., 2020). In a study by Otieno (2014), the use of GGBS in concrete resulted in better corrosion performance than concrete containing FA. This was because of a decrease in chloride diffusion coefficient values, which was attributed to a more refined pore structure of the concrete made with GGBS at different w/b (Scott, 2004).

Studies on the corrosion resistance of concrete made with FA have shown that the inclusion of FA in concrete results in a refined pore structure of the concrete, which subsequently reduces the permeability of the concrete to corrosion agents and increases the concrete's resistivity. As a result, concrete made with FA showed better corrosion performance compared with PC (Maslehuddin *et al.*, 1987; Hussain, 1994; Choi *et al*., 2006). Similarly, in another study, which evaluated the corrosion performance of concrete made with FA for a period of 10 years in a marine tidal zone, it was shown that FA at 30% replacement outperformed the concrete made with PC; owing to the refined pore structure of FA, concrete made with FA exhibited the lowest corrosion (Thomas & Matthews, 2004).

Furthermore, concretes containing SCMs at higher w/b have been reported to show relatively the same corrosion performance as concrete made with PC only at lower w/b, provided the same cover depth is used (Chalee *et al*., 2010). This is because of the pozzolanic reaction of SCMs, resulting in the densification of the concrete pore structure in blended cement concretes (Thomas & Matthews, 2004; Scott & Alexander, 2007; Chalee *et al*., 2010; Otieno *et al*., 2016). The pozzolanic reaction of SCMs results in a fine filling of the pore structure, thereby reducing the ingress of chlorides and other corrosion agents (Vedalkshmi *et al*., 2008).

2.7.3 Cover depth

In a reinforced concrete structure, the concrete cover depth is the shortest distance between the concrete surface and the surface of the reinforcing steel embedded in the RC structure (Neville, 1999). Cover depth influences the ease of transportation of corrosion agents into the concrete cover layer (Yang *et al*., 2020). Hence, it is an important parameter in controlling the rate of corrosion (initiation and propagation) of reinforcing steel in concrete.

Figure 2-13 illustrates the influence of cover depth on oxygen availability and resistivity. From Figure 2-13 it can be observed that, for a given corrosion rate, increasing cover depth reduces oxygen availability (Scott & Alexander, 2007). Therefore, oxygen availability is an important factor in causing corrosion of the reinforcement steel and it depends on the binder type, cover depth, and exposure zone of the marine environment.

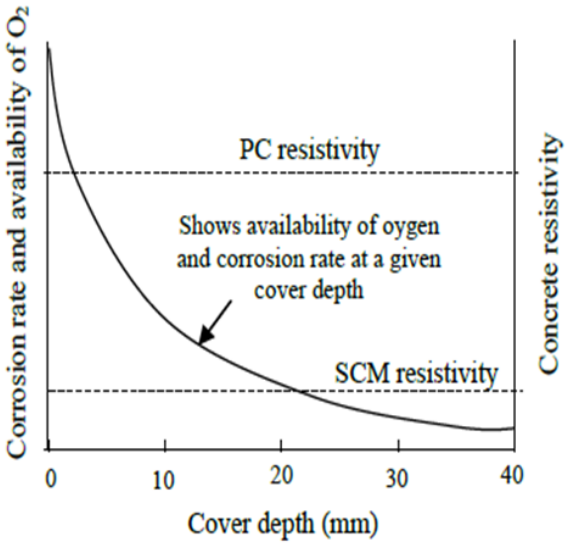

Figure 2-13: Relationship between corrosion rate, oxygen availability and resistivity (Scott & Alexander, 2007)

Moore (2019) conducted an experimental study on the effect of oxygen availability on the corrosion rate of RC structures made with Portland cement in the marine environment. The study simulated the conditions of the tidal zone using 6-hour cycles of wetting and drying. Based on the findings of the study, specimens with higher cover depths exhibited low rate of corrosion. As a result of the higher cover depth, exceeding 30 mm, oxygen was deprived to the steel for concrete in the tidal zone, thereby inhibiting corrosion.

In addition, most national standards worldwide, including the adopted standard in South Africa, prescribe a minimum cover depth for reinforcement. However, they do not take into consideration the performance of the materials (Beushausen *et al*., 2019). According to Alexander *et al*. (2008), for high-performance concrete, the longer service life of a RC structure may be achieved even at lower cover depths. Furthermore, recent research (Luping *&* Lofgren 2016; Al-Ayish *et al*., 2018) indicates that the corrosion assessments conducted based on the effectiveness of the cover thickness may be misleading; thus, advocating for the consideration of materials based on their durability performance.

Lopez-Calvo *et al*. (2018) investigated the effect of cover depth on the corrosion of steel in high-performance concrete (HPC) in relation to concrete quality and specimen crack width. The concrete contained corrosion inhibiting admixtures and

20% fly ash. Two different covers (25 mm and 45 mm) were used. The effectiveness of the cover depth was evaluated based on the wideness of the crack width. From the study, it was concluded that the specimens with a 25 mm cover thickness, on the one hand, exhibited a higher corrosion rate, irrespective of the crack width (90 µm to 300 µm). On the other hand, at 45 mm concrete cover, specimens exhibited a low rate of corrosion of steel up to a crack width of 200 µm and over. Additionally, corrosion was reduced in concrete specimens containing fly ash, regardless of the concrete cover and crack width.

Similarly, Otieno *et al*. (2016) conducted an experimental investigation on chloride-induced corrosion of steel in a simulated and natural marine environment. A variation in cover depth of 20 mm and 40 mm was employed. The concrete specimens were comprised of 100% Portland cement (PC) and 30% FA or 50% GGBS as partial replacements for Portland cement. The results indicated that the thinner the cover to reinforcing steel, the higher the corrosion rate. Hence, relatively higher corrosion currents were observed on the 20 mm cover depth for both laboratory and field specimens. In addition, the incorporation of SCMs resulted in a significant reduction in corrosion rate at a given cover depth (see Figure 2-14). The notations U-L and U-F denote uncracked laboratory and uncracked field specimens, respectively.

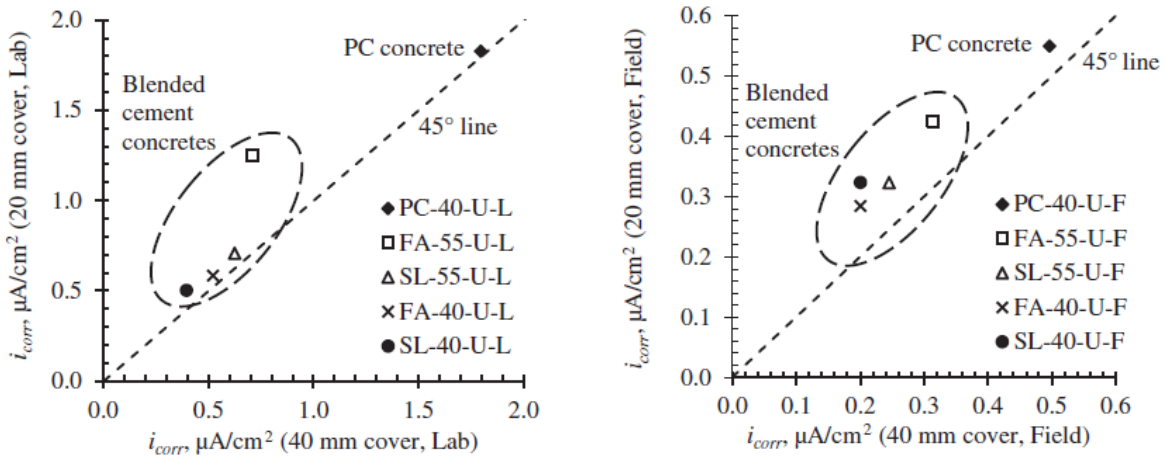

Figure 2-14: Comparison of corrosion rates for (a) uncracked laboratory specimens and (b) uncracked field specimens at varied cover depths (Otieno *et al*., 2016)

Baten *et al*. (2020) studied the corrosion susceptibility of RC structures utilising a variety of blended cements and varying cover depths. The concrete specimens were made PC, FA, GGBS, and a blend of FA and GGBS, as well as a range of cover depths (37,5, 50, 75, 100, 125, 150, and 175 mm). The replacement levels for blended cement concretes were 30% and 40%. On the one hand, concrete mixtures containing 30% and 40%. GGBS exhibited moderate corrosion resistance in comparison to PC specimens for all specified cover depths. The study also showed that the performance of GGBS specimens improved with increasing cover thickness, with a negligible difference in corrosion probability between GGBS and FA specimens. On the other hand, specimens with 30 - 40% FA yielded higher corrosion resistance in comparison with PC and GGBS specimens even at lower cover depths. This can be attributed to a higher silica content and a larger amount of calcium-silicate-hydrate (C-S-H) in FA concretes, with the latter resulting in a more refined pore structure, thereby reducing corrosion (Baten *et al*., 2020).

From the above-reviewed studies, it can be inferred that, provided that sufficient cover depth is used, the desired service life of a structure can be achieved. However, cover depth selection is influenced by the type of binder used. For blended cement concrete, degradation of RC structures due to corrosion can be reduced even at lower cover depths, however, this is not true for RC structures made of PC.

2.7.4 Concrete resistivity

Concrete resistivity is one of the most influential parameters of corrosion rate in RC structures (Gjorv *et al*., 1977; Polder *et al*., 2000). However, when SCMs are used, the assessment of concrete resistivity becomes more complex as there are other factors involved, such as chloride binding, which in turn limits chloride ingress to the level of the reinforcing steel, which affects concrete resistivity (Gjorv *et al*., 1977; Polder *et al*., 2000; Scott & Alexander, 2007). It is a geometry-independent material property that describes the electrical resistance (Polder *et al*., 2000).

Furthermore, concrete resistivity is an indicator of the risk of corrosion degradation of RC structures and can be used to predict the service life of RC structures (Azarsa

& Gupta, 2017). Thus, preventative measures may be employed to prevent an increase in corrosion damage (Polder *et al*., 2000; Azarsa & Gupta, 2017). The likely rate of corrosion of a structure based on concrete resistivity can be assessed using the guidelines in Table 2-2 (Heckroodt, 2002).

Table 2-2: Likely corrosion rate based on the concrete resistivity (Heckroodt, 2002)

Likely corrosion rate for given conditions	Concrete resistivity kΩ.cm
High	< 12
Moderate	12 – 20
Low	> 20

The resistivity of concrete is influenced by intrinsic factors such as cement content, water to binder ratio, concrete pore solution, etc., and extrinsic factors such as moisture content, chloride ingress, temperature, etc. (Polder *et al*., 2000; Otieno, 2008; Azarsa & Gupta, 2017). For example, when temperature rises, more ions move through the concrete, which lowers its electrical resistivity (Layssi *et al*., 2015). Furthermore, the dryness of the concrete (i.e., a decrease in the degree of water saturation) increases the concrete resistivity (Gjorv *et al*., 1977). This was observed when water saturation was reduced from 100% to 20%, resulting in an increase in the electrical resistivity of concrete from 7×10^3 Ω.cm to 6000×10^3 Ω.cm.

Concrete resistivity and conductivity (ingress of ions through an electrical current) have an inverse and direct proportional relationship to the corrosion rate of the RC structure, respectively, at lower moisture content of the concrete (equation (13) (Hunkeler, 2005). Furthermore, as shown in Figure 2-15, this relationship concurs with the results demonstrated by Andrade *et al*. (2004).

$$i_{corr}\ \alpha\ \frac{1}{\rho_c} = \sigma_c \tag{13}$$

Where: i_{corr} denotes the corrosion rate in (A/cm^2); ρ_c is the resistivity of concrete in (Ω.cm); and σ_c is the conductivity.

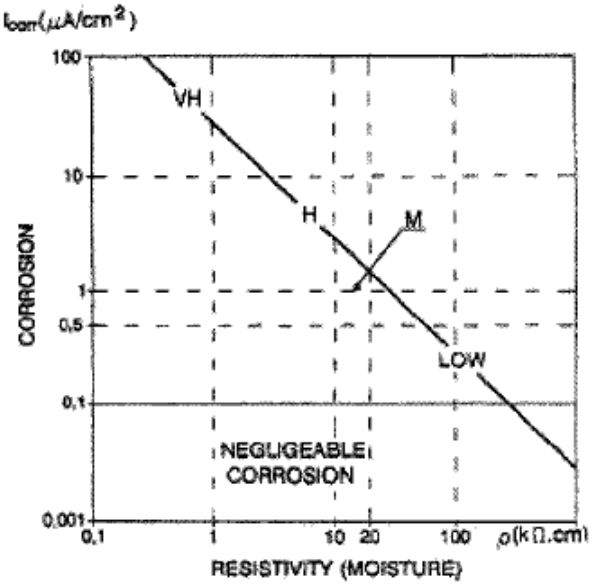

VH – Very high

H – High

M – Moderate

Figure 2-15: Relationship between corrosion rate and the resistivity (Andrade *et al*., 2004)

Furthermore, research on the correlation of concrete resistivity measurements and the corrosion rate is ongoing, considering the corrosion rate's influencing parameters such as exposure zone, chloride ingress, binder type, etc. (Balestra *et al*., 2020). As a result, new resistivity values are proposed based on the corrosion rate's influencing parameters such as chloride ingress (Table 2-3). For example, Balestra *et al*. (2020) conducted a field study on degraded structures in the marine environment to evaluate chloride ion penetration. The results are presented in Table 2-3. It can be seen from Table 2-3 that RC structures associated with high chloride penetrations, similar to those in marine tidal and splash and spray zones, possess a very high risk of corrosion due to high chloride concentration as a result of cyclic wetting and drying.

Table 2-3: Correlation between chloride penetration and concrete resistivity: proposed values (Balestra *et al*., 2020)

Chloride penetration (%)	Concrete resistivity kΩ.cm
Very high	< 5
High	5 – 9
Moderate	9 – 17
Low	17 – 41
Very low	41 – 220
Negligible	> 220

The incorporation of SCMs in concrete increases concrete resistivity, which results in a reduction in the corrosion rate (see Figure 2-13) of steel in reinforced concrete structures (Otieno, 2014). Therefore, the general understanding from the reviewed studies with regard to the influence of concrete resistivity on corrosion rate is that concrete resistivity governs the occurrence of corrosion, but other factors influencing the rate of corrosion, such as oxygen availability, catalyse the rate of corrosion of reinforced concrete structures (Scott, 2004; Golden, 2015).

2.7.5 Oxygen and moisture availability

Oxygen is an essential parameter for the cathodic reaction to occur in RC structures, as can be seen from Figure 2-4 in Section 2.5.1. It is influenced by many factors, including, but not limited to, the quality of concrete, moisture content, binder type, aggregate type, etc. (Real & Bogas, 2017). The ingress of oxygen through the concrete pore structure is mainly through the process of diffusion (Hunkeler, 1996).

It is widely accepted that RC structures that are permanently submerged in seawater pose a low risk of corrosion and are likely to reach their design service life (Tuutti, 1982; Andrade *et al*., 1990; Raupach, 1996; Broomfield, 2007; Hussain, 2011; Walsh, 2015; Walsh & Sagues, 2016; Moore, 2019). This is because concrete pores are filled with water, resulting in low dissolved oxygen diffusivity in the submerged zone to sustain the cathodic reaction on the reinforcing steel and thus the

occurrence of corrosion. However, this is not the case for structures in the marine tidal and splash and spray zones.

In the marine tidal zone, due to short cycles of wetting and drying (6 hours each), depending on the tide range depth (Mehta, 1991), higher moisture content affects the diffusion of oxygen to the level of reinforcement (Ji *et al*., 2015). Also, this provides continuous curing and a prolonged hydration process for RC structures in the marine tidal zone, which results in a more refined concrete pore structure. This results in low penetrability of concrete and, subsequently, low oxygen diffusivity and moisture loss (Hussain & Ishida, 2010; Moore, 2019). Thus, these 2 parameters (oxygen and moisture) are discussed in conjunction with this in this section due to their coupling effect on corrosion of RC structures.

Hunkeler (1994), cited by Hunkeler (2005), attempted to quantify the diffusion of oxygen for partly immersed concrete in correlation with the concrete moisture content using equation (14). The results obtained through the use of this equation are presented in Figure 2-16. It can be seen from the results that moisture increase reduces the diffusivity of oxygen in concrete.

$$D(O_2, C) = \frac{D_L\left(\frac{D_L}{D_W} - W\frac{D_L}{D_W} + 3\right)}{2W\left(\frac{D_L}{D_W} - 1\right) + \frac{D_L}{D_W} + 2} \quad (14)$$

Where: $D(O_2, C)$ is the oxygen diffusion coefficient in concrete in (cm^2/s); D_L denotes the oxygen diffusion coefficient in dry concrete in (cm^2/s); D_W denotes the oxygen diffusion coefficient in wet concrete in (cm^2/s); and W is the water content of the concrete in (vol. %).

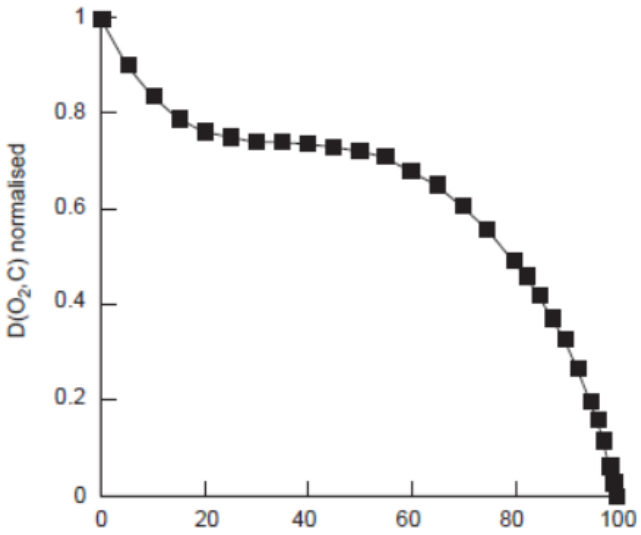

Figure 2-16: The effect of relative humidity on the diffusion of oxygen in concrete (Hunkeler, 1994; cited by Hunkeler, 2005)

Ji *et al*. (2014) quantified the corrosion rate of reinforcing steel under different marine exposure conditions. According to their findings, the availability of oxygen is only an influential parameter for corrosion, but it is not the controlling factor. The rate at which corrosion propagates is a result of the formed corrosion products. The study further indicates that, in the case of partly immersed structures, oxygen and corrosion products are available at high concentrations. As a result, corrosion is high in those structures.

In another study, Ji *et al*. (2015) investigated the effect of moisture content and corrosion products on the corrosion of RC structures. It was found that an increase in relative humidity (RH) reduces the effect of oxygen on reinforcement de-passivation by filling the concrete pores with moisture (see Figure 2-17), while corrosion products increase corrosion as a result of increased RH (from 0 up to 50% RH). Thus, according to their findings, oxygen diffusion plays an important role in corrosion initiation, but the formed corrosion product governs the rate of corrosion propagation.

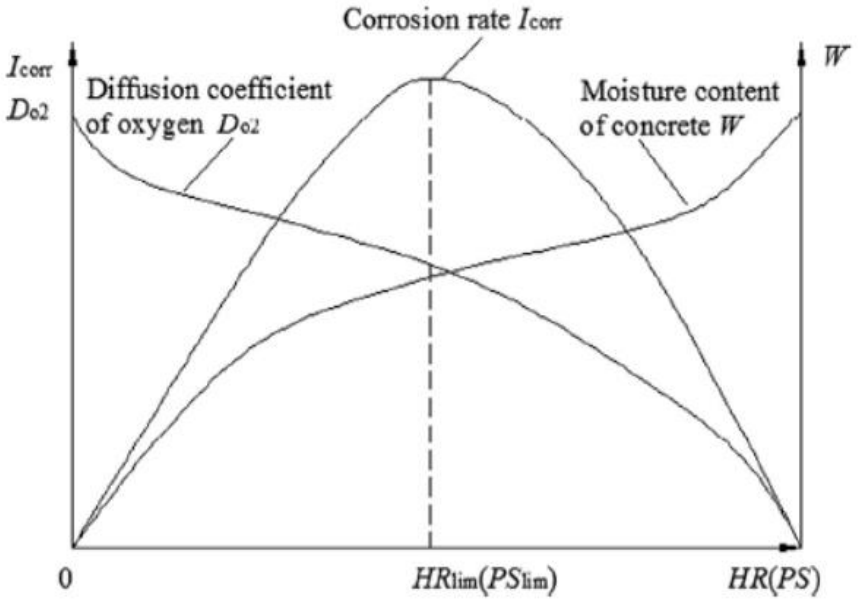

Figure 2-17: Correlation between moisture content and oxygen on corrosion in concrete (Ji *et al*., 2015)

Moreover, Hussain and Ishida (2010) corroborate the above findings that there exists a correlation between RH and oxygen diffusion, where a high RH was reported to inhibit the ingress of oxygen to the level of reinforcement, thus stifling corrosion. Nonetheless, the experimental results of their study showed a high corrosion rate on structures with a RH of up to 95%. However, this may be a result of the formed corrosion product. Also, a correlation between concrete cover and RH under cyclic wetting and drying conditions was found by Hussain *et al*. (2012). The concrete specimens with a thin cover depth exhibited a low corrosion rate compared to those with a thick cover depth due to the prolonged wetting duration (very moist conditions), which inhibited the supply of oxygen to the reinforcing steel. However, Hussain *et al.* (2012) further indicated that if short wetting cycle durations were used the specimens with thick cover depth would undoubtedly exhibit better corrosion resistance.

In addition, the results of Cheng *et al*. (2005) complement those presented in Figure 2-13. The incorporation of GGBS resulted in reduced oxygen concentrations attributed to the densification of the microstructure in blended cement concrete. Therefore, the studies reviewed in this section have shown that oxygen and moisture coexist for structures exposed to cyclic wetting and drying and

that the coupling effect of these parameters plays an important role in the occurrence of corrosion in both initiation and propagation phases. On the one hand, a continuous supply of oxygen is needed to sustain the cathodic reaction during the initiation and propagation phases of corrosion. On the other hand, moisture availability acts as an electrolyte and spreads the formed corrosion product, increasing the corrosion rate. However, short cycles of wetting and drying, as is case in the marine tidal zone, result in highly moist conditions in the concrete pore structure. In addition, the more refined concrete pore structure for concrete made with SCMs reduces moisture loss, making it harder for oxygen to diffuse to the level of the reinforcing steel and thus limiting the risk of corrosion. Therefore, knowledge of the influence of oxygen and moisture content on corrosion rate is paramount, particularly for structures in the marine tidal zone, taking into account the influence of SCMs under various cover depths and drying and wetting durations.

2.7.6 Chloride ingress

Chloride ingress is the root cause of corrosion of reinforcement for concrete structures exposed to sea water. Chlorides are transported primarily through diffusion and convection mechanisms in partially saturated RC structures (Balestra *et al*., 2019). Chloride penetration into concrete is influenced by factors such as the concrete's pore solution, quality, exposure conditions, curing regime, cement composition, etc. (Shi *et al*., 2012).

It is widely accepted that not all the chlorides in the concrete pore structure participate in initiating corrosion of reinforcement in chloride-contaminated concrete structures. Hence, there are bound and free chlorides (Glass & Buenfeld, 1997). The bound chlorides can be defined as adsorption or chemical binding of chlorides due to the hydration process of the concrete matrix (Marinescu & Brouwers, 2010), whereas free chlorides are those that remain in the concrete pore solution (Glass & Buenfeld, 1997). It is generally assumed that only free chlorides pose a corrosion risk in concrete. However, findings from Glass and Buenfeld (1997) and Glass and Buenfeld (2000) suggest that, in some cases, bound chlorides can lead to high corrosion potential in the same manner as free chlorides. This is due to the

accumulation of adsorbed chlorides, which in turn increases corrosion risk (Otieno, 2008).

Furthermore, for corrosion to be initiated, a critical chloride concentration (the chloride threshold value) is required for de-passivation of reinforcement (Angst, 2011). The chloride threshold is generally expressed in three ways, related to the weight of the binder [free chloride content; total chloride content (refers to the total of both free and bound chloride content); and the ratio of chloride ions to hydroxyl ions (which relates the chloride activity to the pH conditions of the concrete, with the higher pH conditions associated with strong inhibiting effect of hydroxide ions)] (Angst *et al*., 2009). However, the expression of total chloride content by mass of cement has been suggested by Glass and Buenfeld (1997). Accordingly, chloride threshold values (total chloride content) ranging from 0.02% to 3.08% are found in the literature, as presented in Table 2-4. An in-depth literature review on chloride threshold is found in Angst *et al*. (2009).

Table 2-4: Chloride threshold values (after Otieno, 2008)

Reference	Cement type	Chloride threshold (%) by mass of cement
Lambert *et al*., 1991	PC & Sulphate resisting Portland cement (SRPC)	1.0 – 3.0
Alonso *et al*., 2000	PC	1.24 – 3.08
Trejo and Pillai, 2003	PC	0.02 – 0.24
Scott, 2004	PC & Blended cements	0.08 – 0.53

2.7.6.1 Chloride profiles in a marine tidal zone

It is important for knowledgeable engineers and concrete researchers to be able to interpret chloride profiles in a concrete structure to predict its service life (de Rincon *et al*., 2004). Figure 2-18 shows a schematic representation of chloride profiles for structures exposed to cyclic wetting and drying in a marine environment. The following observations can be made from the schematic illustration:

- Chloride profiles increase in the convection zone.
- However, a downward trend can be observed at deeper depth (diffusion zone).
- Also, at the end of the convection zone, chloride concentrations are at their maximum peak (Balestra *et al*., 2019).

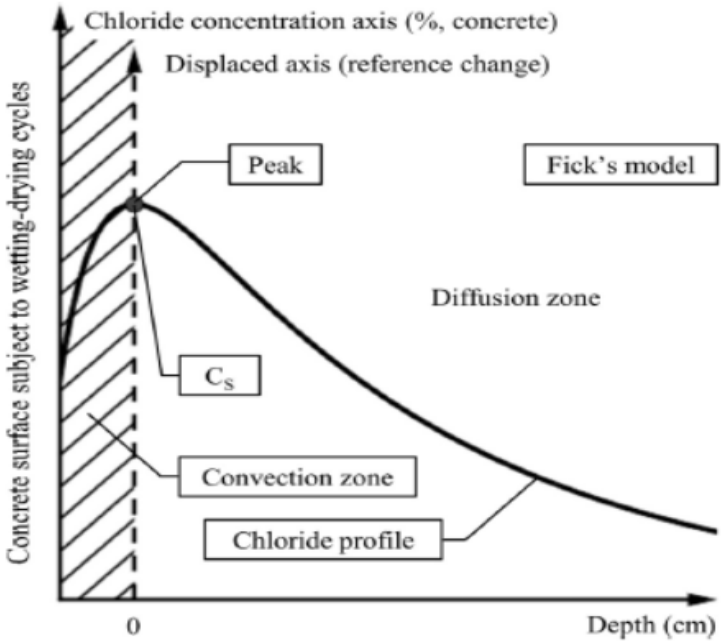

Figure 2-18: Schematic representation of chloride profiles in concrete exposed to cyclic wetting and drying (Balestra *et al*., 2019)

Simcic *et al*. (2015) studied the chloride penetration profiles for mixtures exposed to cyclic wetting and drying conditions. The chloride profiles were measured at 21, 42, 84, 105, and 126 days of exposure to the simulated tidal zone. The concrete specimens were made with PC and blended cement (containing fly ash). From their results, concrete made with FA had a lower chloride concentration than concrete made with PC. This can be attributed to the dense microstructure in blended cement concretes.

The findings of Thomas and Moffatt (2018) corroborate the observations made by Simcic *et al*. (2015), where concrete incorporating SCMs (such as slag, fly ash, and silica fume) exhibited lower chloride penetrations than PC concrete for structures exposed to different marine conditions, including the marine tidal zone for 25 years. Figure 2-19 shows chloride penetration for concrete made with PC and concrete

made with FA under cyclic wetting and drying conditions. It can be observed from Figure 2-19 that with the increase in exposure duration, the depth of the convection zone also increases, especially for concrete made with PC, with a depth difference of 8 mm after 126 days of exposure.

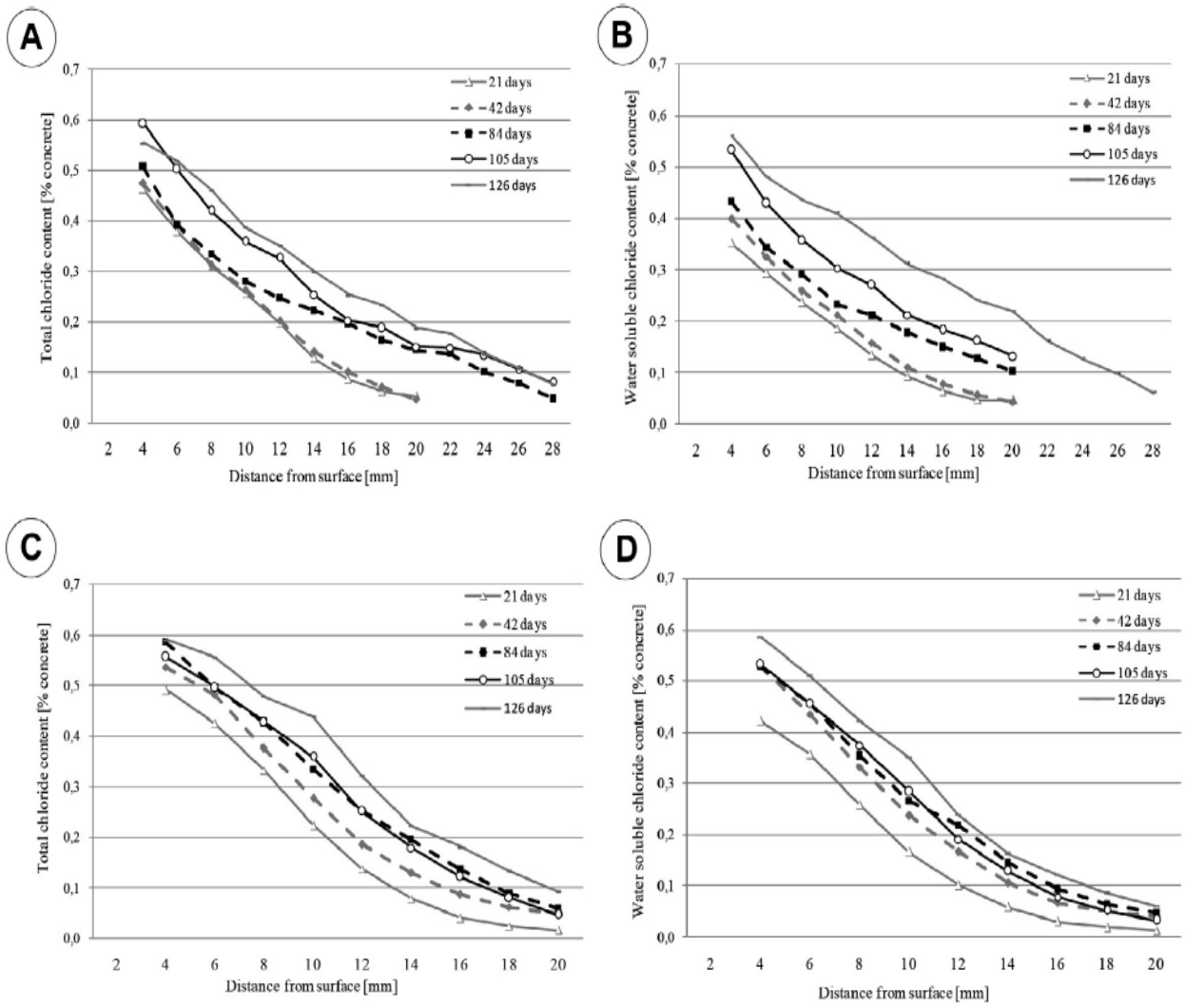

Figure 2-19: Chloride penetration profiles for two concrete mixtures, concrete made with PC (A & B) and concrete made with FA (C & D), exposed to cyclic wetting and drying (Simcic *et al*., 2015)

Another study simulating the tidal and splash zones of the marine environment showed that wave action in the tidal and splash zones plays a significant role in accelerating the rate of chloride ingress into concrete (Sun *et al*., 2018). Furthermore, the results indicate that long-term exposure of concrete structures to seawater leads to high chloride content, thus high corrosion risk (Figure 2-20).

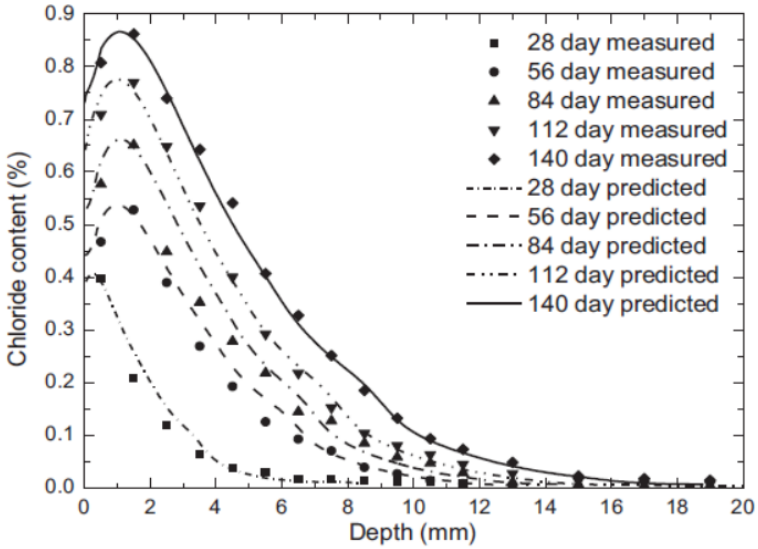

Figure 2-20: Comparison of predicted and measured chloride content profiles of specimens exposed to seawater (Sun *et al*., 2018)

The use of SCMs in concrete applications results in high chloride binding capacity and great resistance to chloride penetration to the level of reinforcing steel (Thomas & Bamforth, 1999; Shi *et al*., 2012; Simcic *et al*., 2015; Tadayon *et al*., 2016; Thomas & Moffatt, 2018). This can be seen in Figure 2-21, where chloride concentration decreases with increasing depth in blended cement concrete after 25 years of exposure in a tidal zone.

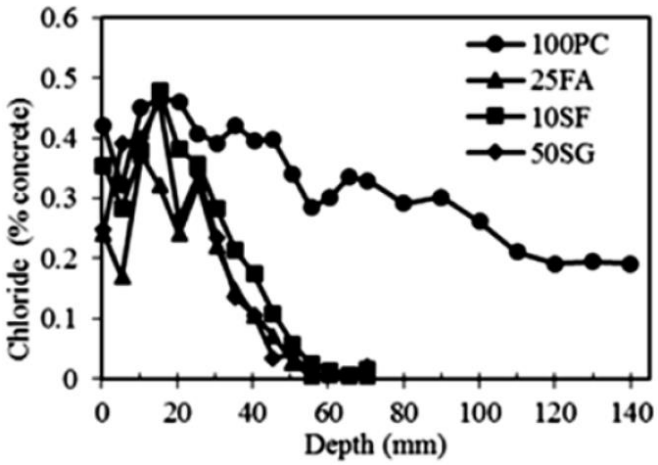

Figure 2-21: Chloride content profiles for RC specimens after 25 years of exposure in a tidal zone (Thomas & Moffatt, 2018)

Therefore, the literature presented in this subsection 2.7.6.1 corroborates Glass and Buenfeld (1997) that to predict the influence of critical chloride content on chloride-

induced corrosion, both laboratory and field investigations should also consider the influence of bound chlorides on the corrosion rate of RC structures, especially with the use of SCMs. In this regard, by employing more appropriate methods and techniques, reliable experimental and field results will be obtained, and the wide variation found in literature regarding the chloride threshold value addressed (Angst *et al*., 2009).

2.7.7 Water to binder ratio

The water to binder ratio (w/b) in concrete influences the quality of concrete (Chalhoub *et al.,* 2020). A low w/b results in a refined concrete pore structure, which in turn reduces the ingress of corrosion agents into concrete, whereas a high w/b promotes the availability of corrosion agents in the concrete pore structure. This is because a higher w/b increases the porosity and permeability of concrete, leading to easier movement of chlorides and oxygen availability at the level of the reinforcing steel and, subsequently, a higher corrosion risk (Meira *et al*., 2014).

Moisture diffusion into the concrete is largely influenced by the amount of moisture content in the concrete pore solution (Sakata, 1983). Consequently, adsorption and desorption of moisture content is dependent on the concrete quality, as shown in Figure 2-22 (Ryu *et al*., 2011). Hence, concrete with an improved microstructure (low w/b, i.e., w/b 0.3) exhibits high moisture retainment compared to those with a less improved microstructure (high w/b, i.e., 0.6) (Figure 2-22). Therefore, a low w/b has a lower diffusivity of moisture migrating or escaping from the concrete pore structure. This results in a moist environment around the reinforcing steel, which inhibits oxygen diffusion and subsequently leads to stifled corrosion.

Moradllo *et al*. (2018) studied the influence of convection zone depth on the chloride profiles and service life prediction of concrete structures in a marine tidal zone. In general, the convection zone consist of high chloride concentrations. In their (Moradllo *et al*., 2018) study, two w/b (0.35 and 0.5) and silica fume were used to make concrete specimens. Due to the high porosity and high permeability of the concrete with a w/b of 0.5, the convection zone depth was reduced by 50% in the concrete with a low w/b of 0.35.

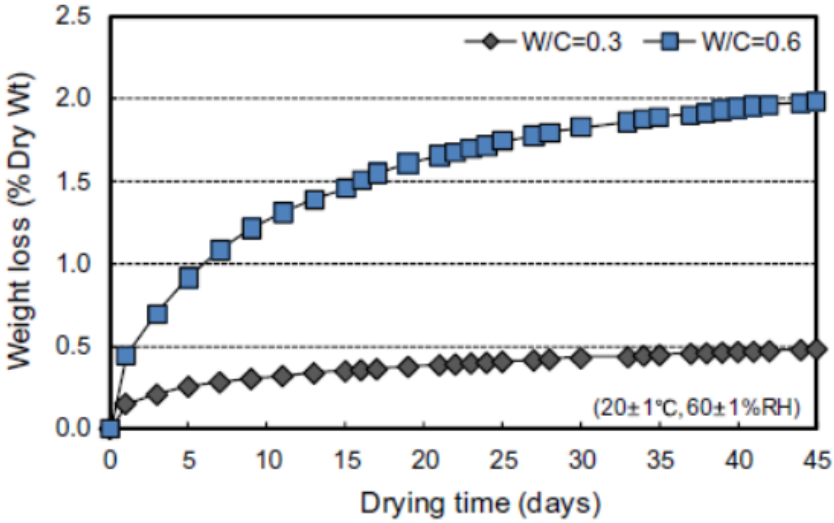

Figure 2-22: Correlation between drying and the amount of moisture evaporation (Ryu *et al*., 2011)

The increased chloride content in the concrete pore structure because of the higher w/b catalyses the onset of corrosion of RC structures and further allows for easier diffusion of oxygen, subsequently increasing the rate of corrosion during the propagation phase (Otieno, 2008; Angst *et al*., 2019). However, it is also important to note the high resistivity of concrete made with SCMs, which becomes the central factor when there is sufficient oxygen and moisture at the level of steel to sustain the corrosion reaction rate (Scott & Alexander, 2007).

Using various binders, Guneyisi *et al*., (2007) investigated the influence of initial curing on chloride ingress and corrosion resistance. The study's findings showed that initial curing influences the chloride penetration into the concrete pore structure, irrespective of the binder type. Chloride ingress and corrosion rate, however, were found to be dependent on w/b and binder type. Similarly, results from van der Wegen *et al*. (2012) corroborate these observations (Figure 2-23). It can be seen from Figure 2-23 that slag concretes exhibited lower diffusion coefficients at different w/b than the other concretes. However, higher values were obtained from the Portland cement concrete.

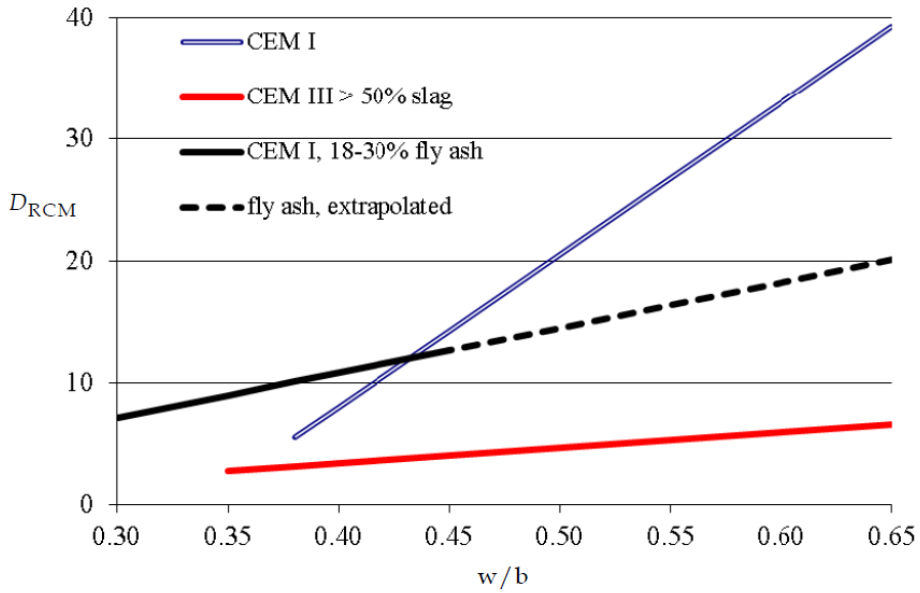

Figure 2-23: Correlation between w/b and chloride diffusion at 28 days (van der Wegen *et al*., 2012)

Also, Chalhoub *et al*. (2020) studied the he chloride threshold values as a function of cement type and steel surface. Low w/b resulted in a higher chloride threshold, while high w/b showed a lower chloride threshold. For the same low w/b, blended cement concretes had higher chloride threshold values. Hence, the rate of corrosion is faster for a high w/b. A similar observation was made by Castro-Borges *et al*. (2013). Table 2-5 presents results obtained from Mangat *et al*. (1994) showing the influence of the w/b on the corrosion rate of specimens exposed to cyclic wetting and drying. The rate of corrosion increases with an increasing w/b.

Table 2-5: Influence of w/b on corrosion rate (Mangat *et al*., 1994; cited by Alexander *et al*., 2012)

w/b	Binder content (kg/m^3)	Corrosion rate $(\mu A/cm^2)$
0.45	430	0.13
0.58	430	0.65
0.58	330	0.62
0.58	530	0.52
0.76	430	2.16

In a nutshell, the literature presented in this section supports the conclusion by Angst *et al*. (2019) that concrete quality (which is affected by w/b and binder type)

influences the transport mechanism of corrosion agents which in turn influences the rate of corrosion of RC structures in the marine environment in concrete, thus its significance in concrete durability assessments as well as service life predictions.

2.7.8 Temperature

Temperature plays a significant role in the process of corrosion, as change in temperature influences the transport mechanism of corrosion agents into the concrete pore solution (Yuan *et al*., 2009). For example, it is generally acknowledged that an increase in temperature is associated with high evaporation of water and thus a reduction in humidity; as a result, the oxygen mobility and absorption of chlorides at the level of the reinforcing steel are increased, resulting in corrosion initiation (Costa & Appleton, 2002; Zivica, 2003; Dousti & Shekcarchi, 2015). Moreover, high temperatures result in de-icing of salts, leading to deep penetration of salt contaminated fluids, which increases the risk of corrosion of RC structures (Yuan *et al*., 2009).

The influence of temperature on the corrosion rate can be determined with the use of the Arrhenius theory, as shown in equation (15) (Scott, 2004).

$$k = A\exp\left(\frac{-Q}{RT}\right) \tag{15}$$

Where: k is the rate constant; A is the frequency factor; Q is the activation energy in (kJ/mol); R is the gas constant 8.31×10^{-3} in (kJ/K/mol); and T denotes temperature in (K).

A non-linear relationship between temperature and bound chlorides was noted by Dousti and Shekcarchi (2015) in a study that examined the effect of temperature on chloride binding capacity using different cementing materials, namely Portland cement (OPC), metakaolin (MK8), natural zeolite (NZ10), and silica fume (SF8), at 8%, 10%, and 8% replacement to PC, respectively. The specimens were exposed to various temperatures (-4, 3, 22, 35, 50 and 70°C). Specimens exposed at -4°C exhibited higher chloride binding capacity than those exposed at 3°C but lower than

the specimens exposed at 22°C (see Figure 2-24). Nonetheless, a notable trend of decrease in chloride binding capacity was observed from 22°C to 70°C.

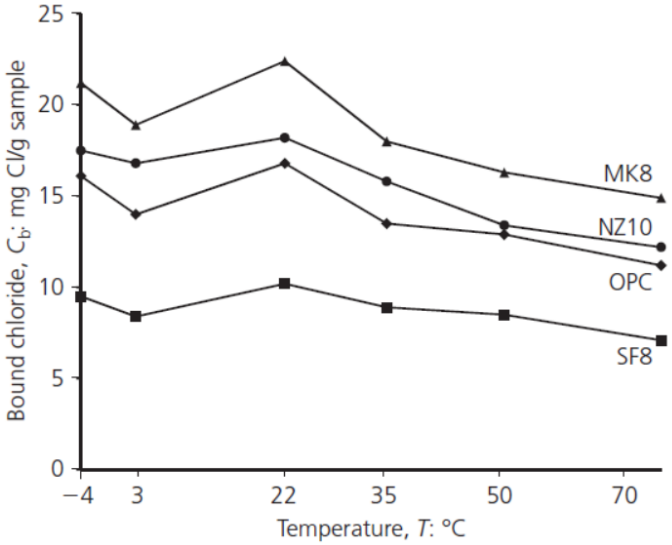

Figure 2-24: Effect of temperature on bound chloride content (Dousti & Shekcarchi, 2015)

Furthermore, high chloride binding capacity at -4 and 22°C resulted in low chloride diffusion coefficients (Figure 2-25). Although Dousti and Shekcarchi (2015) do not discuss the influence of temperature variation on corrosion rate, their findings on the influence of temperature on the chloride binding capacity of the specimens provide a clear understanding that the reduction in chloride binding capacity due to increased temperature leads to high chloride concentrations available to initiate corrosion.

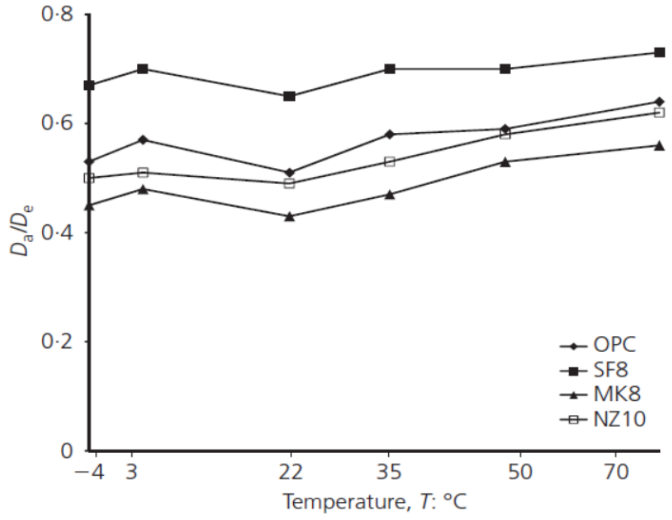

Figure 2-25: Influence of temperature on the ratio of apparent to effective diffusion coefficient (Dousti & Shekcarchi, 2015)

According to a report by Dousti *et al*. (2013), high exposure temperatures (22-50°C) increase the total chloride concentrations due to higher chloride diffusion coefficients and penetration depths. Additionally, the study corroborates the literature that blended cement concrete shows better resistance to chloride than PC concrete. Furthermore, Otsuki *et al*. (2009) reported an increase in oxygen diffusion with increasing temperature, irrespective of the quality of concrete (refer to Figure 2-26).

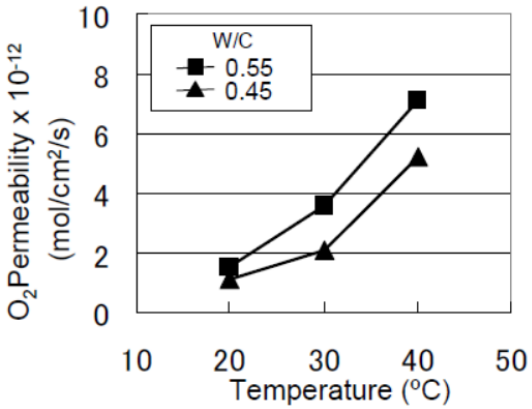

Figure 2-26: Influence of temperature on the oxygen permeability (Otsuki *et al*., 2009)

These studies (Otsuki *et al*., 2009; Dousti *et al*., 2013) further indicate that because of the increased temperature, the rate of corrosion was also increased. On the contrary, Zivica (2003) showed a decrease in dissolved oxygen with an increase in temperature (above 40°C), especially when the w/b was increased, which resulted in a minimal corrosion rate. In addition, a decrease in moisture profiles with increased temperature was noted.

The observation by Zivica (2003) on the corrosion rate and its dependency on the w/b used and varying temperatures further highlights the role of the concrete microstructure in the corrosion rate of the reinforcement steel and its inhibitory influence on the transportation of corrosion agents.

2.8 Techniques for corrosion acceleration in concrete

Conducting laboratory-based corrosion assessments or research studies (for the sake of obtaining a degree) requires a need for faster corrosion initiation. Hence, the use of different corrosion accelerating techniques in the literature. Otieno (2014) describes this process as that which encourages steel corrosion at a rate faster than the corresponding natural corrosion process. Accordingly, accelerated corrosion can be achieved using either one or a combination of the following (Otieno, 2020):

i. Impressed current;
ii. Cyclic wetting and drying;
iii. Use of admixture chlorides, and/or
iv. Accelerated capillary suction.

2.8.1 Impressed current

The impressed current (IC) technique requires the use of an external power supply (either by a potentiostat, a galvanostat or a variable DC power supply) to the embedded steel (anode) and a separate cathode (usually stainless steel) (Otieno, 2020). Additionally, the specimens are immersed in an aqueous solution (NaCl) to create an electric contact between the anode and the cathode (Care & Raharinaivo, 2007; Malumbela *et al*., 2012; Yu *et al*., 2020). This increases the flow of electrons from the anode to the cathode. Hence, the rate of the electrochemical reactions is increased.

When impressed current is used, the ingress of chlorides into concrete is controlled by the migration mechanism, as opposed to natural chloride ingress by diffusion in concrete (Otieno *et al*., 2019). Even though the IC technique has been recommended based on its advantages (Ahmad, 2009; Otieno, 2020), it also has disadvantages. According to Poursaee and Hansson (2009), the method produces considerably different results compared to the natural corrosion of steel from an electrochemical standpoint. This is because of the difference in the chemical composition of the formed corrosion products. Corrosion-induced by IC results in uniform corrosion (the whole steel surface corrodes), whereas natural corrosion leads to pitting (localised) corrosion.

Furthermore, the current applied during the use of the IC varies in order to control the degree of corrosion degradation (El Maaddawy & Soudki, 2003). El Maaddawy and Soudki (2003) further indicate that the current densities applied in laboratory studies found in the literature when using the IC are too high compared to the results obtained from field studies. Thus, they recommend limiting the current density to 200 $\mu A/cm^2$.

2.8.2 Cyclic wetting and drying

The cyclic wetting and drying technique can be achieved in different ways, as each cycle may be conducted using different methods. Accordingly, during the wetting cycle, the following methods have been used in previous research found in literature:

i. Continuous spray or fog with a saline solution (NaCl) solution in an enclosed chamber at a controlled temperature. For example, Vidal *et al*. (2007) continuously sprayed specimens with NaCl solution for 6 years under laboratory conditions before exposing them to drying cycles. The corrosion obtained was quite similar to natural corrosion in terms of distribution, type, and oxides generated.
ii. Full or partial immersion of specimens. For example, Cairns *et al*. (2008) and Liu *et al*. (2014) used 3% and 5% NaCl solutions, respectively.
iii. Ponding the top surface with a saline solution. The technique is commonly used for laboratory studies, and it also resembles the natural corrosion process in terms of chloride distribution (ASTM G109, 2007; Moore, 2019; Otieno *et al*., 2019; Harilal *et al*., 2021).

The drying period, on the other hand, can be achieved through exposure to ambient or elevated temperatures (Otieno, 2020). Subsequently, corrosion initiation or propagation is accelerated due to chloride penetration (through capillary suction) and oxygen availability (Otieno, 2020). Additionally, according to Otieno *et al*. (2019), the drying duration influences the corrosion process of steel. However, the study further stresses the importance of considering the combined influence of drying duration and concrete quality. This is because of the ability to limit oxygen

availability and high resistivity in denser concrete, hence limiting corrosion potential, while the opposite is noted in less dense concrete.

2.8.3 Use of admixture chlorides

The use of the admixture chloride technique, commonly referred to as admixed chlorides, from the experimental point of view, simply describes the mixing of salt (NaCl) with concrete. Different proportions of the salt solution have been used in the literature, ranging from 1% (Mangat & Elgarf, 1999) to 5% (El Maaddawy & Soudki, 2003) by weight of cement. The salt solution is added to immediately cause de-passivation of the reinforcing steel (El Maaddawy & Soudki, 2003).

Nevertheless, Poursaee and Hansson (2009) discouraged this approach. They reported that the technique obstructs the mechanism of natural corrosion. This is because it (as in the case of natural corrosion) does not allow passivation of the reinforcing steel. The study further indicated that the use of chlorides contaminates concrete, which affects the cement hydration process, leading to porous concrete. As a result of the porous pore structure of the concrete, corrosion agents are uniformly distributed around the reinforcement (Malumbela *et al*., 2012). Additionally, mixing chlorides with concrete inhibits chloride binding in concrete (Otieno, 2020).

2.8.4 Accelerated capillary suction

Accelerated capillary suction is a process whereby ingress of chlorides is accelerated to the level of the reinforcing steel through wetting and drying cycles (Allahverdi & Skvara, 2000; Tang *et al*., 2016). Before immersing in a NaCl solution, specimens are allowed to dry to the level of reinforcement under controlled temperature conditions (Otieno, 2020).

The accelerated capillary suction technique results in the fast deposition of chlorides to the level of the reinforcing steel in a short space of time (a few weeks) and subsequently results in immediate corrosion initiation (Garcia *et al*., 2014; Otieno, 2020; Boschmann *et al*., 2021). The technique yields relatively more natural

corrosion results for exposure conditions such as the marine tidal zone (Boschmann *et al*., 2021).

2.8.5 Combined corrosion accelerating techniques

Researchers have successfully explored the application of more than one technique for corrosion acceleration in their experimental set-up. El Maaddawy and Soudki (2003) used the admixed chloride technique in conjunction with the impressed current. Also, Moore (2019) used the admixing chloride technique with cyclic wetting and drying for corrosion initiation before exposing the specimens to a simulated marine tidal zone environment to mimic natural corrosion. Only the anode was contaminated with 5% NaCl, while the cathode side was chloride free. Before opting for a combined use of corrosion accelerating techniques, however, one needs to check the compatibility of the techniques to be combined in relation to specific characteristics of chloride-induced corrosion. The reader is referred to Otieno (2020) for in-depth details regarding the different corrosion accelerating techniques.

In summary, the various corrosion acceleration techniques described in this section (section 2.8) have individual advantages and disadvantages. They all result in faster corrosion initiation. However, some do not correspond to the natural corrosion process of RC structures. Hence, an understanding of one's investigative aim and desired outcomes is crucial to identify before the application of the above techniques (Otieno, 2020). Accordingly, for this study, cyclic wetting and drying was adopted to achieve localised corrosion of the reinforcement, thus resembling the natural corrosion in the marine tidal zone.

2.9 Techniques for corrosion assessment in concrete

Corrosion assessment techniques may either indicate the probability of corrosion (half-cell potential, Wenner probe, cover depth measurement) or demonstrate the extent of corrosion (linear polarisation resistance, macrocell) (Otieno, 2008). The former, on the one hand, aids in determining the risk and nature of corrosion, as well as the corrosion rate measurement method to be used. The techniques that show the extent of the corrosion, on the other hand, aid in identifying the cause and

estimating the extent of corrosion damage. Accordingly, the aforementioned techniques are reviewed in the section that follows.

2.9.1 Half-cell potential measurements

This is an electrochemical method (also known as open circuit or corrosion potential) for calculating the likelihood of steel reinforcement corrosion in concrete (Alexander *et al*., 2012; Rodrigues *et al*., 2021). The method is based on a two-electrode configuration (reinforcement embedded in concrete and a reference electrode connected to a voltmeter, which also has an external attachment to the reinforcement) (Alexander *et al*., 2012) (see Figure 2-27).

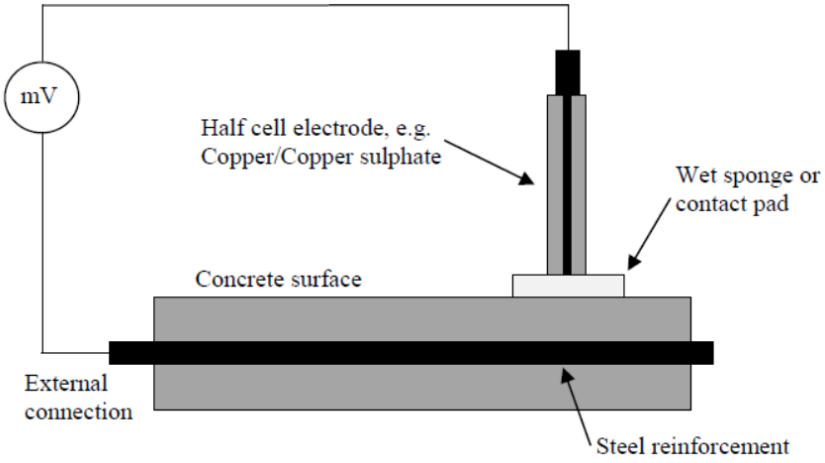

Figure 2-27: Schematic half-cell potential measurement (Alexander *et al*., 2012)

The voltmeter measures the potential difference between the two-electrodes (Rodrigues *et al*., 2021). The reference electrode is either saturated copper/copper sulphate, silver/silver chloride or calomel (the reference electrode, in other words, is a piece of metal immersed in a solution of its own ions) (Alonso *et al*., 2002; Otieno, 2008). The potential difference measured is influenced by the type of reference electrode used as well as the reinforcement conditions (Otieno, 2008).

Moreover, due to the configuration of the half-cell, where anodic and cathodic regions are clearly defined, this technique has been recommended for use in chloride-induced corrosion of reinforcement assessments to detect the risk of

corrosion of steel. Table 2-6 shows the guidelines for interpreting reinforcement potentials measured.

Table 2-6: Guidelines for interpretation of half-cell potentials (Alexander *et al*., 2012)

Reference electrode		Corrosion risk
Copper/Copper Sulphate (mV)	**Silver/Silver Chloride (mV)**	**Likely corrosion condition**
> −200	> −106	Low (10% corrosion risk)
−200 to −350	−106 to −206	Intermediate corrosion risk
< −350	< −206	High (> 90% corrosion risk)
< −500	< −406	Severe corrosion

2.9.2 Resistivity measurements

Concrete resistivity can be measured using different techniques, namely one external electrode, two point uniaxial, and four-point (Wenner) probe techniques (Madhavi & Annamalai, 2016; Rodrigues *et al*., 2021). Nevertheless, the four-point (Wenner) probe technique is commonly used for concrete resistivity measures and will be briefly reviewed herein. The technique uses a small alternating current that is passed between the 2 outermost contacts, thus the resulting potential difference between contacts is measured between the inner 2 probes, as shown in Figure 2-28 (Alexander *et al*., 2012).

The Wenner probe method is fast and simple, and it measures a larger surface area. The Wenner probe technique measurements are sensitive to the surface condition of the concrete, as well as the presence of moisture and voids (Azarsa & Gupta, 2017). Hence, multiple measurements around the concrete specimen are required to obtain a reliable average of the inherent resistivity of concrete (Azarsa & Gupta, 2017). In addition, the measured resistivity is influenced by many factors, such as the aggregate size, probe spacing, specimen size, cover depth, etc. (Morris *et al*., 1996; Presuel-Moreno *et al*., 2013; Ghosh & Tran, 2015).

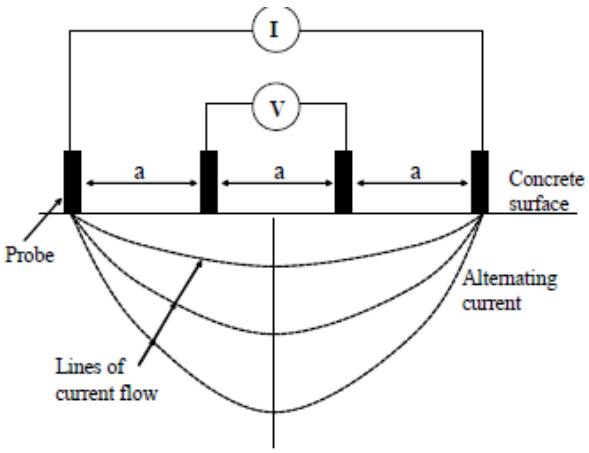

Figure 2-28: Wenner probe measurement principle - Concrete resistivity (Alexander *et al*., 2012)

Electrical resistivity is calculated by dividing the ratio of the applied voltage (V) to the current that results (I), which is carried by ions dissolved in the concrete pore structure, multiplied by a geometric factor which is dependent on the size and shape of the specimen (Azarsa & Gupta, 2017). Therefore, the resistivity of concrete can then be expressed as follows (Otieno, 2008):

$$\rho = \frac{2\pi a V}{I} \tag{16}$$

Where: ρ is the apparent resistivity in (Ω.cm); a denotes the electrode spacing in (cm); V is the measured potential in (volts); I is the applied current (amperes).

2.9.3 Linear Polarisation Resistance

The Linear Polarisation Resistance (LPR) technique (also referred to as the polarisation resistance method) can be used to monitor the corrosion rate during the propagation phase since it gives quantitative information on the rate of corrosion (Rodrigues *et al*., 2021). The LPR can be obtained either by applying a small external potential (ΔE) and measuring the resulting current (ΔI) (potentiostatic approach) or by applying a small current and measuring the resulting potential (galvanostatic approach) (Luping, 2002). The results obtained can then be converted to corrosion current densities with the application of the Stern and Geary (1957) equation.

$$I_{corr} = \frac{B}{R_p} \quad (17)$$

Where: I_{corr} is the corrosion current in ($\mu A/cm^2$); B is the Stern-Geary constant in (mV); R_p denotes the change in potential (ΔE)/change in current (ΔI).

The LPR is considered one of the popular techniques for corrosion rate measurements. However, this technique has been found to yield inaccurate results in localised reinforcement corrosion and that the error could be high by a factor of 10 (Elsener, 2002). Nevertheless, Chen and Su (2021) reported that the inaccuracy of the results may be due to different testing methods, concrete resistivity, etc. Table 2-7 shows guidelines for assessing the rate of corrosion of reinforced concrete structures.

Table 2-7: Guidelines for assessment of corrosion rates (Andrade *et al.*, 2004)

Corrosion rate ($\mu A/cm^2$)	Degree of corrosion
> 1	High
$0.5 - 1$	Moderate
$0.1 – 0.5$	Low
≤ 0.1	Negligible

2.9.4 Macrocell corrosion method

In a chloride exposure environment, localised corrosion of reinforcement is often found. Therefore, the macrocell corrosion mechanism will not be reviewed here again. The macrocell corrosion method can be used to monitor the corrosion rate. However, since the macrocell corrosion technique does not account for localised corrosion, it has been reported (Moore, 2019) that the corrosion rates might be underestimated. Nonetheless, this approach was adopted in ASTM G109 and has been widely used in laboratory corrosion assessments (Harilal *et al.*, 2021).

In this technique, the anode (reinforcing steel) is electrically connected to the cathode (stainless steel) by means of a resistor and the potential measuring

instrument is placed across the resistor for potential difference measurements. Consequently, the resulting corrosion current is calculated. A ponding feature (usually at the top surface) is filled with NaCl solution. Accordingly, Figure 2-29 demonstrates a typical macrocell.

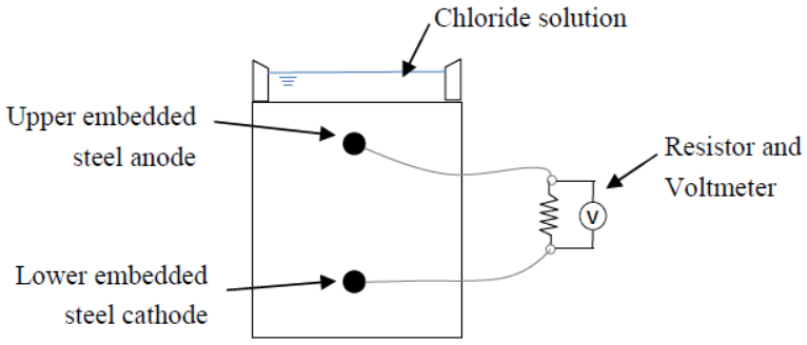

Figure 2-29: Schematic of a macrocell (after Moore, 2019; ASTM G109)

2.10 Review of exposure classification in EN 206-1-1 and SANS 10100-2

Guidelines to safeguard the design of reinforced concrete structures exposed to aggressive environments for them to reach their service life are paramount. Modernised countries have since developed their own standards based on the conditions to which a particular structure is exposed. In South Africa, the Euro code (EN 206-1-1, 2013) has been adopted in SANS 10100-2 (2013) and modified to suit South African conditions (Ballim *et al*., 2009). A review of the exposure classification and the durability requirements for the EN 206-1 and SANS 10100-2 codes is presented hereunder.

2.10.1 The European standard (EN 206-1-1: 2013)

The European standard (EN 206-1-1, 2013) is a standard specification for concrete-related applications that includes the requirements of concrete exposure classification, concrete conformity control, concrete design criteria, concrete production control, etc. The standard provides categories for exposure classification based on the deterioration mechanism by which a structure is induced. Accordingly, in the EN 206 standard, structures prone to chloride-induced damage are categorised by the symbol XS and, due to different exposure conditions within the marine environment, they are further divided into 3 sub-classes, namely: XS1 (RC

structures exposed to atmospheric conditions), XS2 (RC structures permanently submerged in sea water), and XS3 (RC structures exposed to tidal and splash and spray conditions) (Table 2-8).

Furthermore, it can be seen from Table 2-8 that the Euro code is based on a prescriptive approach. The prescriptive approach stipulates requirements such as the w/b, minimum strength grade, and minimum cement content for each exposure condition (Beushausen *et al*., 2019). However, the standard does acknowledge the better durability performance of supplementary cementitious materials in concrete and recommends their use, but at the designer's discretion (EN 206-1-1, 2013).

Table 2-8: Corrosion-induced by chlorides from sea water in RC structures (EN 206-1-1, 2013)

Class designation	**Description of the environment**	**Informative examples where exposure classes may occur**	**Maximum w/c ratio**	**Minimum strength grade**	**Minimum cement content** (kg/m^3)
XS1	Exposed to airborne salt but not in direct contact with seawater	Structures near to or on the coast	0.5	C30/37	300
XS2	Permanently submerged	Parts of marine structures	0.45	C35/45	320
XS3	Tidal, splash and spray zones	Parts of marine structures	0.45	C35/45	340

2.10.2 South African Standard (SANS 10100-2: 2013)

The South African National Standard (SANS 10100-2:2013) specification covers the requirements for structural concrete works. The exposure classification in SANS 10100-2 (2013) was adopted from EN 206-1-1 (2013). Accordingly, depending on the exposure environment, the conditions are categorised as moderate, severe, very severe, and extreme, as shown in Table 2-9.

Table 2-9: Durability requirements in SANS 10100-2: 2013

Conditions of exposure	Description of member/surface to which the cover applies	Minimum concrete class, MPa				
		20	25	30	40	50
		Minimum cover, mm				
Moderate	1. Buried in non-aggressive soils	50	40	45	35	25
	2. Enclosed surfaces					
	3. Continuously under fresh water					
Severe	1. All exposed surfaces	NA	50	45	40	35
	2. Surfaces on which condensation takes place					
	3. Surfaces in contact with soil					
	4. Surfaces permanently under running water					
	1. Cast in-situ piles	50	50	50	50	50
	i. Wet cast against casing	75	75	75	75	75
	ii. Wet cast against soil	75	75	75	75	75
	iii. Dry cast against soil					
Very severe	1. All exposed surfaces of structures within 30 km from the sea	NA	NA	NA	60	50
	2. Surfaces in rivers polluted by industries	NA	NA	NA	60	50
	3. Cast in situ piles, wet against casings	NA	NA	NA	80	80
Extreme	1. Surfaces in contact with sea water of industrially polluted water	NA	NA	NA	65	65
	2. Surfaces in contact with sea water of industrially polluted water					

The standard (SANS 10100-2, 2013) limits the amount of cement content to not exceed 550 Kg/m^3 under any marine exposure condition. Restrictions on the maximum w/b to be used are only made for concrete structures exposed to freeze/thaw attack and for concrete requiring low permeability. Furthermore, it does not consider the performance of the type of SCMs. Moreover, the minimum cover to reinforcement reduces with increasing strength grade, which is contrary to the durability requirements as concrete strength is not considered a durability indicator but rather a basic property of the concrete (Ballim & Alexander, 2018). The durability of a concrete structure is defined by its materialistic performance when exposed to aggressive environments (Ballim & Alexander, 2018).

2.10.3 Critiques on the current approach

Attempts have been made to provide performance-based requirements, such as SANRAL's adoption of Durability Index (DI) tests for oxygen permeability, water sorptivity, and chloride conductivity in 2008 to enhance national infrastructure (Nganga *et al.*, 2017). However, the current South African standard (SANS 10100-2, 2013), as adopted from the European standards (EN 206-1, 2013), is based on a prescriptive approach (Ballim *et al*., 2009; Moore, 2019).

The prescriptive approach considers the concrete mix design parameters such as water to binder ratio, compressive strength, and binder content as the determining factors of the service life of a RC structure in harsh environments. This approach has been criticised by many researchers from the reviewed literature (Kessy *et al*., 2015; Beushausen *et al*., 2019; Alexander & Beushausen, 2019) because it does not take into account material performance, which relates to the durability of concrete. Hence, advocating for the refinement of these standards to performance-based or a combination of both the performance-based and the current prescriptive approach.

Also, Moore (2019) challenges the exposure classification used in the aforementioned standards, arguing that the standards are rather arbitrary. This was after the study found a notable difference in corrosion severity between the marine tidal zone and the splash and spray zones, which are classified in the same category

as the most severe exposure conditions in SANS 10100-2 (2013). The results from the field observations presented by Moore (2019) showed that the RC structures in the tidal zone had little or no corrosion evidence. Furthermore, SANS 10100-2 restricts the designer's innovation as it prescribes minimum requirements depending on the exposure category without considering the wide scatter in durability performance of materials used in concrete, the function, and the location of the structure (Alexander & Beushausen, 2019; Moore, 2019).

Furthermore, a British standard (BS 8500-1: 2006) classifies the part of the RC structure below the mid-tide mark in the same category as the submerged zone (XS2 according to EN 206). This is because the mid-tide mark remains partially dry due to the short wetting and drying cycles in the marine tidal zone, leading to low oxygen level and thus low corrosion risk (McCarter *et al*., 2008). Moreover, other studies (Scott, 2004; Golden, 2015; Otieno *et al*., 2016; Moore, 2019) also found that due to the short wetting and drying cycles in the marine tidal zone, provided sufficient cover or a denser concrete (such as blended cement concrete) is used, negligible corrosion can be observed due to limited access to oxygen and high moisture conditions around the reinforcing steel.

Therefore, to diversify the designer's options when designing RC structures in the marine environment, the standards should highlight the areas with high and low risk, and accordingly expand the existing classification criteria to suit such conditions (Moore, 2019). This will help the designer make design assumptions that will benefit other design implications, such as cost, because the higher the durability requirements, the higher the construction and rehabilitation costs.

2.11 Closure

This chapter reviewed the fundamentals of corrosion of reinforcing steel in concrete. The study mainly focused on chloride-induced corrosion of structures. The transport mechanisms of corrosion agents under different exposure conditions were also reviewed to understand how corrosion agents are transported into the concrete pore structure. Furthermore, this chapter addressed the parameters that influence the

corrosion of RC structures and techniques used for measuring the rate of steel corrosion.

The reviewed studies have shown that reinforced concrete structures in the marine environment are most likely to experience early deterioration problems. This is due to the influence of high chloride concentrations in the marine environment, which makes the reinforcement vulnerable to chloride-induced corrosion. Furthermore, the rate of corrosion of reinforced concrete in the marine environment is mostly dependent on various aspects, such as oxygen, moisture, exposure zone, etc. Therefore, the penetrability of concrete becomes crucial when designing concrete mixes for structures that are exposed to this environment.

The available literature confirms that the influence of SCMs on the properties of reinforced concrete (such as passivation, concrete alkalinity, concrete resistivity, etc.) under different exposure conditions varies. However, a wide range of studies in the literature agree that blended cement concretes result in a more refined concrete pore structure and high resistivity. Thus, the rate of corrosion is reduced. The reviewed studies also show that the exposure classes of the marine environment do not truly represent the actual severity of chloride-induced corrosion damage and, hence, the tidal zone and splash and spray zone fall under the same exposure class.

The studies found and reviewed herein, even though they use acceptable techniques for investigating the corrosion impact on RC structures, do not simulate the exact natural conditions in the marine tidal zone, except Moore (2019). Hence, a correlation between the results from the laboratory-based experiments and field investigations in the marine tidal zone is difficult to find. Also, even though Moore (2019) provided insightful conclusions on the corrosion rate of RC structures in a marine tidal zone, the study focused on the use of PC in concrete, which, as per the reviewed studies, is not recommended for use in marine-exposed RC structures. Therefore, this highlights a need for research that closely simulates the natural conditions in the marine tidal zone when blended cement concrete is used. Subsequently, in this study, a better understanding of the corrosion rate of RC

structures made with blended cement concrete, based on a simulated marine tidal zone laboratory experiment, will be gained.

Furthermore, as indicated in the reviewed literature, the current standards used when designing RC structures in the marine environment must adopt a performance-based approach instead of the prescriptive approach (which is based on limits such as w/b, cover depth, and compressive strength).Therefore, in this study, the possibility of employing relatively higher w/b and lower cover depths when using blended cement concretes for RC structures in the marine tidal zone will be established. The following chapter details the experimental programme and methods used in this study.

3 EXPERIMENTAL PROGRAMME

3.1 Introduction

This chapter details the experimental programme for this study. The experiments were conducted at the Concrete Laboratories of the University of the Witwatersrand, Johannesburg. The purpose of the experimental programme was to investigate the influence of blended cements on the rate of corrosion of RC structures in a marine tidal zone. Therefore, the influence of cover depth variation, oxygen availability, and resistivity on the corrosion rate of RC structures made with blended cement was investigated. An overview of the variables, materials, specimen details, and the experiments/tests that were conducted to achieve the objectives are presented in this chapter.

3.1.1 Variables

To achieve the objectives of this study, the corrosion rate of specimens was evaluated based on the following variables: different binder types, cover depths, and water-binder ratios to investigate their influence on corrosion initiation and propagation as detailed in sections 3.2.1, 3.2.2, and 3.2.3. The exposure zone, aggregate type, and water content were kept constant throughout the experimental programme.

3.2 Materials

The concrete mixes were produced using the following binders: (i) CEM I 52.5N, also known as Portland cement (PC); (ii) Fly ash (FA), and (iii) Ground granulated blast-furnace slag (GGBS). To improve the bond between the concrete and the reinforcing steel, stone (andesite) with a particle size of 13.2 mm was used as a coarse aggregate instead of the normally used 19 mm stone. Crusher sand was used as fine aggregate owing to its improved durability properties compared to natural sand (Menadi *et al*., 2009; Benyamina *et al*., 2019). Also, potable water was used, with the water content kept constant at 190 l/m^3 to produce concrete mixtures with the same water demand and limit the influence of variation in binder content.

To ensure workability of the concrete (between 75- and 150-mm slump, taking into account the relatively wet concrete produced when using FA) was achieved, a polycarboxylate super-plasticiser (Alphaflow 500, Oscrete product) was used. Workability of the concrete refers to the ease with which the concrete can be mixed, placed, compacted, and finished without the loss of homogeneity (Kellerman & Croswell, 2009).

3.2.1 Binder type

Three commonly used binders were considered for this study, namely CEM I 52.5N, FA, and GGBS. The choice of the replacement level was based on the recommendation from the South African National Standard (SANS 50197-1:2013) and the reviewed literature (Samad & Shah, 2017; Vollpracht *et al*., 2018) (see details below):

- CEM I 52.5N, also known as Portland Cement (PC). The sample was procured from PPC Cement factory in Lower Germiston Road, Johannesburg, South Africa.
- Fly ash (FA) was procured from Ulula Ash, a factory in Roodepoort, Johannesburg, South Africa. The FA was proportioned at 30% replacement for the PC by weight as per the recommendations from SANS 50197-1(2013).
- Ground Granulated Blast-furnace Slag (GGBS) was supplied by Slagment, a slag manufacturer for Afrisam, from their factory in Vanderbijlpark, South Africa. The GGBS was used as a 50% replacement for the PC by weight and it is the preferred replacement for the PC (SANS 50197-1, 2013; Samad & Shah, 2017; Vollpracht *et al*., 2018).

3.2.2 Cover depth

Standards such as SANS 10100-2 (2013) and EN 206 (2013) recommend a minimum of 40 mm for structures exposed to the marine environment. Hence, for this study, cover depths of 20 mm and 40 mm were used to investigate the influence of variation in cover depth on the transportation of corrosion agents when using the blended cement concrete in a marine tidal zone. The lower cover depth (20 mm) was adopted to assess the influence of blended cement concretes in limiting the

ingress of oxygen and chlorides to the level of the reinforcing steel bars at a relatively lower cover depth than the recommended minimum cover depth (40 mm). This was done to evaluate the possibility of adjusting the minimum cover depth to 30 mm (Moore, 2019) in SANS 10100-2.

3.2.3 Water-binder ratio

This study used water-binder ratios (w/b) of 0.45 and 0.65. W/b affects the permeability of the concrete microstructure, where higher w/b may result in high permeable concretes, hence the high rate of ingress of corrosion agents. EN 206 (2013) and SANS 10100-2 (2013) specify a maximum w/b of 0.45 to be used for structures in the marine tidal zone.

The high w/b (0.65) was used to produce permeable concrete, allowing the ease of penetrability for chlorides, oxygen, moisture, etc. Therefore, the choice of w/b (0.45 and 0.65) was employed to understand the influence of blended cements on the corrosion rate at varying concrete microstructure and concrete quality.

3.3 Mix design

Concrete mix design was done as per the Cement and Concrete Institute (C&CI) volumetric mix design method (Addis & Goodman, 2009). The concrete mix design was aimed at achieving at least 30 MPa compressive strength after 28 days of curing, taking into account the slower hydration of blended cement concretes. Due to the selection of 3 different binders and 2 w/b, 6 different mixes were required (see Table 3-1).

Table 3-1: Summary of concrete mix proportions

Material (kg/m^3)	PC-45	PC-65	FA-45	FA-65	SL-45	SL-65
	100%PC		70%PC/30%FA		50%PC/50%GGBS	
	0.45	0.65	0.45	0.65	0.45	0.65
CEM I 52.5N	425	295	297.5	206.5	212.5	147.5
Fly ash	-	-	127.5	88.5	-	-
Slag	-	-	-	-	212.5	147.5
Fine aggregate	835	940	790	910	820	930
Coarse aggregate	924	924	929	929	924	924
Water	190	190	190	190	190	190
Super-plasticiser (% by weight of binder)	0.22	-	0.15	-	0.22	-
Slump measured (mm)	80	90	85	125	90	90

3.4 Details on the number and the manufacturing of specimens

3.4.1 Compressive and durability test specimen details

A total of 84 cubes (100 mm × 100 mm × 100 mm) were cast for compressive strength and durability tests. For each mix, 14 cubes were cast (6 for compressive strength test and 8 for durability index tests). For further details regarding the tests, see sections 3.8.1 and 3.8.2, respectively.

3.4.2 Corrosion specimen details

A total of 12 corrosion specimens (100 mm × 100 mm × 200 mm) were cast. For each mix, 2 corrosion specimens were cast. The corrosion specimens consisted of a 10 mm diameter high yield reinforcing steel bar, which was embedded in the

concrete to act as a working electrode (anode). Also, two 10 mm diameter stainless steel bars (316 grade) were embedded in the concrete, acting as a counter electrode (cathode) (see Figure 3-1). The reason for the use of 2 cathode steel reinforcing bars and 1 anode steel bar was to ensure that the cathode does not limit the oxygen reduction rate (Moore, 2019). The corrosion specimen (corrosion cell) is depicted schematically in Figure 3-1.

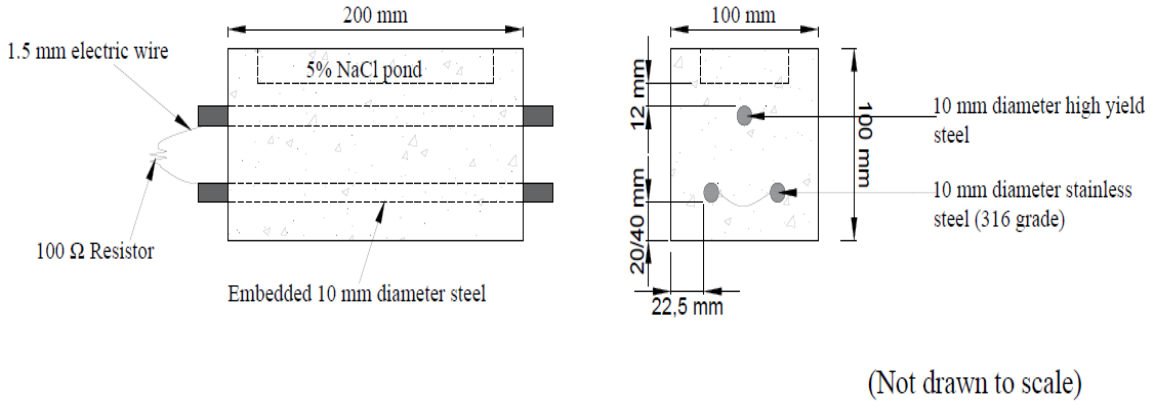

Figure 3-1: Schematic representation of the corrosion cell (modified after ASTM G109, 2007)

The specimens were made of chloride-free concrete to allow for localised corrosion, thus a true representation of the natural corrosion of RC structures. A ponding feature, hereafter referred to as the NaCl pond, was incorporated on top of the corrosion specimen to continuously supply chlorides to the working electrode throughout the exposure period (see Figure 3-2).

The NaCl pond was made by inserting and nailing a plyboard (18 mm × 60 mm × 160 mm) centred into the top side of the mould. To avoid damaging the NaCl pond, caution was required when de-moulding the specimens. Moreover, due to the design of the moulds used, the electrical wire connection between the anodic and cathodic steels and coating of the reinforcing steel bars was done after curing. The design of the corrosion specimens was adopted from ASTM G109 (2007) and Moore (2019).

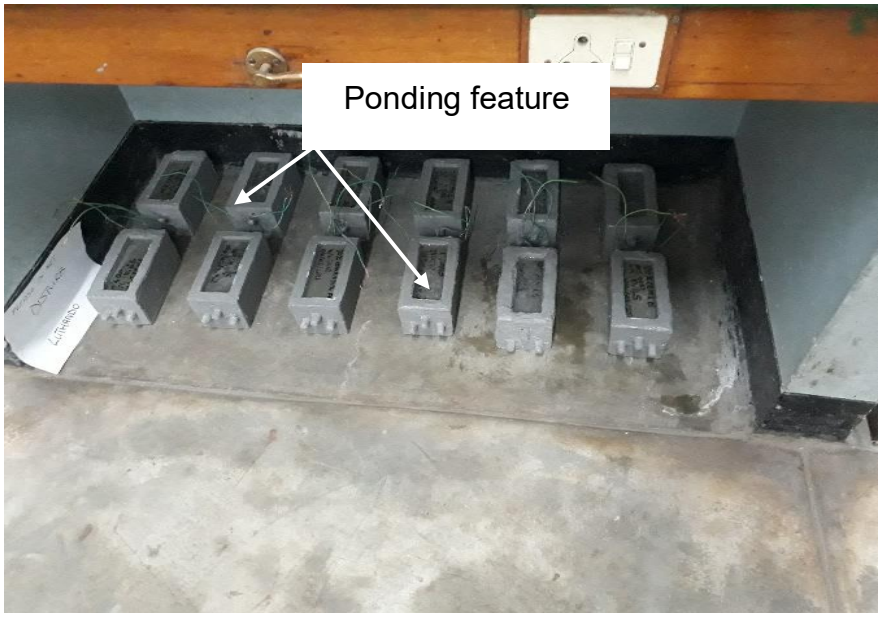

Figure 3-2: A photograph showing the NaCl ponding feature

3.4.3 Steel preparation for corrosion cells

Before casting of specimens, both the anode and cathode reinforcing steels bars were cut to 240 mm length (see Figure 3-3), grooved to a depth of 2 mm on the one end for electrical wire connection and wire brushed. The connection between the anode and the cathode was tested using a Multimeter to ensure a proper connection was achieved. Following that, the reinforcing steels (anode and cathode) were sealed with insulating tape and thereafter epoxy-coated for 20 mm on both ends. This was done to ensure that only 200 mm length of the steel surface was exposed. The details of the steel preparation and electrical wire connection are shown in Figure 3-3.

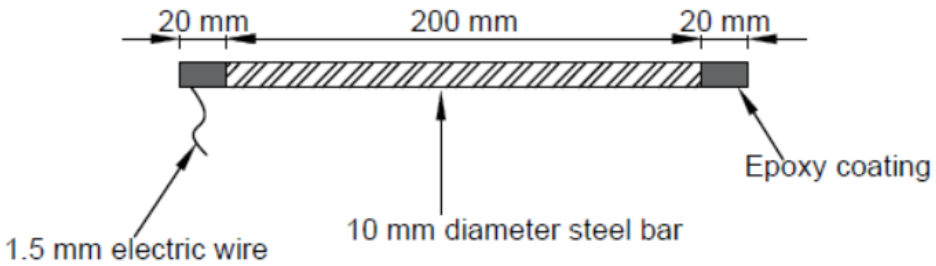

Figure 3-3: Steel configuration

3.4.4 Casting

Batching of material (by mass) was done using a calibrated scale. After batching, aggregates (sand and stone) and binder were fed into the pan mixer and properly mixed, and thereafter, water was slowly added (while the machine was running) until the required workability was achieved. For concrete mixes with very low workability, a percentage of super-plasticiser by weight of binder (see Table 3-1) was slowly added until the desired workability was achieved. The corrosion cells were cast upside down due to the incorporation of the NaCl pond. After casting, all specimens (corrosion cells and cubes) were covered with a polyethylene sheet and allowed to set for 24 hours in the laboratory, under room temperature (Figure 3-4). Thereafter, the specimens were de-moulded and placed in the curing bath (see section 3.5 for further details).

(a) (b)

Figure 3-4: Photograph showing (a) the direction of casting of corrosion specimens and (b) polyethylene covering

3.5 Curing

When the specimens were de-moulded after setting (in the order of casting), they were immediately placed in a water curing bath (Figure 3-5). The temperature of the curing bath was maintained at 23 ℃ ± 2 ℃ for all mixes. All the corrosion specimens

were removed from the curing tank after 28 days for further preparations before they were placed in their exposure environment (see section 3.6). The cubes were removed after 28 and 90 days for compressive strength and durability tests.

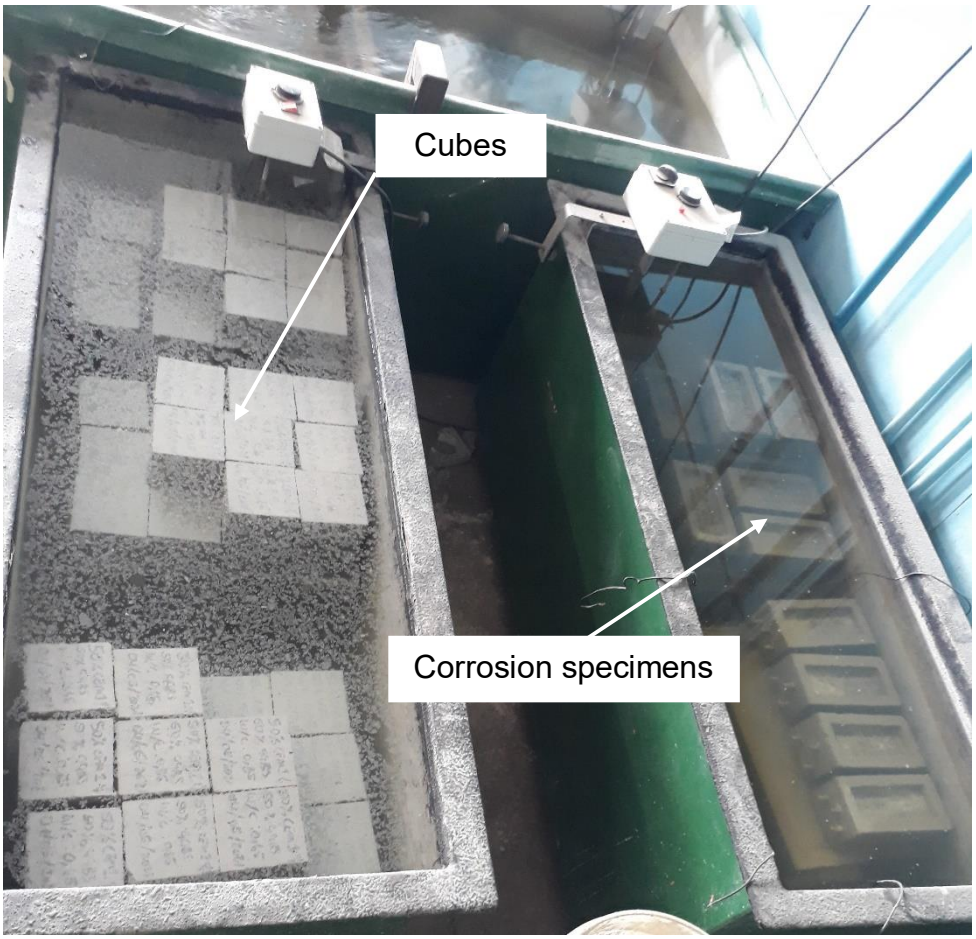

Figure 3-5: Photograph of specimens in curing baths

3.6 Corrosion activation

The procedure (wetting and drying) outlined in ASTM G109 (2007) was adopted in this study for the initiation of corrosion of the reinforcing steel. However, as mentioned in section 3.4.2, only chloride-free concrete was used when casting corrosion cells to allow for localised corrosion – thus a true representation of the natural corrosion of RC structures. Therefore, after curing, the specimens were left to dry for a period of 1 week and were thereafter epoxy-coated on all sides (including the edges of the ponding feature) except the top and bottom sides of the corrosion specimen. The epoxy on the specimens was allowed to set for 24 hours before the corrosion activation period commenced.

To accelerate the corrosion activation process, the specimens were exposed to 3 days of wetting and 4 days of air-drying, respectively (ASTM G109, 2007). The duration of the drying cycle was made longer to allow for more oxygen diffusion in dense concrete specimens. During the wetting cycle, the NaCl pond was filled with a 5% NaCl solution, which was prepared using potable water. During the drying cycle, chloride penetration is accelerated through capillary suction, subsequently catalysing the corrosion initiation. Also, during the drying cycle, some chloride ions that were stuck in the concrete pores were further absorbed to the level of the reinforcing steel during the wetting cycle.

The wetting and drying cycles result in diffusion and sorption of chlorides and allow for de-passivation of the anode steel, leading to active corrosion (Chang *et al*., 2019). Due to the time constraints of this study, the corrosion activation process was carried out for a period of 3 weeks before the specimens were exposed to the simulated marine tidal environment. One of the specimens (FA for w/b of 0.65) showed signs of corrosion having been initiated before the last cycle of wetting and drying (after 2 weeks) (Figure 3-6).

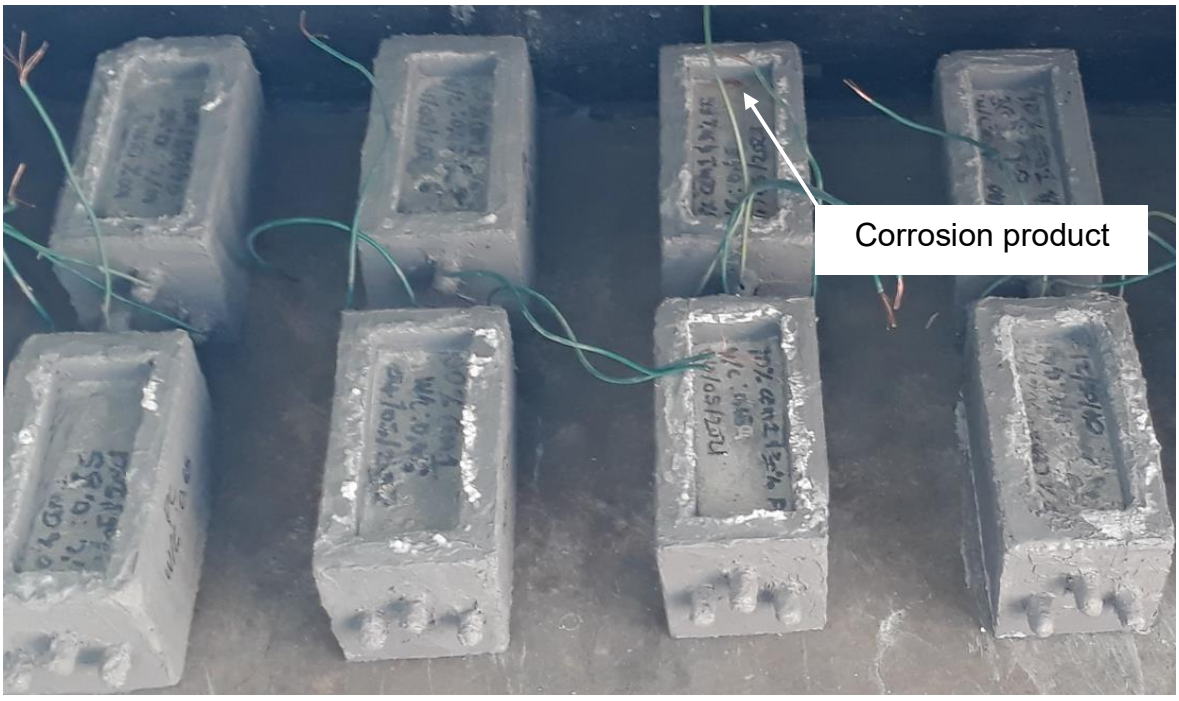

Figure 3-6: A photograph showing signs of active corrosion

3.7 Exposure zone set-up

After the corrosion activation period, specimens were immediately placed in their exposure zone (see Figure 3-8). Thereafter, 100 Ω Resistors were connected to each specimen to create an electrical connection between the anodic and cathodic steel. In order to simulate the marine tidal zone, the corrosion cells were subjected to wetting and drying cycles. A 12-hour cycle comprising of 6 hours wetting (high tide) and 6 hours air-drying (low tide) was adopted.

The wetting and drying cycles were achieved through the use of 2 pumps with timers, which transferred the 5% NaCl solution from the reservoir into the containers holding the corrosion cells and back as shown in Figure 3-7 and Figure 3-8. The first pump was programmed to turn on every 12 hours to transfer the NaCl solution to the containers holding the corrosion cells (wetting cycle). The second pump was set to switch on 6 hours after the first pump, allowing the transfer of the NaCl solution back to the reservoir and subsequently lowering the tide (drying cycle).

Adjustable irrigation valves were used to control the rate at which the tide rises or falls (see Figure 3-8). The use of adjustable valves was employed to ensure that it took 10 minutes to transfer the NaCl solution from the reservoir to the container holding the corrosion specimens and vice versa. Moreover, an orifice was made in the tubing to prohibit water from draining back from the containers to the reservoir during the wetting cycle and vice versa during the drying cycle (see Figure 3-8). Due to the time constraints of the study, the corrosion specimens were exposed to the wetting and drying cycles for a period of 3 months.

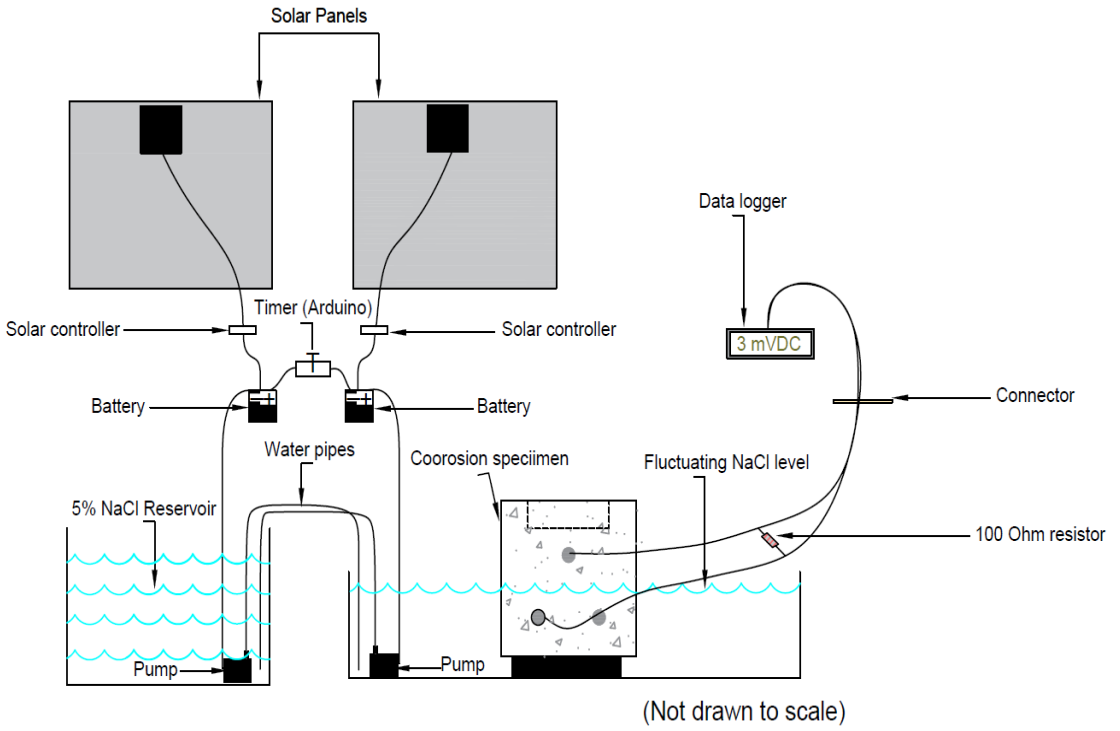

Figure 3-7: Diagram showing the experimental set-up

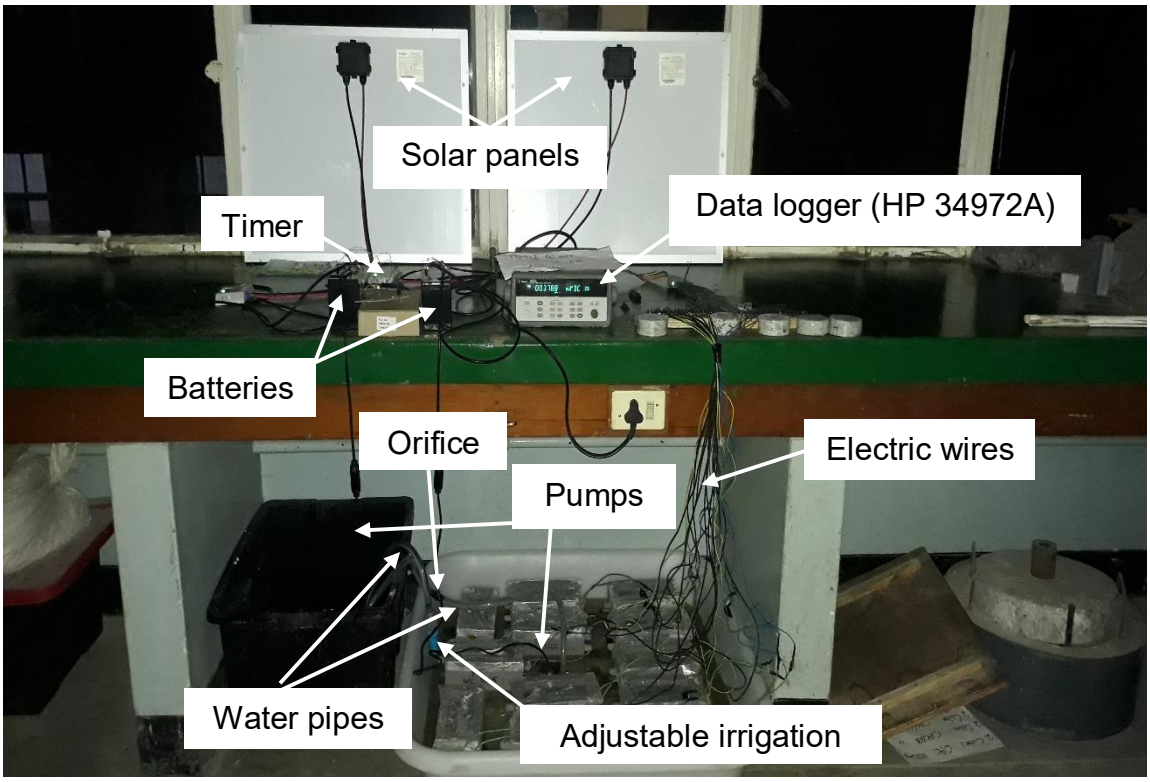

Figure 3-8: Photograph showing the experimental set-up

3.8 Testing

3.8.1 Compressive strength

A total of 6 cubes (100 mm) were cast for each mix for compressive strength testing at 28 and 90 days. Since blended cements have a slow hydration reaction, the 90th day of testing was also included. The tests were conducted in accordance with SANS 5863 (2006) procedure. This was done using a manually operated AMSLER compression testing machine, at a loading of 0.3 MPa/sec until the specimen fails. SANS 5863 (2006), specifies a continuous loading rate of 0.3 MPa/sec ± 1 MPa/sec. Subsequently, the compressive strength of each specimen was calculated. Details of the compressive strength results are presented in Appendix A. An example of the definition of failure of the concrete specimens after compression is shown in Figure 3-9.

Figure 3-9: Photograph showing the positioning of concrete specimens on the AMSLER machine and their definition of failure after compression

3.8.2 Durability index testing

Durability index tests were conducted to characterise the concrete cover based on the transport mechanisms related to durability of the concrete. Accordingly, 8 cubes

(100 mm × 100 mm × 100 mm) were cast per mix. From the 8 cubes, 4 cubes were used for Oxygen Permeability Index (OPI) and Water Sorptivity Index (WSI), and the remaining 4 cubes were used for Chloride Conductivity Index (CCI) testing. Concrete discs of 70 × 30 mm were cored and sliced from concrete cubes (see Figure 3-10) after 28 and 90 days of casting (SANS 3001-CO3-1, 2015) and the following durability indicators were determined:

- Oxygen Permeability Index (SANS 3001-CO3-2) – Test for permeation
- Water Sorptivity Index (Alexander, 2018) – Test for water absorption
- Chloride Conductivity Index (CCI) (SANS 3001-CO3-3) – Test for chloride ion diffusion

(a) (b)

Figure 3-10: Photograph showing (a) drilling of cores and (b) specimens after slicing

3.8.2.1 Oxygen Permeability Index (OPI)

The Oxygen Permeability Index (OPI) is used to get a general evaluation of the concrete microstructure and macrostructure (Alexander, 2018). This method is most sensitive to some conditions (macro-voids and cracks) that may allow excessive permeation of oxygen, thus altering the results (Alexander, 2018). Therefore, the test was conducted to develop a general understanding of the susceptibility of the concrete pore structure to allow for oxygen diffusion due to the effect of cyclic

wetting and drying based on the permeability coefficient. The apparatus used in conducting experiments for OPI is shown in Figure 3-11.

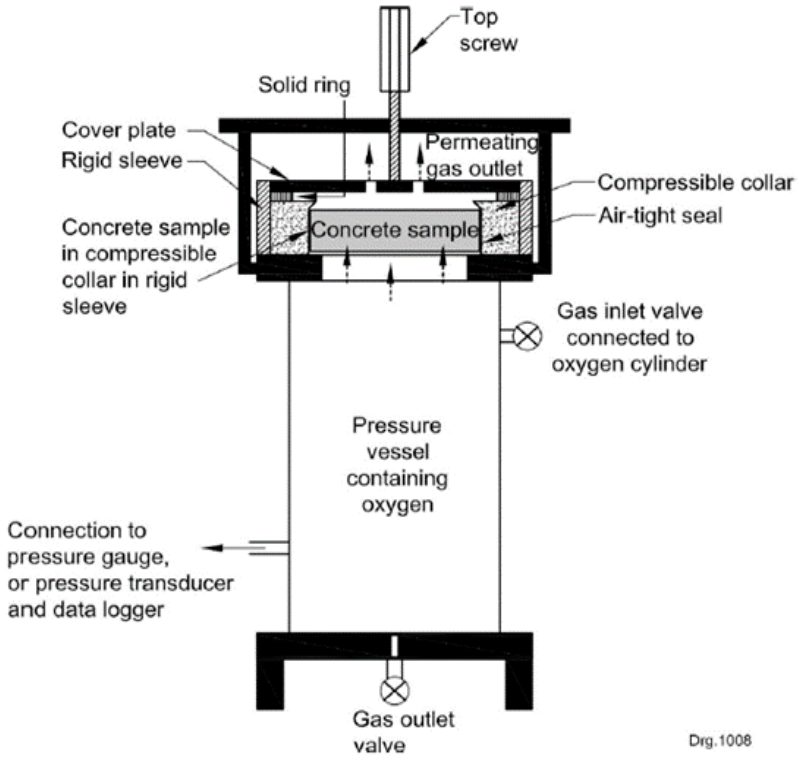

Figure 3-11*:* Oxygen permeability test apparatus (Alexander, 2018)

From the 4 specimens that were cast for the OPI test, 2 specimens were used for the test after 28 days and the remaining 2 specimens after 90 days. Accordingly, the specimens were cored and sliced in accordance with the dimensions mentioned in section 3.8.2. A total of 4 disc samples (hereafter referred to as specimens) were cored, 2 from each specimen. Immediately after coring, the 4 specimens from each mix were placed in an oven for 7 days of conditioning at 50 ℃ ± 2 ℃ and were then removed for testing. After removal from the oven, the specimens were placed inside the desiccator for cooling for 3 hours. Before starting the test, specimen thickness and diameter measurements were taken. Thereafter, specimens were placed in oxygen permeability cells (see Figure 3-12) and pressure was applied by opening the permeability cell's valve until it reached 100 ± 5 kPa, after which the valve was closed, and the pressure recording commenced. Pressure readings were recorded every 15 minutes for 6 hours, and the testing was terminated thereafter.

Figure 3-12: Photograph of oxygen permeability test set-up

The best fit line for each specimen was determined using linear regression, forced through the (0, 0) point as demonstrated in the following equation:

$$z = \frac{\sum\left[\ln\left(\frac{P_0}{P_t}\right)\right]^2}{\sum\left[\ln\left(\frac{P_0}{P_t}\right)t\right]} \quad (18)$$

Where: z is the slope of the linear regression; t is the time since the start of the test in (seconds); P_0 is the initial pressure at start of the test in (kPa); P_t is the pressure reading at time t in (kPa).

The oxygen permeability coefficient (k) was determined for each specimen through the application of Darcy's law:

$$k = \frac{\omega \times V \times g \times d \times z}{R \times A \times T} \quad (19)$$

Where: k is the coefficient of permeability in (m/s); ω is the molecular mass of oxygen in (kg/mol); V is the volume of the permeability cell in (m^3); g is the

gravitational acceleration in (m/s^2); d is the average specimen thickness in (m); z is the slope of the linear regression; R is the universal gas constant in (Nm/Kmol); A is the cross sectional area of the specimen in (m^2); and T is the absolute temperature in (K).

The average oxygen permeability index (OPI) of the 4 specimens was determined as the negative log of the permeability coefficient (k):

$$OPI = -\log_{10}(k) \quad (20)$$

3.8.2.2 Water Sorptivity Index (WSI)

The Water Sorptivity Index (WSI) test is used to measure the transport properties of concrete by means of capillary suction mechanism (Alexander *et al*., 1999; Alexander, 2018) and, thus, the rate of flow of water through the concrete near-surface (Moore *et al*., 2021). The test was used to characterise the water absorption of the concrete microstructure for the different mixes. Furthermore, it helped in understanding of the influence of moisture availability to the level of steel and its influence on rate of corrosion of structures subjected to the marine tidal zone. For example, the concrete with dense microstructure will exhibit low absorption of fluids and high moisture retention. An experimental setup used for this test is shown in Figure 3-13 below.

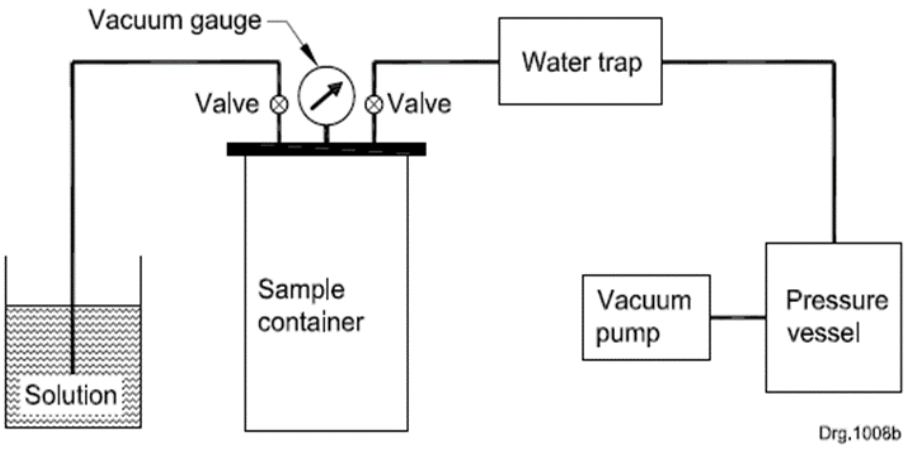

Figure 3-13: Vacuum Saturation Facility (Alexander, 2018)

The same specimens that were used for OPI were used for this test. Immediately after the OPI test, the specimens were sealed on the edges with a tape and their dry mass measured. In preparation for the test, 10 layers of paper towel were placed on a tray and a calcium hydroxide (CaOH) solution was poured into the tray until the solution was visible at the top surface, which should be at most 2 mm above the bottom edge of the specimen (Alexander, 2018) (see Figure 3-14a).

A ruler was used to remove bubbles by smoothening the paper towel towards the edges of the tray. Following that, the specimens were placed in CaOH solution and weighed at 3, 5, 7, 9, 12, 16, 20 and 25 minute to determine mass gain (see Figure 3-14a). Thereafter, the specimens were placed in a tank and vacuumed at 80 kPa pressure for 3 hours (see Figure 3-14b). After 3 hours, the tank was isolated and filled with calcium hydroxide solution (the solution level was at least 40 mm above the specimen) and vacuumed at 80 kPa pressure for 1 hour. After 1 hour, the vacuum was released, and specimens were allowed to soak into the solution for 18 hours. Thereafter, the specimens were weighed to get the saturated mass. Sorptivity and porosity of the specimens were determined using the following equations.

Equation for water sorptivity:

$$S = \frac{Fd}{M_{sv} - M_{s0}} \tag{21}$$

Where: S is the water sorptivity of the specimen in (mm/√h); F is the slope line of best fit in (grams (g)/√h); d is the average specimen thickness in (mm); M_{sv} is the vacuum saturated mass in (g); M_{s0} is the mass of the specimen at the initial time in (g).

Equation for porosity:

$$n = \frac{M_{sv} - M_{s0}}{Ad\rho_w} \times 100 \tag{22}$$

Where: n is the porosity in (%); M_{sv} is the vacuum saturated mass in (g); M_{s0} is the mass of the specimen at the initial time in (g); A is the cross-sectional area of the specimen in (mm^2); d is the average specimen thickness in (mm); ρ_w is the density of water in (g/mm^3).

(a)

(b)

Figure 3-14: Photograph of (a) sorptivity measurements and (b) vacuum saturation facility

3.8.2.3 Chloride Conductivity Index

The Chloride Conductivity Index (CCI) method is specifically used to assess the resistance of concretes in the marine environment towards the ingress of chloride ions (Alexander, 2018). Hence, it was used to evaluate the concrete specimen's pore structure. An example of a sample cell arrangement used to conduct this test is shown in Figure 3-15.

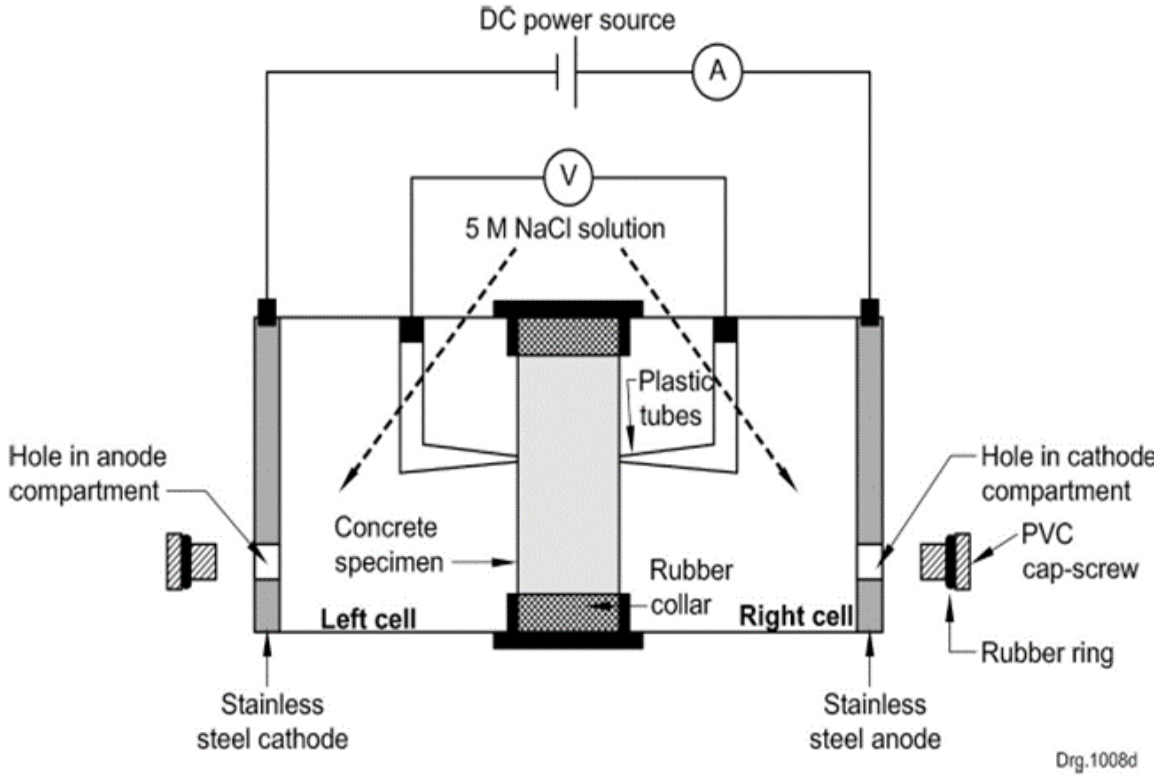

Figure 3-15: Sample cell arrangement (Alexander, 2018)

Similar to OPI and WSI tests, of the 4 specimens that were cast for the CCI test, 2 specimens were used for the test after 28 days and the remaining 2 specimens after 90 days. The specimens were cored and sliced in accordance with the dimensions mentioned in section 3.8.2. A total of 4 disc samples were cored, 2 from each specimen. Thereafter, the specimens were placed in an oven for 7 days of conditioning at 50 ℃ ± 2 ℃ and were then removed for further test preparations. After removal from the oven, the specimens were placed inside the desiccator for cooling for 3 hours before starting the test.

The thickness and diameter as well as the dry mass of each specimen were measured. Thereafter, the specimens were placed in a vacuumed saturation tank which was evacuated to between -75 kPa and -80 kPa pressure (Alexander, 2018). The tank was sealed with a lid and the pressure maintained for 3 hours. After 3 hours, the tank was isolated and filled with sodium chloride (NaCl) solution to a level of at least 40 mm above the sample and vacuumed at 80 kPa pressure for 1 hour. After 1 hour, the vacuum was released for air to enter into the tank and the samples were allowed to soak into the solution for 18 hours and weighed to get the saturated mass.

Following the aforementioned, samples were placed in the conduction cell (Figure 3-16). The conduction cell consists of anode and cathode compartments. A NaCl solution is filled in each compartment. The ammeter and voltmeter were connected, and the DC power adjusted until the voltmeter applied across the sample was at a range of 10 V. Thereafter, for each sample, the voltage and current readings were simultaneously recorded. The chloride conductivity and porosity were calculated using the following equations and the CCI determined from the average chloride conductivity of each specimen:

Chloride conductivity:

$$\sigma = \frac{id}{VA} \tag{23}$$

Where: σ is the chloride conductivity of the sample in (mS/cm^2); i is the electric current in (mA); d is the average sample thickness in (cm); V is the voltage difference (V); A is the cross-sectional area of the specimen in (cm^2).

Porosity:

$$n = \frac{(M_s - M_d)}{Ad\rho_s} \times 100 \tag{24}$$

Where: n is the porosity in (%); M_s is the vacuum saturated mass of the sample in (g); M_d is the dry mass of the sample in (g); A is the cross-sectional area of the specimen in (mm^2); d is the average sample thickness in (mm); ρ_s is the density of salt solution in (g/mm^3).

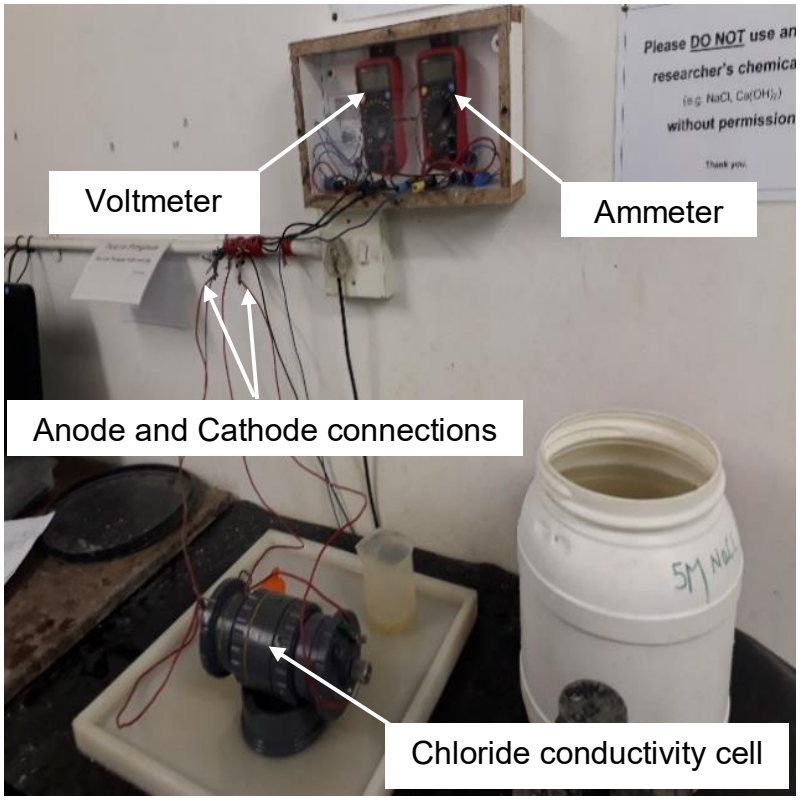

Figure 3-16: Photograph showing chloride conductivity test set-up

3.8.3 Corrosion monitoring

The macrocell corrosion method was used to monitor the corrosion rate of the RC specimens (as detailed in section 2.9.4). This method has been adopted in the ASTM G109 standard and has been explored in some laboratory-based corrosion investigations (Moore, 2019; Harilal *et al*., 2021). In this method, the anode and the cathode steels are electrically connected by means of a resistor, and the potential difference across the resistor is measured using a potential measuring instrument (such as data logger). After the resistors were successfully connected to the anode and cathode steels, all 12 corrosion specimens were connected to a data logger, which measured the corrosion cell's voltage across the known resistance (100 Ω) between the anode and cathode (see Figure 3-17).

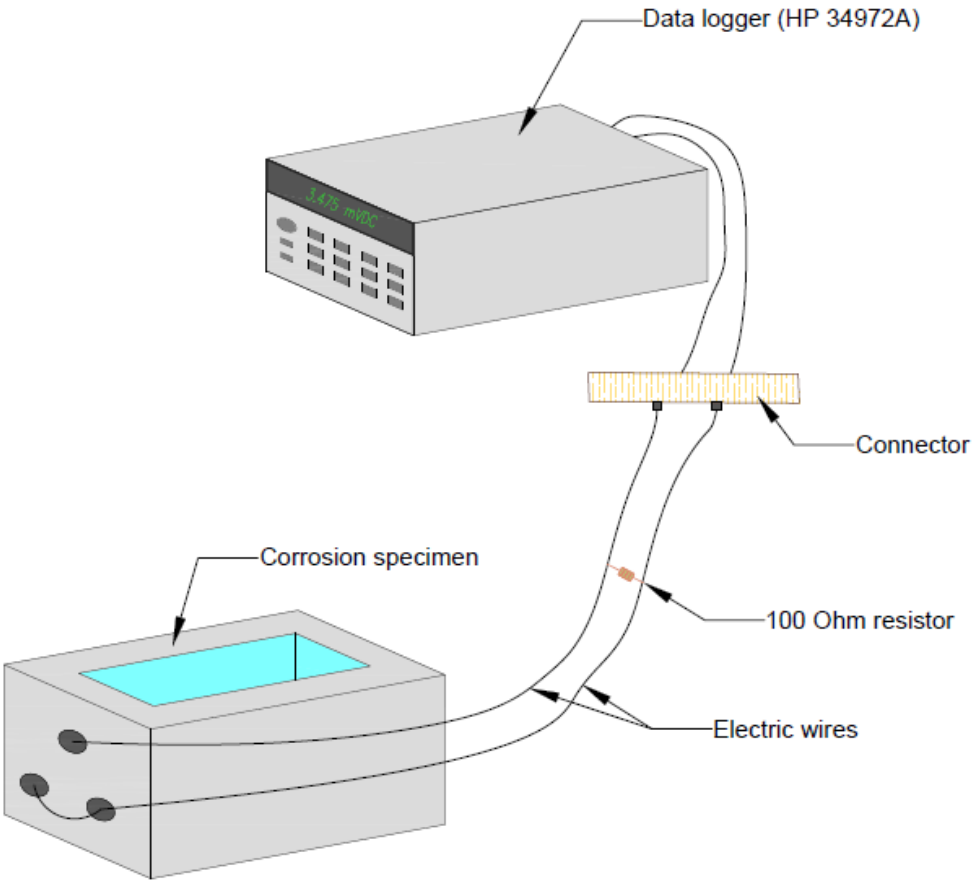

Figure 3-17: Schematic showing corrosion specimen connection to the data logger

The measured voltage across the known resistance was used to calculate the current flow between the anode and the cathode. This was done using Ohm's law, as demonstrated in equation (25) (ASTM G109, 2007). The readings were recorded once a week during the drying cycle for 13 weeks. The duration was influenced by the limited timeframe of this study as well as the availability of the laboratory facilities.

$$I = \frac{V}{R} \tag{25}$$

Where: I is the current in (amperes/A); V is the voltage in (volts/V) and R is the resistance in (Ohm's).

Furthermore, in accordance with the ASTM standard, an integrated corrosion current (TC) can be determined using the following equation (26). In this way, the total corrosion that has occurred over the test duration may be determined. This

formula helps to identify the area under the corrosion current curve against time and thus the gross corrosion that has occurred (Moore, 2019).

$$TC_j = TC_{j-1} + \left[(t_j - t_{j-1}) \times \left(\frac{(i_j - i_{-1})}{2} \right) \right] \quad (26)$$

Where: TC_j is total corrosion in (coulombs/C); t_j denotes time in (seconds); i_j is the macrocell current in (amps).

3.8.4 Resistivity

The four-point Wenner probe technique (described in section 2.9.2), with the probe spacing of 50 mm, was used in this study to measure concrete resistivity of the corrosion specimens. The resistivity measurements were taken once a week during the drying cycle for a period of 13 weeks due to the limitations mentioned in the preceding section 3.8.3 for this study. The resistivity measurements were used as corrosion rate indicators for the corrosion specimens. Accordingly, 4 resistivity measurements were taken on each corrosion specimen (2 resistivity measurements on both sides of the longitudinal section of the specimen) (see Figure 3-18). Thereafter, the resistivity value of a particular specimen was calculated by averaging the results of the 4 resistivity measurements.

Figure 3-18: Photograph of resistivity measurements with the four-point Wenner probe

In summary, section 3.8 presented the test methods that were used in order to achieve the objectives of this study. On the one hand, tests like the compressive strength and durability index were conducted to evaluate the microstructure of the concrete specimens, subsequently providing an idea of the susceptibility of the specimens to the transportation of corrosion agents and catalysing the rate of reinforcement corrosion. On the other hand, the resistivity test was used as a corrosion rate indicator of the specimens. This section also outlined how the corrosion rate was monitored and the analytical methods used. The following chapter provides an analysis and discussion of the results obtained through the experimental programme outlined in this section.

4 RESULTS, ANALYSIS AND DISCUSSION

The rate of corrosion of RC structures is generally influenced by a variety of factors, as discussed in Chapter 2, such as cover depth, oxygen availability, w/b, concrete resistivity, moisture, and binder type. Therefore, it is essential to have a broad understanding of how each of these parameters affects the corrosion rate individually.

This study investigated the influence of blended cements on the corrosion rate of RC structures while taking into consideration some of the influencing parameters of corrosion of RC structures, namely cover depth, oxygen availability, and concrete resistivity. Consequently, the preceding chapter provided an experimental programme for this study; materials used for mix preparations and proportions; specimen details; curing, and exposure set-up. Also, the techniques employed for testing and monitoring of corrosion rate, concrete resistivity, durability index tests, and compressive strength testing were discussed in detail.

In this chapter, the results, analysis, and discussion of the experimental observations for this study are presented. The discussions are outlined to cover the aim and objectives of this study. Therefore, the influence of parameters such as cover depth, binder type, w/b, and concrete resistivity in relation to the corrosion rate of the specimens is discussed. More emphasis is given to the corrosion performance of blended cement specimens compared to the control mix (PC) specimens. Also, durability index test results are presented and discussed to understand the concrete pore structure and the likelihood of the transportation of corrosion agents through the concrete cover depth to trigger corrosion.

4.1 Compressive strength test results

The compressive strength results are shown in Figure 4-1. The results shown in Figure 4-1 represent the average compressive strength of three specimens per mix. A summary of the compressive strength test results calculations at 28-day and 90-day testing is provided in Appendix A. In general, the compressive strength of concrete mixes increases over time.

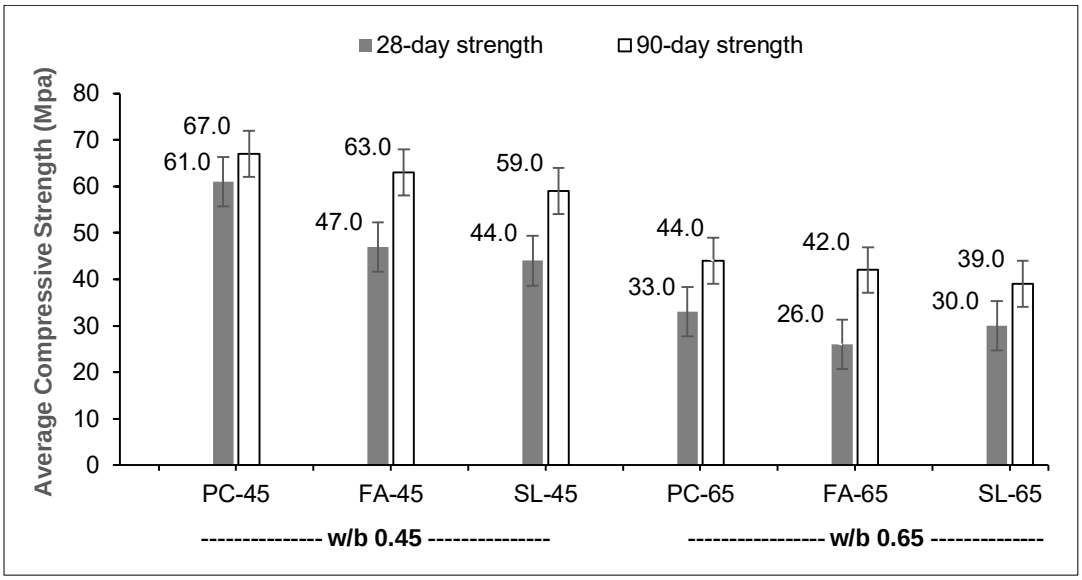

Figure 4-1: Compressive Strength results over 28 days and 90 days

As expected, due to the high degree of hydration (reactivity) of tricalcium silicate (C_3S) in Portland cement (PC) to form calcium silicate hydrate (CSH) gel and high portlandite [$Ca(OH)_2$] (Grieve, 2009; Samad *et al*., 2017; Wang *et al*., 2022), the concrete made with PC had the highest compressive strength at 28 and 90 days, irrespective of the w/b. However, from 28 to 90 days, the PC specimens showed lower strength gain compared to the blended cement concretes. For example, for w/b 0.45, PC exhibited about 11% strength gain, while FA and GGBS specimens exhibited a strength gain of 32% and 36%, respectively.

The delayed strength development of FA and GGBS concrete specimens can be attributed to the prolonged hydration process of GGBS and the slow pozzolanic reaction of FA. The slow strength development of blended cement concretes corroborates Scott's (2004) findings. Furthermore, FA concrete specimens, for the specified w/b, had a compressive strength in the same range as the PC concrete specimens at 90 days, which is attributed to the fine-filling effect of FA and the continued pozzolanic reaction [FA's reaction with $Ca(OH)_2$ and water to generate more CSH gel] to form more CSH gel. A similar trend was observed in the literature (Islam & Islam, 2013).

Notable is also the lower strength of concrete made with a higher w/b compared to the lower w/b, irrespective of the binder type and age. In general, concrete with a higher w/b will have a less dense pore structure (larger pores). Consequently, it is understood that an increase in concrete porosity due to a higher w/b results in a decrease in concrete strength (Perrie, 2009).

4.2 Durability index tests

The durability index (DI) tests were conducted to evaluate the ease with which the concrete cover depth allows the transportation of corrosion agents such as chlorides, oxygen, and moisture to the level of the reinforcement, thus providing an idea of the durability performance of the concrete. The results presented in the following sections will provide an indication of the potential durability performance of the different mixes based on the type of binder used (Ballim & Alexander, 2018). Detailed DI test results are presented in Appendix B.

4.2.1 Oxygen Permeability Index

The Oxygen Permeability Index (OPI) results over time (28 and 90 days) are shown in Table 4-1 and presented in more detail in Appendix B for each specimen. The OPI test indicates the ease of oxygen penetrability through the concrete pore structure. Therefore, concrete with a more refined pore structure is expected to have high OPI, which would indicate less permeability of oxygen through the concrete pore structure.

Table 4-1: Oxygen Permeability Index results at 28 and 90 days

Mix label	OPI	
	28-day	90-day
PC-45	10.46	10.22
PC-65	10.30	10.32
FA-45	9.50	9.86
FA-65	9.45	10.60
SL-45	10.39	10.46
SL-65	10.19	10.67

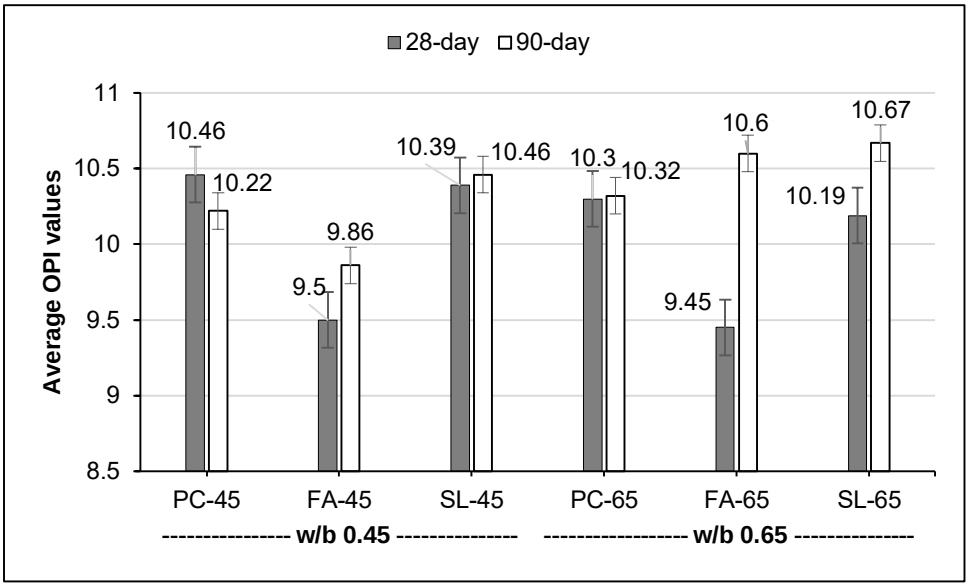

Figure 4-2: Oxygen Permeability Index results at 28 and 90 days

From the OPI test results obtained, it is notable that PC specimens had higher OPI values than FA and SL specimens on the 28th day of testing, irrespective of the w/b (see Figure 4-2). Starting from high to low OPI for both w/b at 28-day testing, the OPI can be ranked in the following manner: PC > SL > FA. The high OPI of PC can be attributed to its high degree of hydration and strength development compared to blended cement concretes, thus a more refined pore structure at an early age (Khan & Lynsdale, 2002; Golden, 2015; Wang *et al*., 2022).

It is generally understood that a low w/b will result in less permeable concrete (high OPI) than a higher w/b. At 28 days, the OPI test results of this study, corroborate this understanding. The OPI values decreased with increasing w/b at 28 days, which can be attributed to a more porous concrete microstructure when higher w/b is used. Khan and Lynsdale (2002) and Otieno (2008) also observed an increase in the permeability of concrete due to an increase in w/b.

At 90-day testing, SL specimens had higher OPI values than PC and FA specimens for the specified w/b, with the FA specimen, however, demonstrating significant improvement from the 28-day test due to continued pozzolanic reaction, leading to a more refined pore structure after 90 days. Also, at the 90-day test, the OPI value for PC-45 specimens decreased with age (from 28 to 90 days). This observation was not expected as the permeability of concrete, generally, decreases with curing

age, i.e., the permeability of specimens at 90 days is expected to be less than the permeability of specimens at 28 days due to continued hydration of cement. However, due to the high degree of hydration for PC concrete, this observation may be an indication that not much reactivity occurred after 28 days for PC specimens. A similar trend to the PC-45 specimen was observed in the literature (Golden, 2015).

Contrary to the trend observed at 28 days, at 90 days, specimens with a higher w/b had a higher OPI than specimens with a lower w/b. This trend is contrary to the established literature (Khan & Lynsdale, 2002) that a higher w/b will likely result in a more permeable concrete than a lower w/b due to the less dense microstructure of concrete with a high w/b. Therefore, due to the contradictory observations for the 90-day testing, the 90-day OPI test results will not be considered for further analysis and interpretation in this study.

From the above analysis of the OPI as a durability indicator of concrete structures, even though the overall trends contradict the established understanding found in literature, it can be seen that blended cement specimens showed less oxygen penetrability on the 90-day of testing than PC specimens at a higher w/b. The low oxygen permeability of blended cement specimens is attributed to the modified concrete microstructure of FA and GGBS binders (Scott, 2004; Otieno, 2008). As a result, FA and SL specimens are expected to show better durability performance over time.

4.2.2 Water Sorptivity Index

The Water Sorptivity Index (WSI) test results from the 28 and 90 days of testing are shown in Table 4-2. This test evaluates the degree of water absorption through the concrete pore structure by means of capillary suction (Alexander, 2018). Generally, concrete with lower sorptivity and porosity values indicates the high resistance of the concrete to the inward movement of water through the concrete cover (Scott, 2004). This relates to the concrete quality, binder type, and curing age (Otieno, 2008). The lower the w/b and the longer the curing period, the lower the sorptivity and porosity values (Liu *et al*., 2014).

Table 4-2: Water Sorptivity Index results at 28 and 90 days

Mix label	WSI $(mm/\sqrt{hour})$		Porosity (%)	
	28-day	90-day	28-day	90-day
PC-45	10.33	5.50	8.38	7.01
PC-65	10.16	7.09	11.67	10.99
FA-45	11.75	4.47	11.69	6.49
FA-65	8.66	6.31	14.24	9.15
SL-45	5.75	5.45	7.99	8.01
SL-65	7.61	5.71	11.31	7.30

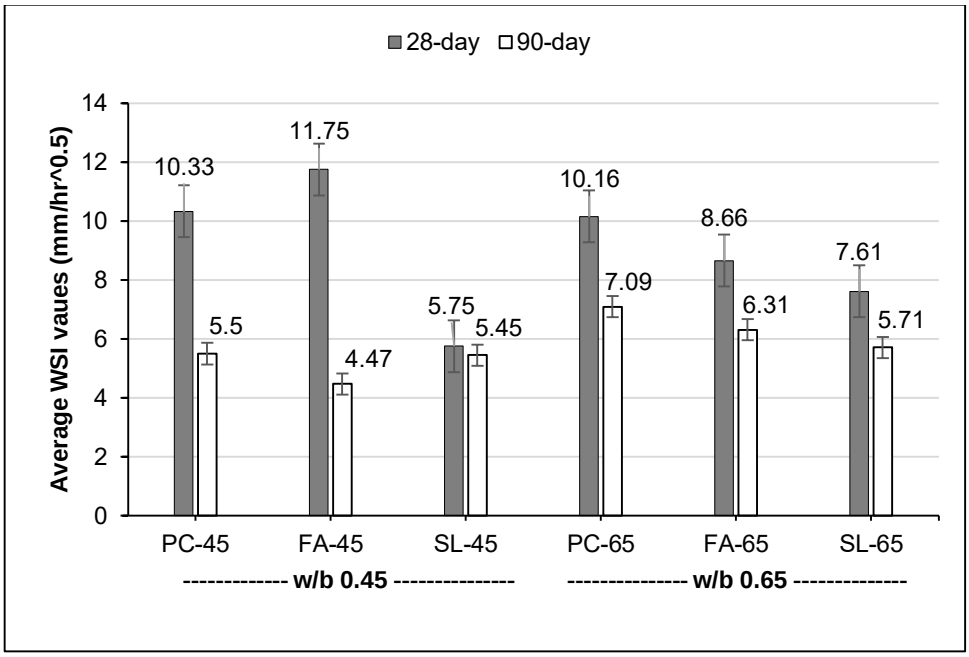

Figure 4-3: Water Sorptivity Index test results at 28 and 90 days

The test results presented in Figure 4-3 clearly show that the WSI values of the specimens decreased over time, irrespective of the w/b and the type of binder used, owing to the improved microstructure of the concrete over time. Similar observations were made by Scott (2004) and Otieno (2008). Due to the prolonged hydration and pozzolanic reaction of blended cement concrete, it should be noted that the incorporation of SCMs played a significant role in the decrease of WSI values with time. On the 90-day testing, for a low w/b (0.45), the WSI values can be ranked (from low to high WSI values) in the following order: FA > SL > PC. The low

sorptivity of FA specimens can be attributed to the fine-filling properties of the FA binder and the pozzolanic reaction products (CSH gel), resulting in a refined concrete pore structure (Yahia *et al*., 2005; Islam & Islam, 2013).

For 0.65 w/b, SL specimens had low WSI values compared to FA and PC specimens, with WSI values ranked in the following order: SL > FA > PC. This trend further shows the improved durability performance of blended cement concretes over time due to their resistance to the ingress of aggressive fluids (Scott, 2004). In addition, a decrease in the porosity of the specimens with curing age can also be observed for all specimens for the specified w/b, with the exception of SL-45, which showed a slight increase in porosity from 28-day to 90-day testing.

In addition to the statement above, a contradiction to the expected trend was also observed for PC and FA specimens in relation to the w/b on the 28th day. PC-45 and FA-45 exhibited higher sorptivity values than PC-65 and FA-65. Also, for SL specimens, SL-65, at 90-day testing, showed lower porosity than SL-45. The concrete with low w/b is expected to have lower absorption of water than a high w/b owing to its refined concrete pore structure (Scott, 2004; Otieno, 2008). The contradicting result from the expected trend in the application of the WSI test was also observed by Beushausen and Alexander (2008). Nevertheless, the results obtained in this study are indicative that blended cement concretes show better water resistance than PC specimens, with the effect of curing noted.

4.2.3 Chloride Conductivity Index

The Chloride Conductivity Index (CCI) assesses the resistance of concrete to the ingress of chlorides, thus determining the potential durability of the concrete (Streicher & Alexander, 1995). Therefore, with the use of equation (23), the CCI value of a specimen was determined from the recorded voltage and current that pass through the specimen in a conductivity cell to evaluate its resistance to chloride ingress. It has been widely established that for corrosion to occur, a sufficient amount of chloride is required (Angst *et al*., 2009). Therefore, concrete exhibiting low chloride conductivity will have a low corrosion risk (Scott, 2004).

The CCI test results for the 28 and 90 days are presented in Table 4-3. From the results obtained, higher w/b showed low resistance to chloride diffusion for all concrete mixes. The low chloride resistance at a higher w/b relates to the poor refinement of the concrete pore structure compared to the denser pore structure at a low w/b. Also, the movement of chlorides in the concrete pore structure decreased over time (from 28 to 90 days) (see Figure 4-4). This was due to the continued hydration, resulting in a more refined concrete pore structure. A similar observation was made by Otieno (2008).

Table 4-3: Chloride Conductivity Index results at 28 and 90 days

Mix label	CCI (mS/cm)	
	28-day	90-day
PC-45	0.58	0.33
PC-65	0.96	0.78
FA-45	1.20	0.43
FA-65	1.39	0.99
SL-45	0.21	0.10
SL-65	0.46	0.13

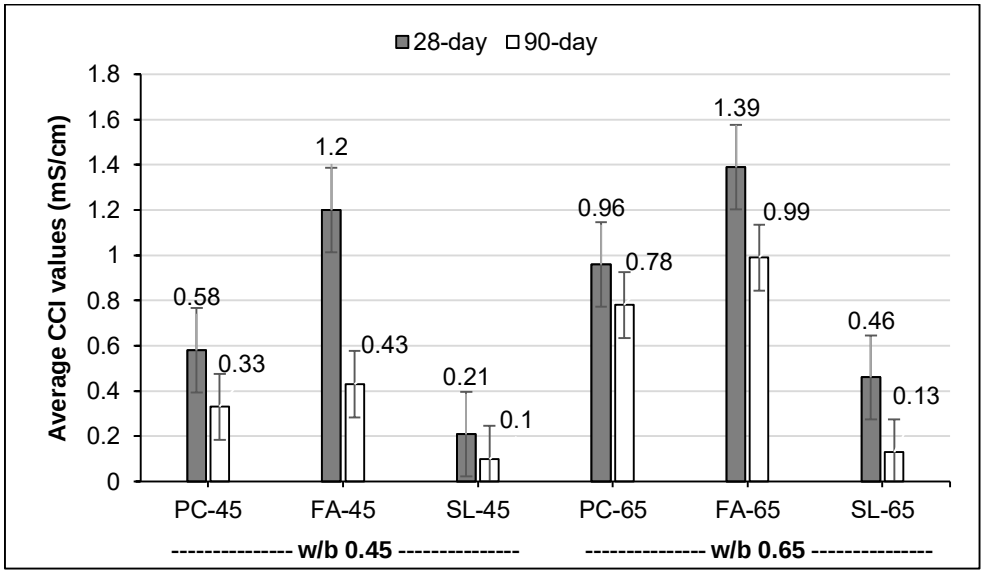

Figure 4-4: Chloride Conductivity Index results at 28- and 90-day testing

The CCI values for both w/b and the testing times can be ranked from a high to a low resistant concrete in the following order: SL > PC > FA. Scott (2004) and Otieno (2008) also reported the high resistance of SL specimens to chloride diffusion compared to other binders, which is attributed to the refinement of the concrete pore structure for concrete made with the GGBS binder.

Notably, FA specimens exhibited lower chloride resistance than PC and SL specimens. This indicates that FA specimens have a high corrosion risk during the early ages of exposure due to high permeability, which is attributed to the delayed pozzolanic reaction (Islam & Islam, 2013). However, over time, FA specimens are expected to have a more refined pore structure. Additionally, the early age corrosion risk of FA specimens can be seen from the TC values presented in section 4.4.

Despite the fact that FA specimens had the highest CCI values at 28-day testing, a significant decrease in CCI values can be observed on the 90th day of testing (see Figure 4-4). The decrease in CCI of the FA specimens can be associated with the refined pore structure development of concrete made with FA binder due to prolonged hydration and pozzolanic reaction, resulting in a reduction in the diffusion of chlorides in concrete (Kanjee, 2015).

From the CCI test results obtained, it can be inferred that blended cements improve the pore structure of the concrete, which in turn reduces the diffusion of chlorides in concrete structures, subsequently reducing the risk of corrosion. Furthermore, the CCI values obtained also highlight the importance of curing to allow for the development of the concrete pore structure, especially in the use of blended cements.

4.3 General observations on corrosion current (I_{corr}) results

In this section, general observations on the fluctuation of the corrosion current over time are given, while an understanding of how cover depth, w/b, binder type, and resistivity influence the rate of corrosion is discussed in more detail in section 4.4. Before the corrosion specimens were exposed to the simulated marine tidal zone 6-hour wetting and drying cycles, the specimens underwent corrosion activation for 3

weeks (3 days of wetting and 4 days of air-drying) (see section 3.6). Even though not directly measured, corrosion was assumed to have been initiated.

Figure 4-5 to Figure 4-8 depict the corrosion current (corrosion rate) measurements for each mix during the simulated marine tidal zone wetting and drying cycles at different cover depths, measured once a week after the wetting cycle. The figures illustrate the influence of cyclic wetting and drying on the corrosion rate, over time, in a simulated marine tidal zone.

The influence of oxygen availability was not directly measured for this study. Instead, the increase in corrosion currents is assumed to indicate high diffusion of dissolved oxygen to the level of steel. The notations used to differentiate the corrosion specimens are labelled according to the mix design and cover depth in brackets. For example, PC-45 (20) and PC-45 (40) denote corrosion specimens made of PC with a w/b of 0.45 and concrete cover depths of 20 mm and 40 mm, respectively.

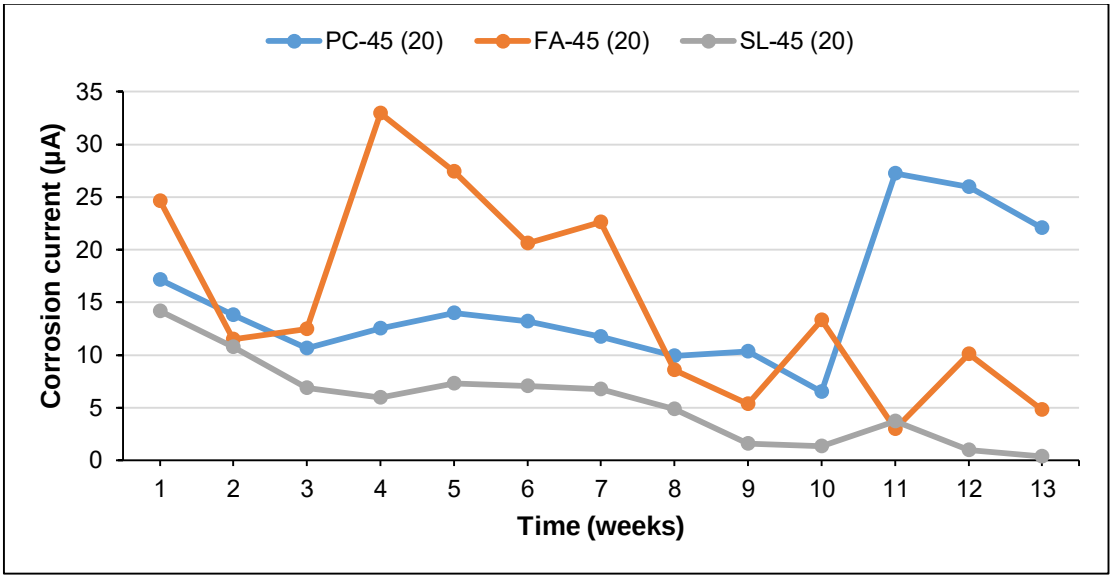

Figure 4-5: Corrosion current for w/b 0.45 specimens at 20 mm cover depth

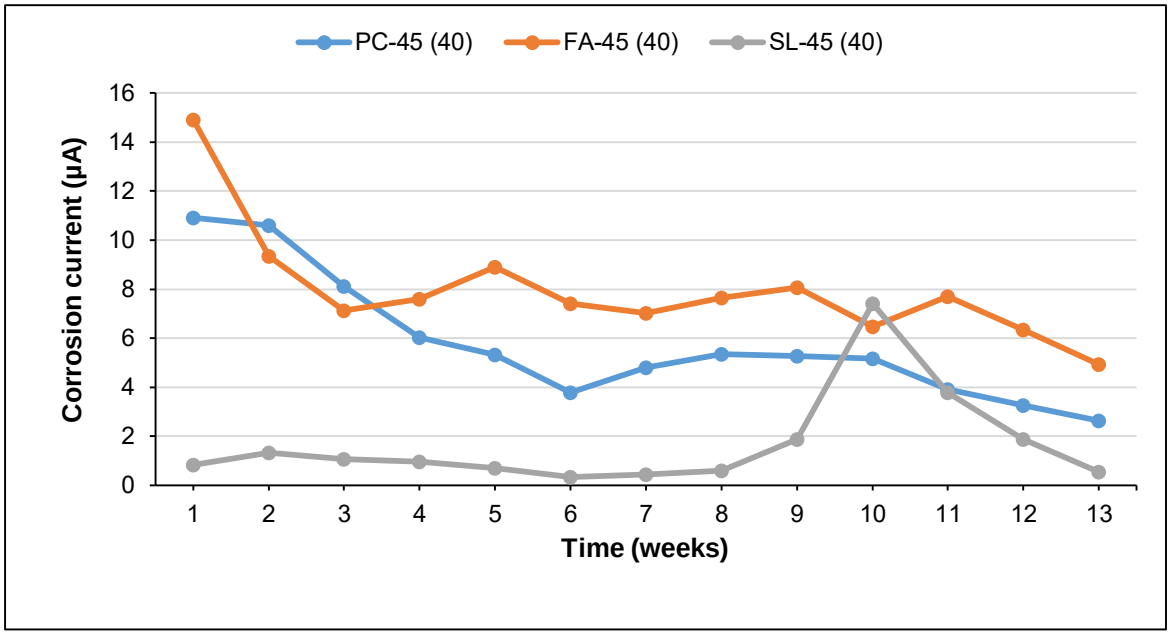

Figure 4-6: Corrosion current for w/b 0.45 specimens at 40 mm cover depth

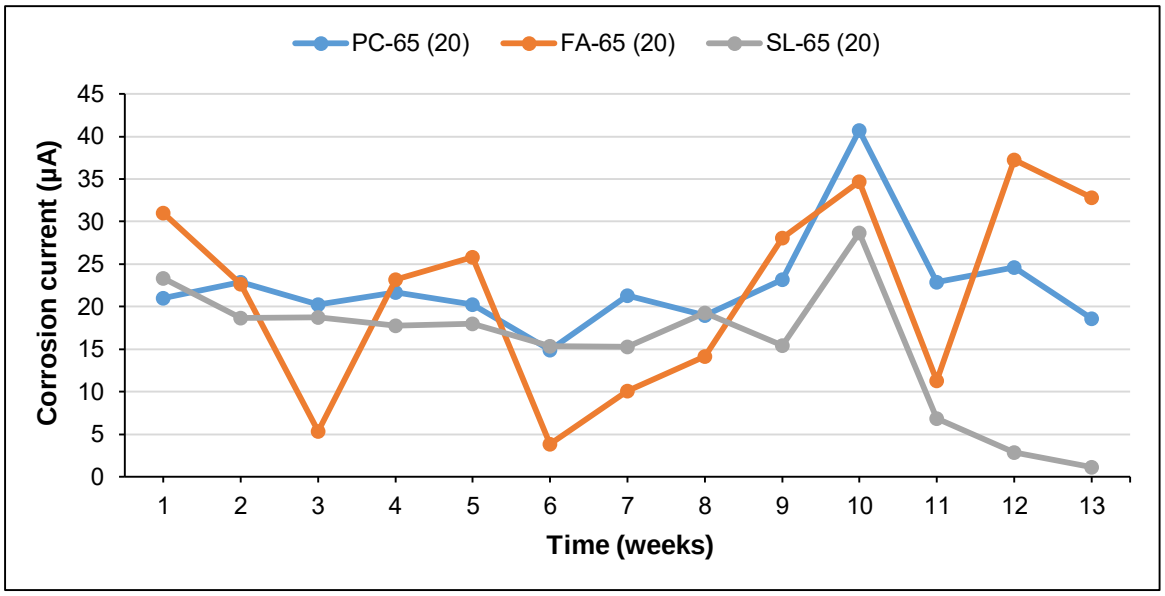

Figure 4-7: Corrosion current for w/b 0.65 specimens at 20 mm cover depth

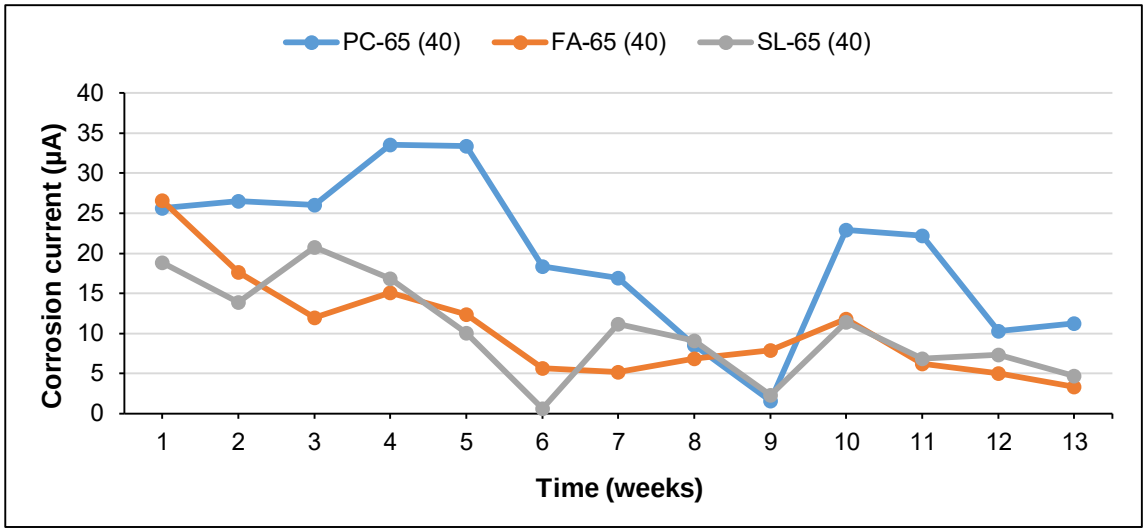

Figure 4-8: Corrosion current for w/b 0.65 specimens at 40 mm cover depth

From the above figures, Figure 4-5, Figure 4-6, and Figure 4-8, on the one hand, show a gradual decrease in corrosion current (indicating a low corrosion rate) between the 1st and the 9th weeks of exposure to the simulated marine tidal zone (except for SL-45 specimen in Figure 4-6). The decrease in corrosion current can be attributed to deprived oxygen availability and an increase in moisture content as a result of short cycle duration for wetting and drying, leading to a partially dry concrete pore structure, corroborating literature findings (Golden, 2015; Moore, 2019). During the activation period, there was sufficient oxygen supplied to the level of the reinforcing steel bars as a result of a longer drying cycle (4 days); hence, it can be observed that the corrosion was higher after the activation period. On the other hand, Figure 4-7 shows a slight fluctuation of the corrosion current from the beginning of the exposure of the specimens to week 9.

The observations made in the paragraph above highlight the influence of the concrete microstructure, coupled with the influence of cover depth, on the corrosion rate of RC structures. For example, from Figure 4-5 , the influence of a refined pore structure in reducing the ingress of corrosion agents such as oxygen can be observed, thus reducing the corrosion current, owing to the use of a low w/b (Meira *et al*., 2014). Whereas, from Figure 4-6, the improved pore structure of blended cement concrete (e.g., SL specimen) results in a reduction in corrosion rate, even though the influence of concrete cover depth is noted.

Furthermore, as it can be observed in Figure 4-8, the refined pore structure of blended cement concretes (FA and SL specimens) (Scott, 2004; Otieno, 2008; Golden, 2015) resulted in a reduction in corrosion current compared to the concrete made with PC. However, it is notable that, even though the corrosion currents of PC were higher than the corrosion currents of blended cement concretes, due to the use of higher cover depth (Scott, 2004), the corrosion current was decreasing over time.

Contrary to Figure 4-5, Figure 4-6, and Figure 4-8, Figure 4-7 shows that the use of higher w/b and relatively lower cover depths promote the availability of oxygen and ingress of chloride as well as loss of moisture content at the level of the reinforcing steel. This is due to less dense concrete microstructure and a shorter travel path for oxygen and chlorides (Scott, 2004; Andrade, 2019). Notably, the SL-45 specimen for 40 mm cover depth (Figure 4-6) remained in a passive state with a corrosion current of less than 10 µA (ASTM G109, 2007). The SL-45 (40) recorded the lowest total corrosion current (8.14 µA) from the 1st week to the 9th week of exposure. This could be an indication that some of the chlorides are absorbed into the concrete pore structure due to a delayed hydration process in blended cement concrete (Marinescu & Brouwers, 2010).

A significant increase in corrosion current on SL-45 (40) is noted in the 10th week of Figure 4-6. This could be an indication that a sufficient amount of chlorides reached the reinforcing steel, leading to high conductivity at the reinforcement level and, thus an increase in corrosion current. A similar trend of occasionally significant increase in corrosion current was also observed in the literature (Broomfield, 2007; Andrade, 2019; Wei *et al*., 2019; Xu *et al*., 2022). The high peak in corrosion current is also observed on other specimens, followed by a gradual decrease (for example, the PC specimen in the 11th week in Figure 4-5 and all specimens on the 10th week in Figure 4-7).

According to ASTM G109 (2007), a corrosion current of 10 µA is required to indicate the active corrosion, even though other studies (Andrade *et al*., 2004; Otieno, 2008; Golden, 2015) considered activeness of corrosion from 0.1 µA/cm^2, which is equivalent to 2.5 µA (Moore, 2019). Nevertheless, since in this study the procedure

outlined in ASTM G109 to measure macrocell corrosion of the specimens was adopted, 10 µA was accepted as an indicator of active corrosion in the specimens. Accordingly, all specimens, except SL-45 (40), showed active corrosion from the first week of exposure to the simulated marine tidal zone. However, in general, the corrosion currents gradually decreased over time due to the limited oxygen availability attributed to the short cycles of wetting and drying.

4.4 Integrated corrosion current

Figure 4-9 to Figure 4-12 show an integrated corrosion current of specimens at varying w/b and cover depths. The integrated corrosion current (TC) provides the cumulative corrosion current that has occurred over the test duration of this research, which is determined using the method described in section 3.8.3. The TC gives the gross corrosion current incurred over the duration of this study for each corrosion specimen. In other words, the integrated corrosion current indicates how much corrosion current has been accumulated by a particular specimen over time. Thus, from the TC values, a specimen that demonstrated better corrosion resistance can be identified. This section discusses some of the influencing parameters of chloride-induced corrosion, such as cover depth, w/b, and binder type on the total corrosion current.

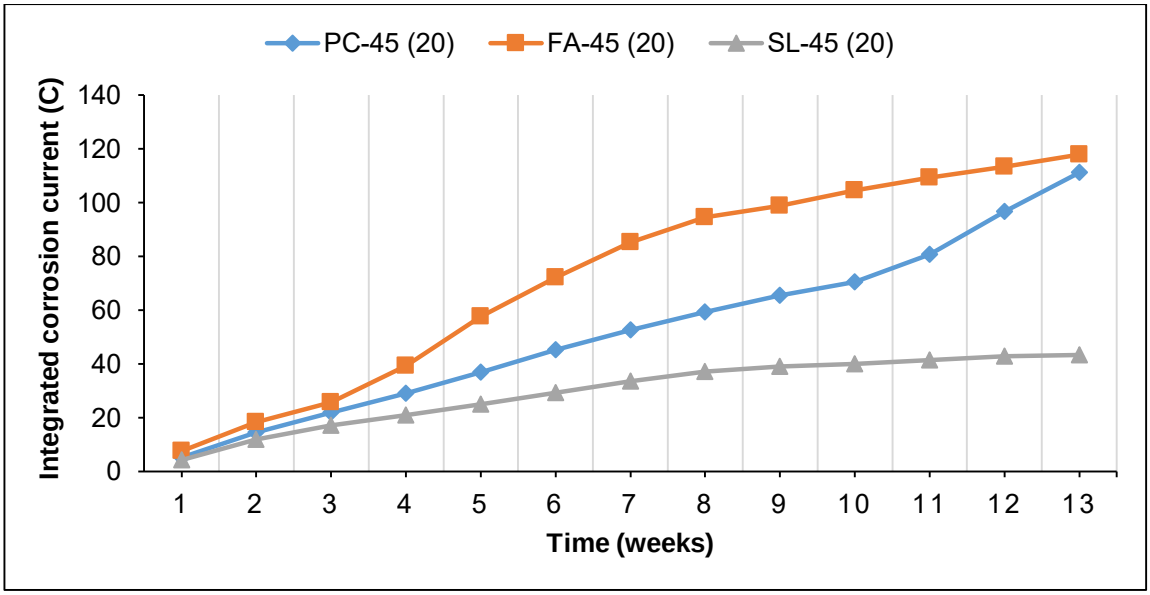

Figure 4-9: Integrated corrosion current for w/b 0.45 specimens at 20 mm cover depth

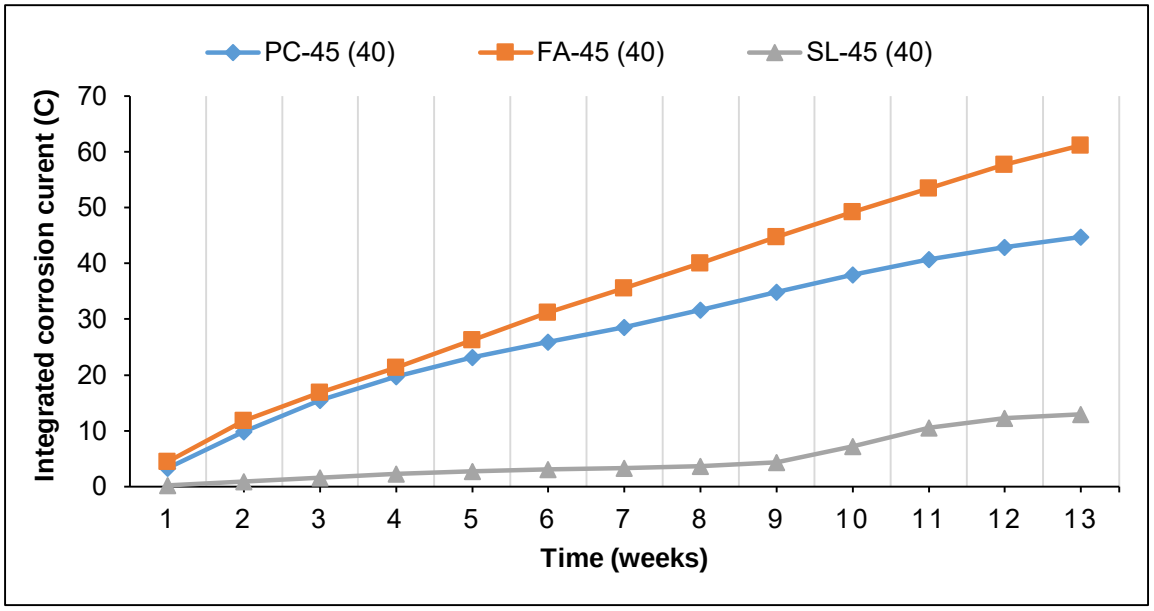

Figure 4-10: Integrated corrosion current for w/b 0.45 specimens at 40 mm cover depth

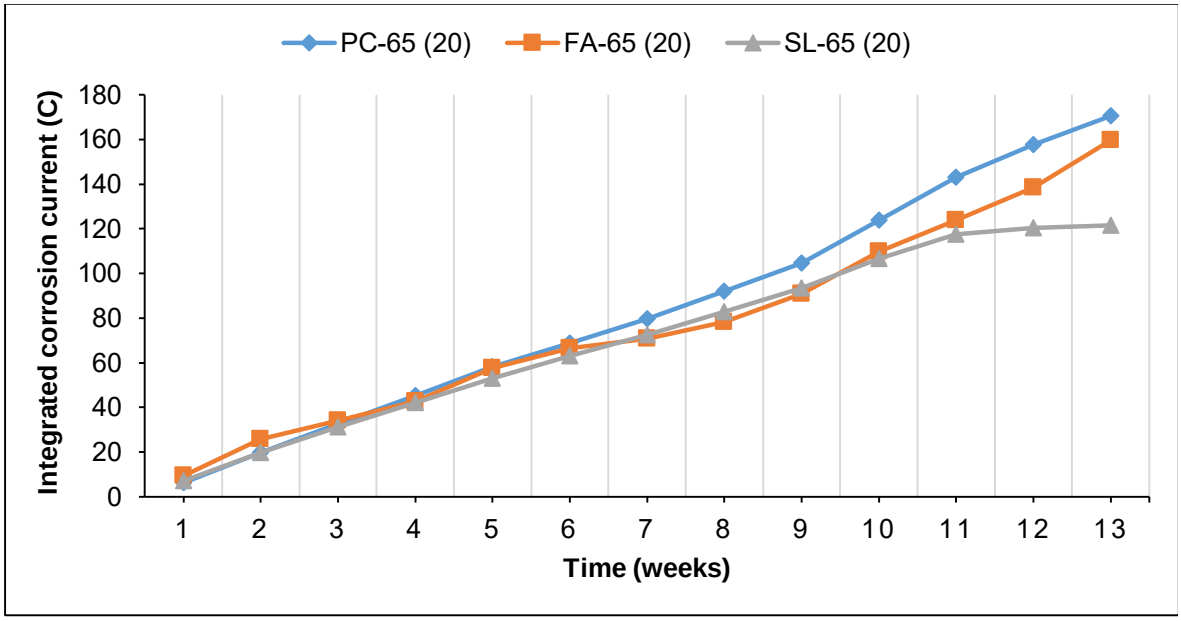

Figure 4-11: Integrated corrosion current for w/b 0.65 specimens at 20 mm cover depth

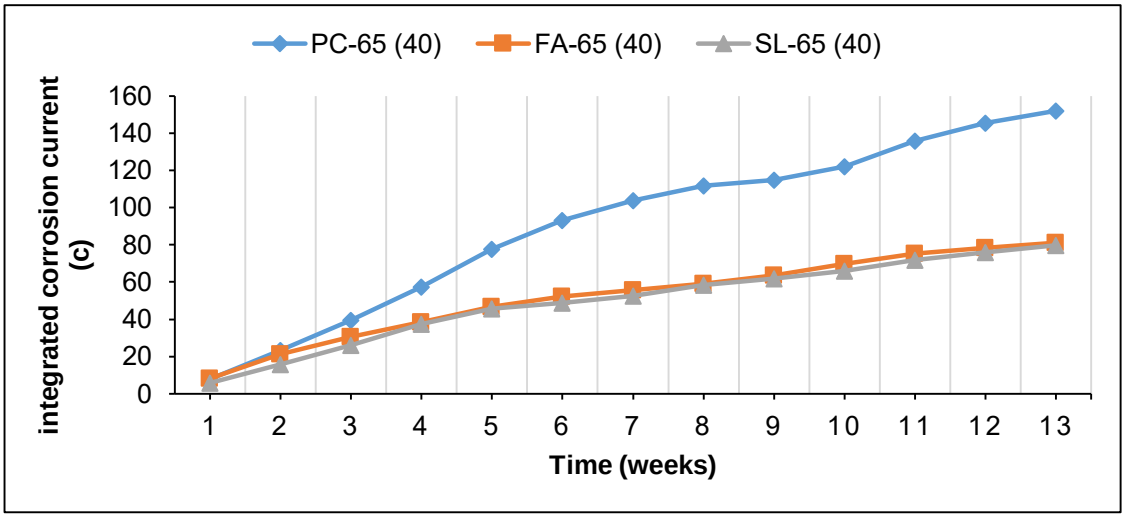

Figure 4-12: Integrated corrosion current for w/b 0.65 at 40 mm cover depth

4.4.1 Influence of cover depth on corrosion rate

Figure 4-9 and Figure 4-10 show the integrated corrosion current for w/b 0.45 specimens for cover depths of 20 mm and 40 mm, respectively. The observations made on the influence of cover depth on the TC for specimens PC-45, FA-45, and SL-45 indicate that an increase in cover depth results in a reduction in corrosion rate. For example, by week 13, PC-45 (20) had a TC of 111.23 C, whereas PC-45 (40) yielded a TC of 44.68 C. This trend is also observed on the blended cement concrete specimens of the same w/b. FA-45 (20) and SL-45 (20) had a TC of 117.83 C and 43.24 C, while FA-45 (40) and SL-45 (40) had a TC of 61.10 C and 13.01 C, respectively.

From Figure 4-11 and Figure 4-12, which shows the integrated corrosion current for w/b 0.65 specimens for specified cover depths of 20 mm and 40 mm, respectively, a similar trend as above is observed for all the specimens (i.e., PC, FA, and SL specimens). For all specimens, the corrosion rate decreased with an increase in cover depth. For example, PC-65, FA-65, and SL-65 specimens with a 20 mm cover depth exhibited TC values of 170.63 C, 159.67 C, and 121.58 C, respectively, by week 13. Meanwhile, PC-65, FA-65, and SL-65 for 40 mm cover depth had TC values of 152.13 C, 81.11 C, and 79.67 C, respectively. A similar trend was observed by Otieno *et al*. (2016).

The decrease in TC values with an increase in cover depth is an indication of the reduction of oxygen availability at the level of steel due to the increased travel path for oxygen to reach the reinforcement, which corroborates the observations made by Scott (2004) and Otieno *et al*. (2016). Additionally, due to the short cycles of wetting and drying employed in this study, the low TC values could be an indication that the specimens do not completely dry to the level of reinforcement for higher cover depth, resulting in highly moist conditions around the steel, thus low oxygen diffusion. Similar observations were made by Golden (2015) and Moore (2019).

In relation to the influence of increased cover depth on the corrosion rate of concrete containing SCMs, these results contradict Scott (2004), who reported a negligible influence of increased cover depth for concrete made with SCMs. However, due to the age of the specimens for this study compared to those of Scott, the specimens may yield different results if the study were to continue for a longer time period.

4.4.2 Influence of w/b on the corrosion rate

Overall, all specimens showed a significant increase in TC with an increase in w/b. For example, after 13 weeks, PC-45 (40) and PC-65 (40) had a TC of 44.68 C and 152.13 C, respectively. Also, at 20 mm cover depth, with an increase in w/b from 0.45 to 0.65, the TC values of PC specimens increased from 111.23 C to 170.63 C. Similarly, increasing the w/b for FA specimens resulted in an increase in TC, where FA-45 (20) and FA-65 (20) had a TC of 117.83 C and 159.67 C, respectively, after 13 weeks.

Also, by week 13, FA-45 (40) and FA-65 (40) exhibited a TC of 61.10 C and 81.11 C, respectively. For SL specimens, increasing the w/b at 20 mm cover depth resulted in an increase in total corrosion current from 43.24 C to 121.58 C. While at 40 mm cover depth, it increased the TC values from 13.01 C to 79.67 C. These results corroborate the observations found in literature (Meira *et al*., 2014) that low w/b results in a more refined concrete microstructure, which in turn reduces the ingress of chlorides and oxygen diffusion into concrete. In contrast, a higher w/b increases the concrete penetrability, leading to oxygen and chloride access at the level of reinforcement and thereby increasing the corrosion risk.

Therefore, due to a more refined pore structure for low w/b concretes, ease of transportation of corrosion agents (inward and outward), such as oxygen, moisture, and chlorides, is reduced. Hence, low TC values for low w/b. A similar trend was observed by Moore (2019). Furthermore, it is noted that PC specimens exhibited the highest TC values compared to the blended cement concretes at a higher w/b. Alexander *et al*. (2012) and Golden (2015) made similar observations. The high susceptibility of PC to corrosion at higher w/b is attributed to a less dense microstructure and low resistivity compared to blended cement concretes.

4.4.3 Influence of binder type on the corrosion rate

Based on the comparison of the TC values for the specified binders, SL specimens for the specified cover depths of 20 mm and 40 mm and for both 0.45 and 0.65 w/b demonstrated better corrosion resistance when compared to PC and FA specimens (see Figure 4-13). Golden (2015) made a similar observation of GGBS showing better corrosion resistance than PC and FA at w/b of 0.65. At low w/b, the corrosion performance of the specimen can be ranked from high to low corrosion resistant, as follows: SL > PC > FA, while at higher w/b they can be ranked in the following order: SL > FA > PC, irrespective of the cover depth.

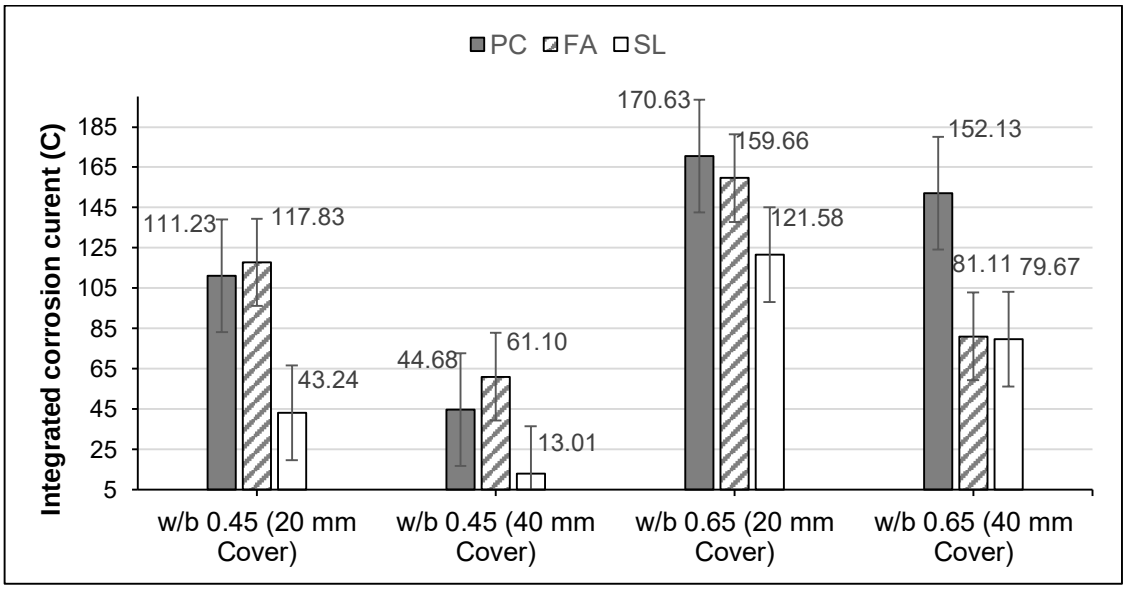

Figure 4-13: Total integrated corrosion current of the specified binders for varying w/b and cover depth after 13 weeks

From Figure 4-13, it can be observed that FA specimens at low w/b (0.45) exhibited the highest corrosion current over the duration of exposure, irrespective of the cover depth. In general, concrete made of FA has a delayed strength development as a result of continued pozzolanic reaction, which in turn has an effect on the refinement of the concrete microstructure. Hence, high corrosion risk due to the ease of movement of chlorides and oxygen to the level of reinforcement at lower cover depth (Kosior-Kazberuk & Lelusz, 2007).

The observation above corroborates the CCI results for w/b 0.45, which indicated the ease of movement of chlorides at an early age for concrete made with FA. Similar observations regarding the less dense microstructure of FA concretes at an early age were made by Kosior-Kazberuk and Lelusz (2007) and Islam and Islam (2013). Based on the observations above, it can be inferred that the refinement of the concrete microstructure based on the binder type plays an influential role in the rate of corrosion, especially at lower cover depths.

It is notable from Figure 4-13 that the control mix (PC) specimen shows better corrosion performance at a lower w/b (0.45) and higher cover depth (40 mm), based on the relatively lower TC value accumulated. The overlapping standard error bars (see Figure 4-13) further indicate that there is no statistically significant difference in the corrosion performance of all the specimens at 0.45 w/b and 40 mm cover depth. However, this was not the case for the higher w/b, due to high penetrability of the pore structure. The better corrosion resistance of PC at lower w/b was also observed by Scott (2004) and Golden (2015). Furthermore, Golden (2015) also highlights that the use of PC for RC structures in the marine tidal zone is only suitable provided there is a sufficient cover depth and lower w/b (maximum of 0.45), which corroborates the findings of this study, and Moore (2019) recommends a minimum concrete cover depth of 30 mm.

Blended cement concretes showed a slower rate of corrosion compared to the concrete made with PC at higher w/b and 40 mm cover depth. This was assessed by checking the difference in the TC values between w/b 0.45 and w/b 0.65. FA and SL specimens showed a minimal difference in TC values between low and high w/b

(20.01 C and 66.66 C, respectively) compared to PC specimens with a TC variation of 107.45 C. FA specimens showed better corrosion resistance at higher w/b due to the fine-filling effect, resulting in an improved microstructure (Jones *et al*., 2015), with the influence of higher cover depth noted.

The better corrosion performance of blended cement concretes is further highlighted by the non-overlapping standard error bars between PC and blended cement concrete specimens at 0.65 w/b and 40 mm cover depth (see Figure 4-13), which indicates a statistically significant difference in the corrosion rate of the specimens. Therefore, it can be inferred that the minimal variation in TC values between low and high w/b for blended cement concretes compared to PC specimens at higher cover depths is due to the increased travel path for chlorides to reach the reinforcement and the improved microstructure in blended cement concretes (Jones *et al*., 2015).

These observations in the above paragraph are also an indication of the influence of the concrete microstructure, though the influence of high cover depth is also noted. Therefore, these observations indicate that the concrete quality and cover depth have a significant influence on a structure's corrosion performance during the early stages of exposure to the marine tidal zone.

After the termination of the experimental programme, the reinforced steel bars embedded in the concrete specimens were extracted to visually observe the corrosion damage that had occurred (see Figure 4-14). The visual inspection of the anode steels at the end of the experiment corroborates the trends observed in the total integrated corrosion current graphs in section 4.4, which indicated that SL specimens had a slow rate of corrosion compared to PC and FA specimens (see Figure 4-14c).

From Figure 4-14c, it can be seen that SL specimens show no significant signs of corrosion damage. Evidence of rust was only observed on the edges of the epoxy-coated surface of the reinforcement. However, it was observed that SL-65 (20) showed active corrosion between the 1st and 10th weeks. The behaviour of SL-65 (20) is in agreement with Andrade (2019) that high corrosion current measurements

do not necessarily indicate the actual corrosion damage of the reinforcement, but are rather an indication of active corrosion, even if no visible signs of corrosion can be observed.

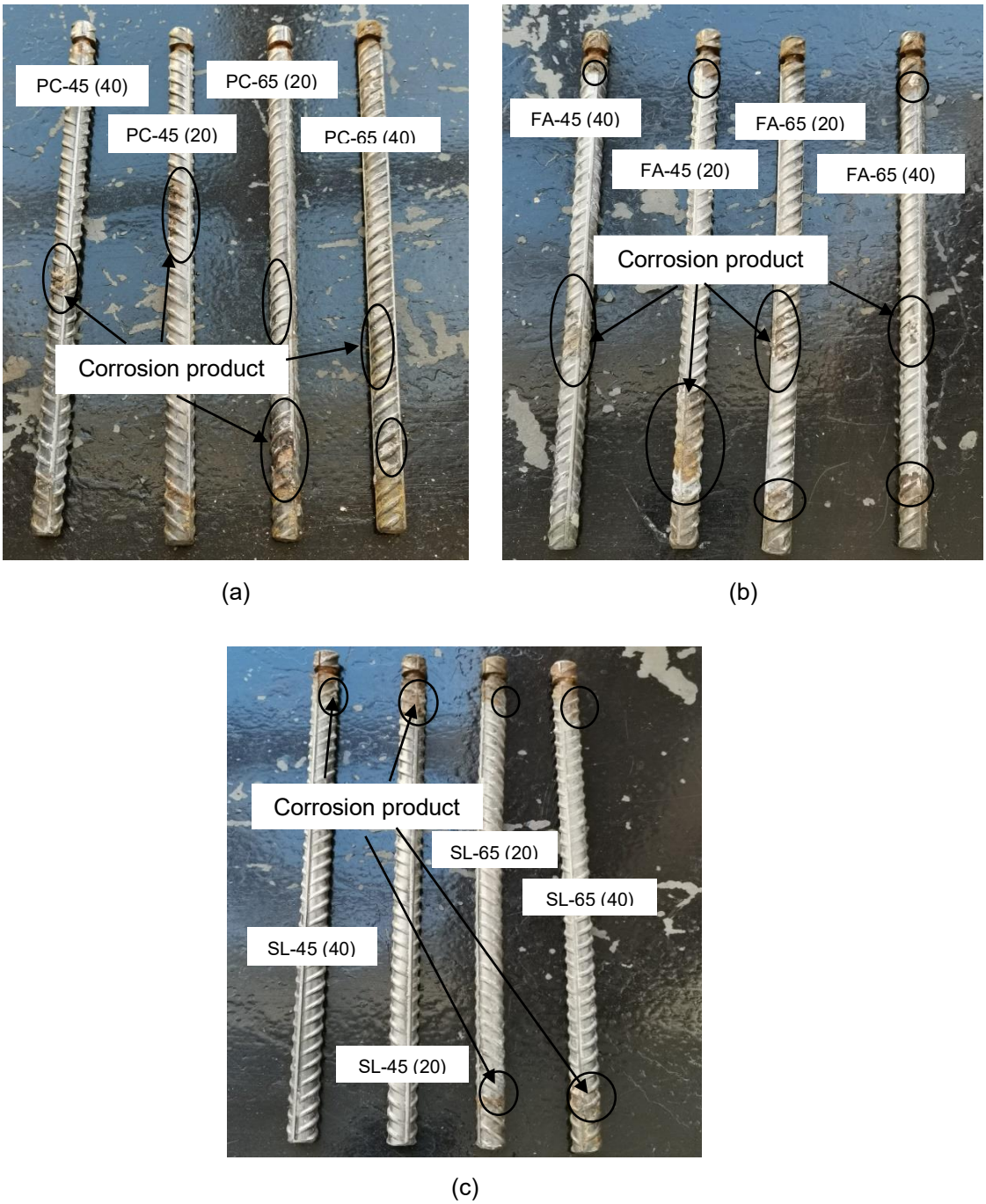

Figure 4-14: Photograph showing the visible corroded area of the reinforcing steels for (a) PC, (b) FA, and (c) SL specimens

For PC and FA concrete specimens (Figure 3-14a and Figure 3-14b), respectively, the influence of an increase in cover depth (40 mm) in limiting the rate of corrosion

can be observed. The corrosion damaged areas on the reinforcing steels are relatively wider for 20 mm cover depth than for 40 mm cover depth. Also, the visual observations corroborate the observation that concrete made with FA has a high corrosion risk at an early age, provided a smaller cover depth (less than 20 mm) is used because of the delayed pozzolanic reaction, which prolongs pore structure refinement.

4.5 Resistivity measurements

Resistivity of concrete determines the ease of ionic movement through the concrete pore structure from the anode to the cathode. The measuring of concrete resistivity commenced concurrent with the measurements of corrosion rate during the exposure of specimens to the 6-hour wetting and drying cycles (see Figure 3-18). This was done to relate the concrete resistivity results to the corrosion rate. Accordingly, the resistivity measurements were taken once a week after the wetting cycle. Figure 4-15 to Figure 4-18 show the concrete resistivity of specimens measured during the 13 weeks of exposure to the simulated marine tidal zone.

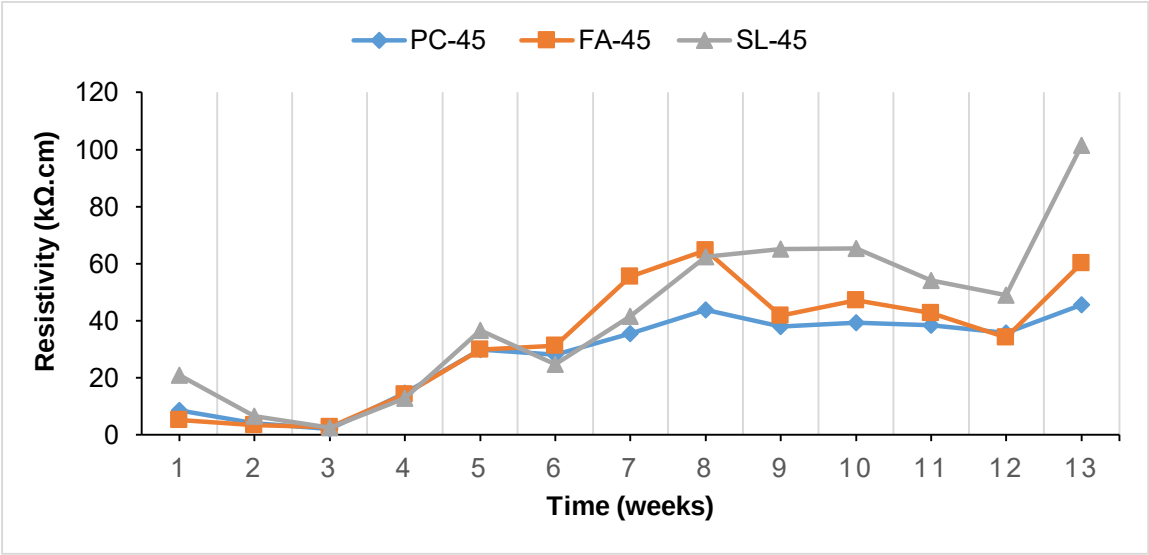

Figure 4-15: Resistivity measurements for w/b 0.45 at 20 mm cover depth

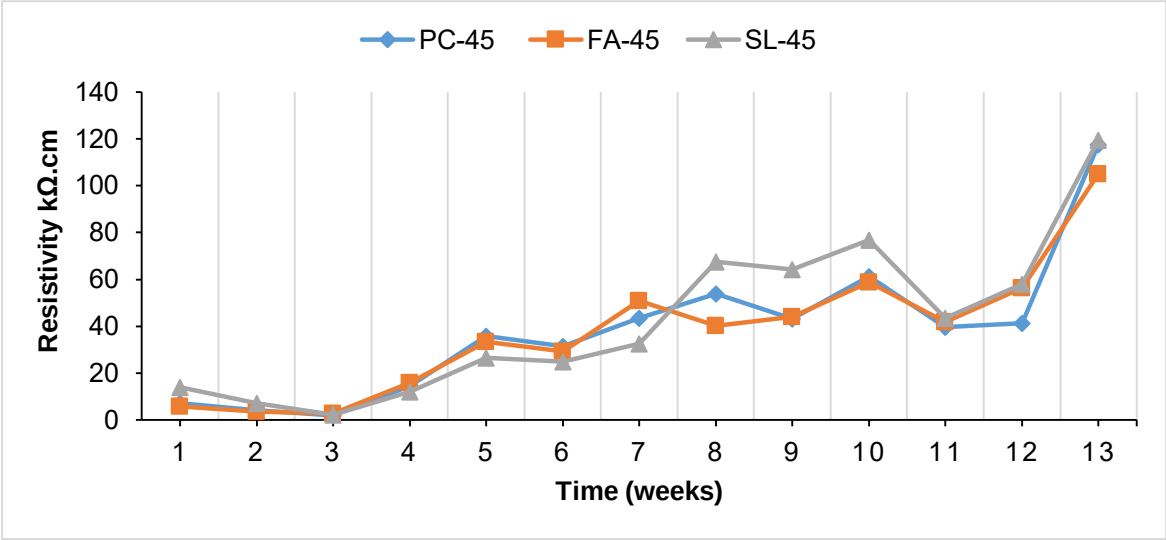

Figure 4-16: Resistivity measurements for w/b 0.45 at 40 mm cover depth

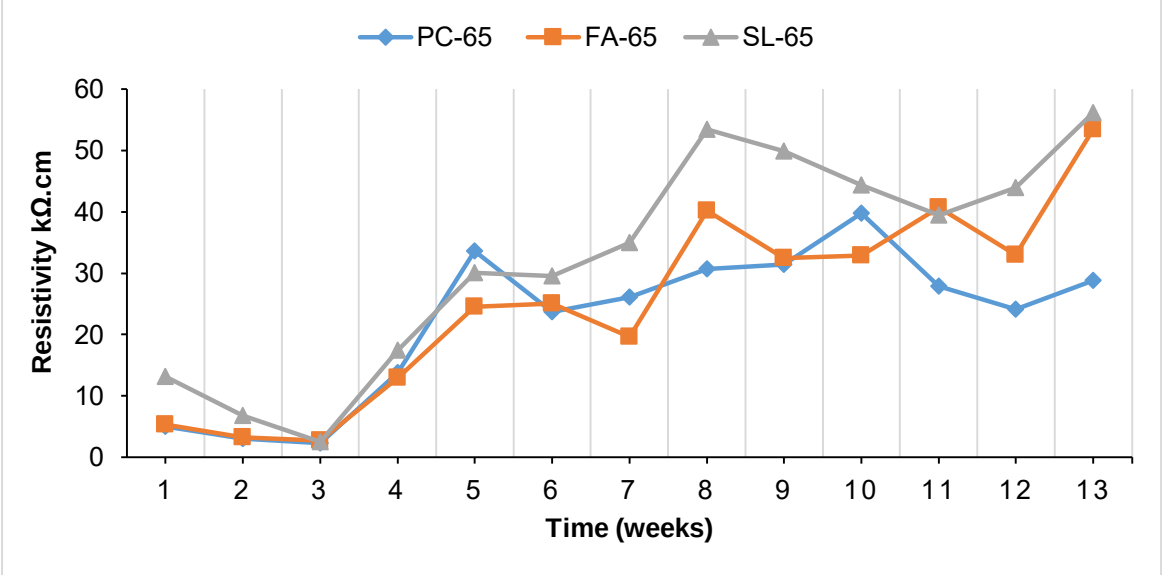

Figure 4-17: Resistivity measurements for w/b 0.65 at 20 mm cover depth

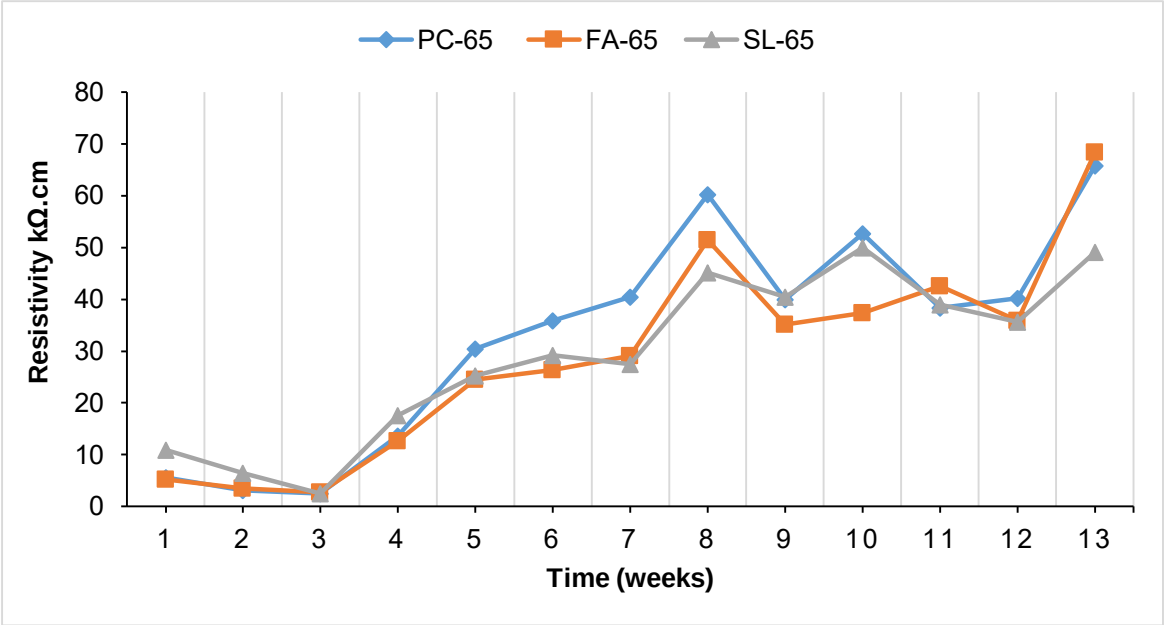

Figure 4-18: Resistivity measurements for w/b 0.65 at 40 mm cover depth

From Figure 4-15 to Figure 4-18, it can be seen that from the 1st week to the 3rd week, the resistivity of all concrete specimens decreased. The decrease in concrete resistivity to values ranging from 2 to 2.9 kΩ.cm on the 3rd week indicates that during the initial stages of exposure of concrete specimens, there was a high ionic movement (high chloride penetration) in the concrete pore structure (refer to Table 2-3). This was due to the high absorption (capillary suction) of chlorides as the specimens were dry after the corrosion activation period. In addition, the lowest resistivity values measured on the 3rd week (<12 kΩ.cm) indicate high likelihood of corrosion rate (see Table 2-2) (Heckroodt, 2002).

However, from the 4th to the 13th week, an increasing trend in the resistivity values can be observed, irrespective of the w/b and binder type. The increase in resistivity values is attributed to the continued hydration and pozzolanic reaction of the respective specimens, which results in a more refined concrete pore structure (Scott, 2004; Otieno, 2008; Golden, 2015). The continuous hydration of the specimens can further be supplemented by the short cycles of wetting and drying, which further prolongs the curing of the specimens (Moore, 2019).

Notably, in Figure 4-15 and Figure 4-17, which present the resistivity trends of the specimens for the specified w/b at 20 mm cover depth, blended cement concretes

(FA and SL) exhibited higher resistivity values than the PC concrete. In comparison to FA and PC specimens, the SL-45 and SL-65 specimens had relatively high resistivity values. The mean (average) resistivity of the specimens presented in Appendix C shows that the resistivity of the specimens for a cover of 20 mm was in the following order, from highest to lowest: SL-45 > FA-45 > PC-45 and SL-65 > FA-65 > PC-65. The high concrete resistivity of SL specimens to ionic movement corresponds to the CCI results provided in Table 4-3.

The above trend, however, was not observed for w/b 0.45 specimens with a cover depth of 40 mm. It should also be noted that PC-65 at 40 mm cover depth had high resistivity values almost throughout the duration of exposure of specimens to the simulated marine tidal zone (see Figure 4-18). The high resistivity values of the PC-65 (40) specimen do not correspond to the high rate of corrosion observed on the embedded reinforcement of the specimen. This further confirms the observation in the literature (Scott, 2004; Golden, 2015) that at higher cover depths the resistivity of the concrete is not the controlling factor of corrosion rate; rather, the availability of oxygen controls the corrosion rate. Concrete made with PC only, at high w/b, is expected to have a porous microstructure that allows ions and oxygen to easily move into the concrete, thus the high corrosion risk.

4.6 General discussion and closure

In this chapter, the influence of blended cements on the corrosion rate of reinforced concrete structures in a marine tidal zone was examined based on the experimental results obtained. The results of this study have shown that blended cements improve the microstructure of the concrete over time, as can be seen from the compressive strength and durability index test results. The concrete microstructure, which is influenced by binder type, w/b, etc., gives the designer an idea of the choice of concrete cover depth to be used for a particular structure.

An increase in concrete cover depth from 20 mm to 40 mm reduced the corrosion rate of all the specimens, irrespective of the w/b. The reduction in corrosion rate was attributed to the increased travel path, leading to oxygen deprivation at the steel as a result of an increased cover depth. Furthermore, the reduction in corrosion rate at

higher cover depth also indicated that the short cycles of wetting and drying do not provide enough drying time for concrete, leading to moist conditions around the reinforcing steel, which inhibited oxygen diffusion to sustain the occurrence of corrosion.

The increase in cover depth was not expected to have a significant influence on FA and SL specimens, as the literature (Scott, 2004) reports a negligible influence of increased cover depth for blended cement concretes, owing to their improved pore structure over time. However, the findings of this study showed that, at an early age, all concretes are susceptible to the ingress of corrosion agents; hence the necessity to provide a sufficient cover depth, irrespective of the type of binder used.

The influence of cover depth in limiting the corrosion of blended cement concrete could be attributed to the slow densification of the pore structure. This observation strengthens the general understanding that low cover depths are not suitable for RC structures exposed to aggressive environments such as the marine tidal zone. Thus, it can be inferred that using concrete cover depth less than 20 mm should not be recommended for the design of RC structures in the marine environment.

An increase in w/b from 0.45 to 0.65 increased the susceptibility of all the specimens to high corrosion risk, especially at lower cover depth. However, it is notable that PC concretes are more vulnerable to high corrosion risk than blended cement concretes, as the increase in cover depth did not make much of a difference in reducing the total corrosion measured. This observation further proved the poor corrosion resistance of PC concrete compared to blended cement concrete, which can be attributed to the less dense microstructure and low resistivity of PC concrete. In addition, the susceptibility of PC concrete to corrosion risk at higher w/b than the blended cement concrete proves that corrosion of RC structures made with PC is highly controlled by oxygen availability.

Therefore, it can be inferred that blended cement concretes can be used for RC structures with a high w/b but with concrete cover that is greater than 40 mm. The results of this study, regarding the use of high w/b RC structures in a marine environment, corroborate the observations made in the literature (Otieno, 2008) that

the use of blended cement would assist in the elimination of strength-based design approaches. This is because blended cement concretes show better corrosion performance despite their relatively low strength compared to PC. Moreover, Otieno (2008) further recommended the use of a maximum w/b of ≤ 0.55 for RC structures in the marine environment.

It is also worth noting that the SL specimens in general showed better performance towards corrosion resistance at lower w/b. The corrosion resistance of SL specimens is also confirmed by the CCI and concrete resistivity values obtained. The low CCI values and resistivity values recorded for SL specimens indicate a slow chloride diffusion and low electrical conductivity of SL specimens. This can be attributed to the refined pore structure of SL specimens due to prolonged hydration.

Overall, the durability index (DI) tests (OPI, WSI, and CCI) and resistivity measurements provided an idea of the durability performance (based on the ease of movement of corrosion agents) of blended cement concrete mixtures compared to the control mix (PC), and thus the corrosion probability of the specimens. Accordingly, from the DI test and resistivity measurements, it was observed that blended cement concretes have an improved microstructure over time compared to PC concrete due to the prolonged hydration and pozzolanic reaction, limiting the ingress of corrosion agents. As a result, blended cement concrete can potentially reduce the corrosion risk of RC structures in the marine tidal zone.

The results of this study provide an indication that, provided a sufficient cover depth is used, blended cement concrete reduces the corrosion risk of RC structures in a marine tidal zone compared to concrete made with PC. Therefore, in line with objective number 4 of this study, the current standards (SANS guidelines) need to be refined (in terms of exposure classification) taking into account the improved durability performance of blended cement concretes.

Moore (2019) recommended that the exposure classification in SANS guidelines be refined and, on the one hand, allow for the classification of the marine tidal zone in the same category as the submerged zone when a concrete cover depth greater than 30 mm is used. On the other hand, the guidelines should allow for RC

structures with a cover depth of less than 30 mm to be classified in the same category as the splash and spray zone.

The findings of this study corroborate Moore's (2019) notion. However, in addition to Moore's recommendation, the exposure classification should also include the w/b. For example, the RC structures in the marine tidal zone, classified in the same category as the submerged zone, should have a maximum w/b of 0.45. Due to the corrosion resistance demonstrated by blended cement concretes at higher w/b and higher cover depth, RC structures with relatively higher w/b and a cover depth greater than 40 mm can be categorised in the same category as the splash and spray zone. Nevertheless, further research is needed for a longer exposure period in the marine tidal zone, which should also investigate the corrosion performance of blended cements in the submerged zone.

In summary, this chapter presented the results and findings of this study, where the corrosion performance of blended cement was investigated in conjunction with influencing parameters of corrosion. The results demonstrated that blended cement concretes have high corrosion resistance and that, provided a sufficient cover depth and a low w/b, the RC structures in the marine tidal zone can be classified in the same category as the submerged zone. The following chapter will present the concluding remarks and recommendations for future research based on the analysis presented in this chapter.

5 CONCLUSIONS AND RECOMMENDATIONS

In order to understand the deterioration impact due to reinforcement corrosion in reinforced concrete (RC) structures exposed to aggressive environmental conditions, such as the marine environment, one needs to understand the influencing parameters (both intrinsic and extrinsic factors) of the corrosion of steel phenomena. Accordingly, this study investigated the influence blended cements have on the corrosion rate of RC structures in a marine tidal zone. This chapter presents the conclusions and recommendations derived from the findings and experimental results of this study.

5.1 Conclusions

This study aimed to investigate the influence of blended cement on the corrosion rate of RC structures in a marine tidal zone, taking into account the influence of cover depth variation, concrete resistivity, and oxygen availability. Therefore, the corrosion performance of blended cements and their role in limiting the transportation of corrosion agents, such as oxygen availability, chlorides, etc., along with some of the influencing parameters of the rate of corrosion, such as the concrete cover depth, w/b, and concrete resistivity, have been discussed based on the literature review and findings of this study.

Even though the study was conducted for a short period of time due to study constraints, the results obtained, to some extent, provide compelling evidence that the use of blended cements in the construction of RC structures in a marine tidal zone can yield better durability performance of RC structures in this region. In relation to the study's aim and objectives, the following conclusions were drawn from the findings and results presented in the preceding chapters:

5.1.1 Influence of concrete cover depth on the corrosion rate

One of the objectives of this study was to investigate the influence of cover variation on the corrosion rate of RC structures in a marine tidal zone. It is generally understood that higher cover depths reduce the corrosion risk of RC structures in

the marine environment. This is because of the increased travel path for oxygen to reach the level of steel reinforcement, subsequently delaying the occurrence of the cathodic reaction.

The results of this experimental study showed that the influence of increasing the concrete cover depth is beneficial on the less dense concretes (e.g., at an early age and for concrete made with higher w/b). Less dense concrete has large pores that allow the ease of movement of oxygen to the level of steel. Interestingly, this study observed that the corrosion rate of FA and SL specimens was influenced by an increase in cover depth. This was attributed to the slow densification of the pore structure for concrete made FA and SL at an early age, as confirmed by the compressive and DI tests. For example, at a higher w/b (0.65), increasing the cover depth from 20 mm to 40 mm for FA and SL specimens resulted in a reduction of TC values by 49% and 35%, respectively, whereas for PC specimens' TC values decreased by 11%.

It should be noted, however, that the increase in cover depth was more beneficial for PC concrete specimens at a lower w/b than at higher w/b. Hence, the consideration to use concrete made with 100% PC in the construction of RC structures in the marine tidal zone should only be made at relatively higher cover depth (>40 mm). For SL specimens at lower w/b, the corrosion rate was rather controlled by the resistivity of the concrete than oxygen availability, as opposed to PC and FA specimens. Moreover, the reduced corrosion rates at higher cover depths indicate that the 6-hour wetting and drying cycles in the marine tidal zone create a huge demand for oxygen supply for higher cover depths. This is because the concrete pore structure does not fully dry, thereby lowering the corrosion risk. Therefore, increasing the cover depth reduces the drying rate of the concrete pore structure, resulting in reduced corrosion rates.

Hence, based on these observations, it can be concluded that in any case where the need to use a relatively low cover depth arises (e.g., due to cost implications), the use of PC should be avoided for RC structures in a marine tidal zone when lower cover depths (like 20 mm) are used.

5.1.2 Influence of binder type and water to binder ratio on corrosion rate

The results of this study have shown that higher w/b promotes the corrosion risk of RC structures in the marine tidal zone, particularly at lower cover depths. This is attributed to high porosity, a shorter travel path for chlorides, and easier access to oxygen at the reinforcement level at lower cover depths. The increase in w/b resulted in an increase in the rate of corrosion of all the specimens. Nevertheless, the influence of binder type on the concrete pore structure was observed to be the key factor in limiting the corrosion rate of specimens.

At a high w/b, PC specimens exhibited the highest total integrated current compared to FA and SL specimens and increasing the cover depth did not make much of a difference either. This observation highlighted the improved microstructure of blended cement concretes. Hence, it can be concluded that blended cement concretes can be used at relatively higher w/b. However, a sufficient cover depth should be used to limit the oxygen availability and the ingress of chlorides.

The corrosion performance of FA specimens was superior to PC at increasing w/b. Due to its fine-filling effect on the pore structure of the concrete as a result of the pozzolanic reaction, which resulted in a reduction in the diffusion of chlorides and oxygen to reach the reinforcing steel level, the improved corrosion resistance of FA specimens is indicative of the improved microstructure. Additionally, all the SL specimens showed a relatively slow rate of corrosion compared to the FA and PC specimens from the first 9 weeks of exposure, which could possibly highlight the low chloride concentration in SL specimens due to chloride binding.

Furthermore, from the reinforcement visual inspections at the end of the experiment, the reinforcements that were embedded in SL specimens showed little signs of corrosion damage (small pits). Therefore, it can be concluded that blended cement concretes can potentially reduce the corrosion rate of RC structures in a marine tidal zone even at higher w/b, provided a higher cover depth is used.

5.1.3 Influence of concrete resistivity on reinforcement corrosion

The concrete resistivity of the corrosion specimens was measured for this study to understand the ionic mobility in the concrete pore structure. The resistivity measurements for this study corroborate the general understanding that blended cement concretes have high resistivity compared to PC concrete, with SL specimens showing higher resistivity.

The resistance of SL concretes to ionic movement can also be supported by the CCI results. Notwithstanding these findings, the results obtained in this study also indicate that the incomplete drying process of the concrete pore structure extends the hydration process, thus refining the concrete pore structure. As a result, PC concretes showed relatively higher resistivity, even though, on average, they exhibited lower resistivity than the blended cement concretes.

5.1.4 Exposure classification of the marine environment

The results of this study could be used to support the notion of refining the exposure classification for marine-exposed RC structures. The current standards (SANS 10100-2: 2013) classify the marine tidal zone as the most severe exposure zone, in the same category as the splash and spray zone. However, based on the reviewed literature and the observations made on the results of this study, it is clear that the exposure classification in the SANS guideline is overly simplified.

The results of this study indicate that blended cement concrete can limit the corrosion risk of RC structures in the marine tidal zone. Also, the findings of this study are in agreement with the cover depths limit for the marine tidal zone (greater than 30 mm) provided by Moore (2019), to potentially provide the same corrosion risk as the submerged. Therefore, based on these findings, it can be concluded that the exposure classification in the SANS guidelines needs to be refined and the classification of RC structures in the marine tidal zone should be subcategorised based on the limits of cover depth and w/b.

Therefore, the exposure classification in SANS should be improved in the following manner. Firstly, RC structures exposed to the marine tidal zone with a cover depth greater than 30 mm and a w/b of 0.45 can be classified in the same category as those in the submerged zone. Secondly, RC structures made with blended cement concrete for w/b 0.45 but for a lower cover depth (less than 30 mm) and at relatively higher w/b can be categorised in the same category as the splash and spray zone. However, in the case of higher w/b, a minimum cover depth of 40 mm should be adopted. This will assist in providing the designer with various options during the design stage of RC structures based on the functionality of the structure and the owner's requirements as well as the budgetary constraints.

5.2 Recommendations

This section provides recommendations for future research studies based on the results of the analysis in the preceding chapters.

- **Further laboratory experiments** – As previously stated, due to the time constraints of this study, the experimental programme duration was short. It was observed during the experimental programme that concrete made with SCMs such as FA needs more time to develop a more refined pore structure. Thus, conclusions drawn from this study represent the early age influence of blended cements on the corrosion rate of RC structures exposed to the marine tidal zone. Hence, a similar experimental programme for a longer duration of exposure in the simulated marine tidal zone, is required. Furthermore, to support the notion that the exposure classification in the design standards must categorise the tidal zone in the same category as the submerged RC structures at higher cover depth, future research should also compare the corrosion performance of blended cement for both regions. This will allow for more precise and sustainable durability designs for RC structures in the marine environment.
- **Quantification of chloride profiles** – Further research could also aim at quantifying the chloride profiles of the laboratory specimens. This will enable a better understanding of the chloride binding capacity of blended cement concretes in the marine tidal zone, thus, understanding their influence on the corrosion risk of RC structures in this region.

- **Moisture profiles** – The influence of moisture on the corrosion rate was not investigated in this study. Therefore, future studies should consider this factor. This will assist in understanding the influence of moisture in blended cement concretes exposed to the marine tidal zone, particularly when higher cover depths are used.
- **Corrosion depth measurements** – Corrosion depth was not measured in this study. Corrosion depth measurement determines the depth of the generated pits over time. Therefore, similar research should consider quantifying it. This would assist in developing service life prediction models for RC structures in a marine tidal zone.

References

ACI Standards. (2005). ACI 318-05 & PCA Notes on 318-05., Building Code Requirements for Structural Concrete and Commentary, American Concrete Institute, Farmington Hills, United States of America.

Addis, B. & Goodman, J. (2009). Durability of Concrete. In ed. Owens, G., *Fulton's Concrete Technology*, Chapter 11, 219-218. Cement & Concrete Institute, Midrand, South Africa.

Ahmad, S. (2009). Techniques for inducing accelerated corrosion of steel in concrete. *Arabian Journal for Science and Engineering* 34(2):95.

Aldred, J.M., Rangan, B.V. & Buenfeld, N.R. (2004). Effect of initial moisture content on wick action through concrete. *Cement and Concrete Research* 34(6):907-912.

Alexander, M., Ballim, Y. & Mackechnie, J.R. (1999). *Concrete durability testing manual*. Research Monograph No. 4, Department of Civil Engineering, University of Cape Town and University of Witwatersrand.

Alexander M.G., Ballim Y. & Stanish K. (2008). A framework for use of durability indexes in performance-based design and specifications for reinforced concrete structures. *Materials and Structures* 41(5):921-936.

Alexander, M., Beushausen, H. & Otieno, M. (2012). *Corrosion of steel in reinforced concrete: Influence of binder type, water/binder ratio, cover and cracking*. Research Monograph No. 9, Department of Civil Engineering, University of Cape Town and University of Witwatersrand.

Alexander, M.G. (2016). *Concrete durability testing procedure manual*. Cambridge, England.

Alexander, M.G. (2018). *Durability Index Testing Procedure Manual*. Engineering and the Built Environment, University of Cape Town and University of Witwatersrand.

Alexander, M. & Beushausen, H. (2019). Durability, service life prediction, and modelling for reinforced concrete structures – review and critique. *Cement and Concrete Research* 122(2019):17-29.

Allahverdi, A. & Skvara, F. (2000). Acidic corrosion of hydrated cement based materials. *Ceramics − Silikaty* 44(4):152-160.

Alonso, C., Castellote, M. & Andrade, C. (2002). Chloride threshold dependence of pitting potential of reinforcements. *Journal of Electrochimica Acta* 47(21):3469-3481.

Andrade, C., Alonso, C. & Garcia, A.M. (1990). Oxygen availability in the corrosion of reinforcements. *Advances in Cement Research* 3(11):127-132.

Andrade, C. (1993). Calculation of chloride diffusion coefficients in concrete from ionic migration measurements. *Cement and Concrete Research* 23(3):724-742.

Andrade, C., Alonso, C. & Polder, R. (2004). Recommendations of RILEM TC-154-EMC: Electrochemical techniques for measuring metallic corrosion. Test methods for on-site corrosion rate measurement of steel reinforcement in concrete by means of the polarization resistance method. *Materials and structures* 37(273):623-643.

Andrade, C. (2019). Propagation of reinforcement corrosion: principles, testing and modelling. *Materials and Structures* 52(1):1-26.

Angst, U., Elsener, B., Larsen, CK. & Vennesland, O. (2009). Critical chloride content in reinforced concrete – A review, *Cement and Concrete Research* 39(12):1122-1138.

Angst, U. (2011). Chloride induced reinforcement corrosion in concrete. PhD thesis, Department of Structural Engineering, Norwegian University of Science and Technology, Trondheim, Norway.

Angst, U., Geiker, M.R., Alonso, M.C., Polder, R., Isgor, O.B., Elsener, B., Wong, H., Michel, A., Hornbostel, K. & Gehlen, C. (2019). The effect of the steel–concrete interface on chloride-induced corrosion initiation in concrete: a critical review by RILEM TC 262-SCI. *Materials and Structures* 52(4):88.

Al-Ayish, N., During, O., Malaga, K., Silva, N. & Gudmundsson, K. (2018). The influence of supplementary cementitious materials on climate impact of concrete bridges exposed to chlorides. *Construction and Building Materials,* 188(2018):391-398.

Arito, P. (2012). Discrete Sacrificial External Anodes and Their Use in Service Life Extension of Chloride Contaminated Reinforced Concrete Structures. MSc thesis, Department of Civil Engineering, University of Cape Town, Cape Town, South Africa.

ASTM, C125-15b. (2016). Standard Terminology Relating to Concrete and, Concrete Aggregates. Columbia University, West Conshohocken, United States.https://courseworks2.columbia.edu/files/580900/download?download_frd=1&verifier=NQIMOio8ovm0lzDml9S16Hjj5ezeNDEMQBd7E5hq. [Accessed 07 December 2020].

ASTM G109. (2007). Standard test method for determining effects of chemical admixtures on corrosion of embedded steel reinforcement in concrete exposed to chloride environments. ASTM International: West Conshohocken, United States of America.

Azarsa, P. & Gupta, R. (2017). Electrical Resistivity of Concrete for Durability Evaluation: A Review. *Advances in materials science and engineering* 2017:1-30.

Babaee, M. & Castel, A. (2018). Chloride diffusivity, chloride threshold, and corrosion initiation in reinforced alkali-activated mortars: Role of calcium, alkali, and silicate content. *Cement and Concrete Research* 111(September):56-71.

Balestra, C.E.T., Reichert, T.A., Pansera, W.A. & Savaris, G. (2019). Chloride profile modeling contemplating the convection zone based on concrete structures present for more than 40 years in different marine aggressive zones, *Construction and Building Materials* 198(2019):345-358.

Balestra, C.E.T., Reichert, T.A., Pansera, W.A. & Savaris, G. (2020). Evaluation of chloride ion penetration through concrete surface electrical resistivity of field naturally degraded structures present in marine environment. *Construction and Building Materials* 230(2020):116979.

Ballim, Y., Alexander, M. & Beushausen, H. (2009). Durability of Concrete. In ed. Owens, G., *Fulton's Concrete Technology*, Chapter 9, 155-188. Cement & Concrete Institute, Midrand, South Africa.

Ballim, Y. & Alexander, M. (2018). Guiding principles in developing the South African approach to durability index testing of concrete, *Sixth International Conference on Durability of Concrete Structures*, 18-20 July 2018. University of Leeds, Leeds, West Yorkshire, United Kingdom.

Baten, B., Manzur, T. & Ahmed, I. (2020). Combined effect of binder type and target mix-design parameters in delaying corrosion initiation time of concrete, *Construction and Building Materials,* 242(2020):118003.

Baten, B., Torsha, T. & Manzur, T. (2021). Corrosion vulnerability of reinforced concrete structures with different blended cement due to chloride ingress. *Materials Today: Proceedings*, 43(2021):1018-1024.

Benyamina, S., Menadi, B., Bernard, S.K. & Kenai, S. (2019). Performance of self-compacting concrete with manufactured crushed sand. *Advances in concrete construction* 7(2):87-96.

Bertolini, L., Carsana, M., Gastaldi, M.M., Lollini, F. & Redaelli, E. (2016). Corrosion of steel in concrete and its prevention in aggressive chloride-bearing environments. *In 5th International Conference on the Durability of Concrete Structures* 30 June – 01 July 2016. Shenzhen University, Shenzhen, Guangdong Province, China.

Beushausen, H. & Alexander, M.G. (2008). The South African durability index tests in an international comparison. *Journal of the South African institution of civil engineering* 50(1):25-31.

Beushausen, H., Torrent, R. & Alexander, M.G. (2019). Performance-based approaches for concrete durability: State of the art and future research needs. *Cement and Concrete Research* 119(2019):11-20.

Boschmann Kathler, C., Poulsen, S.L., Sorensen, H.E. & Angst, U.M. (2021). Investigations of accelerated methods for determination of chloride threshold values for reinforcement corrosion in concrete. *Sustainable and Resilient Infrastructure* 2021:1-12.

Bouzoubaa, N., Zhang, M.H., Bilodeau, A. & Malhotra, V.M. (1998). Laboratory-Produced High-Volume fly ash blended cements: Physical properties and compressive strength of mortars. *Cement and Concrete research* 28(11):1555-1569.

Broomfield, J.P. (2007). *Corrosion of Steel in Concrete: Understanding, Investigation and Repair*. 2nd ed. Tailor & Francis Group, London, England.

BS 8500- 1. (2006). Complementary British Standard to BS EN 206- 1: Method of Specifying and Guidance for the Specifier. British Standard Institution, London, England.

Byfors, K. (1987). Influence of silica fume and fly ash on chloride diffusion and pH values in cement paste. *Cement and Concrete Research* 17(1):115-130.

Cairns, J., Du, Y. & Law, D. (2008). Structural performance of corrosion-damaged concrete beams. *Magazine of Concrete Research* 60(5):359-370.

Care, S. & Raharinaivo, A. (2007). Influence of impressed current on the initiation of damage in reinforced mortar due to corrosion of embedded steel. *Cement and Concrete Research* 37(2007):1598-1612.

Castro-Borges, P., Balancan-Zapata, M. & Lopez-Gonzalez, A. (2013). Analysis of tools to evaluate chloride threshold for corrosion onset of reinforced concrete in tropical marine environment of Yucatan, Mexico. *Journal of Chemistry* 2013:1-8.

Chalee, W., Ausapanit, P. & Jaturapitakkul, C. (2010). Utilization of fly ash concrete in marine environment for long term design life analysis. Materials & Design 31(3)1242-1249.

Chalhoub, C., François, R. & Carcasses, M. (2020). Critical chloride threshold values as a function of cement type and steel surface condition. *Cement and Concrete Research* 134(2020):106086.

Chang, H., Zuo, Z., Qu, M., Wang, F., Ge, Z. & Liu, J. (2019). Influence of Pore Structure on Chloride Penetration in Cement Pastes Subject to Wetting-Drying Cycles. *Advances in Materials Science and Engineering*, *2019*.

Chen, L. & Su, R.K.L. (2021). Corrosion rate measurement by using polarization resistance method for microcell and macrocell corrosion: Theoretical analysis and experimental work with simulated concrete pore solution. *Construction and Building Materials* 267(2021):121003.

Cheng, A., Huang, R., Wu, J. & Chen, C. (2005). Influence of GGBS on durability and corrosion behavior of reinforced concrete. *Materials Chemistry and Physics* 93(2005):404-411.

Choi, Y.S., Kim, J.G. & Lee, K.M. (2006). Corrosion behaviour of steel bar embedded in fly ash concrete. Corrosion Science 48(7):1733-1745.

Costa, A. & Appleton, J. (2002). Case studies of concrete deterioration in a marine environment in Portugal. *Cement and concrete composites* 24(1):169-179.

Damtoft, J.S., Lukasik, J., Herfort, D., Sorrentino, D. & Gartner, E.M. (2008). Sustainable development and climate change initiatives. *Cement and concrete research* 38(2):115-127.

De Rincon, O.T., Castro, P., Moreno, E.I., Torres-Acosta, A.A., de Bravo, O.M., Arrieta, I., García, C., García, D. & Martinez-Madrid, M. (2004). Chloride profiles in two marine structures – meaning and some predictions. *Building and Environment* 39(9):1065-1070.

Dousti, A., Rashetnia, R., Ahmadi, B. & Shekarchi, M. (2013). Influence of exposure temperature on chloride diffusion in concretes incorporating silica fume or natural zeolite. *Construction and Building Materials* 49(2013):393-399.

Dousti, A. & Shekarchi, M. (2015). Effect of exposure temperature on chloride-binding capacity of cementing materials. *Magazine of Concrete Research* 67(15):821-832.

DuraCrete. (1998). Probabilistic performance based durability design: modelling of degradation. In: eds. Lindvall, A., *2nd Int. PhD Symposium in Civil Engineering,* 412-96. Chalmers University of Technology, Gothenburg, Sweden.

Detwiler, R. (2002). The role of Fly Ash Composition in Reducing Alkali-Silica Reaction. PCA R&D Serial No. 2092. Portland Cement Association, Skokie (Illinois), United States of America.

El Maaddawy, T.A. & Soudki, K.A. (2003). Effectiveness of impressed current technique to simulate corrosion of steel reinforcement in concrete. *Journal of Materials in Civil Engineering* 15(1):41-47.

Elsener, B. (2002). Macrocell corrosion of steel in concrete – implications for corrosion monitoring, *Cement and Concrete Composites* 24(1):65-72.

EN 206-1-1. (2013). Concrete – specification, performance, production and conformity. European Standard.

Fib Model Code for Service-life Design (fib MC-SLD). (2006). fib Bulletin 34, first ed., *Federation International du Beton*, Lausanne, ISBN: 978-2-88394-074-1.

Gao, Y., Zhang, J., Zhang, S. & Zhang, Y. (2017). Probability distribution of convection zone depth of chloride in concrete in a marine tidal environment. *Construction and Building Materials* 140(2017):485-495.

Garcia, V., Francois, R., Carcasses, M. & Gegout, P. (2014). Potential measurement to determine the chloride threshold concentration that initiates corrosion of reinforcing steel bar in slag concretes. *Materials and structures* 47(9):1483-1499.

Ghods, P., Chini, M., Alizadeh, R. & Hoseini, M. (2005). The effect of different exposure conditions on the chloride diffusion into concrete in the Persian Gulf region. [Internet]. The Pennsylvania State University, University Park, United States of America.

http://citeseerx.ist.psu.edu/viewdoc/summary?doi=10.1.1.471.4766. [Accessed 20 June 2020].

Ghosh, P. & Tran, Q. (2015). Influence of parameters on surface resistivity of concrete. *Cement and Concrete Composites* 62(2015)134-145.

Gjorv, O.E., Vennesland, O.E. & El-Busaidy, A. (1977). Electrical resistivity of concrete in the oceans, *Offshore Technology Conference*, 1-4 May 1977, Houston, Texas.

Glass, G.K. & Buenfeld, N.R. (1997). The presentation of the chloride threshold level for corrosion of steel in concrete. *Corrosion Science* 39(5):1001-1013.

Glass, G.K. & Buenfeld, N.R. (2000). The influence of chloride binding on the chloride induced corrosion risk in reinforced concrete. *Corrosion Science* 42(2):329-344.

Golden, G. (2015). The effect of cyclic wetting and drying on the corrosion rate of steel in reinforced concrete. MSc Eng thesis, Department of Civil Engineering, University of Cape Town, Cape Town, South Africa.

Grieve, G. (2009). Cementitious materials. In ed. Owens, G, *Fulton's Concrete Technology*, Chapter 1, 1-16. Cement & Concrete Institute, Midrand, South Africa.

Guneyisi, E. Ozturan, T. & Gesoglu, M. (2005). A study on reinforcement corrosion and related properties of plain and blended cement concretes under different curing conditions. *Cement and Concrete Composites* 27(4):449-461.

Guneyisi, E., Ozturan, T. & Gesoglu, M. (2007). Effect of initial curing on chloride ingress and corrosion resistance characteristics of concretes made with plain and blended cements. *Building and Environment* 42(7):2676-2685.

Harilal, M., Kamde, D.K., Uthaman, S., George, R.P., Pillai, R.G., Philip, J. & Albert, S.K. (2021). The chloride-induced corrosion of a fly ash concrete with nanoparticles and corrosion inhibitor. *Construction and Building Materials* 274(2021):22097.

Hansson, C.M., Poursaee, A. & Laurent, A. (2006). Macrocell and microcell corrosion of steel in Portland cement and high performance concretes. *Cement and Concrete Research* 36(11):2098-2102.

Heckroodt, R.O. (2002). *Guide to the deterioration and failure of building materials*. Thomas Telford Publishing, London, England.

Hunkeler, F. (1994). Fundamentals of corrosion and potential measurements of reinforced concrete structures. *Bericht* 510.

Hunkeler, F. (1996). The resistivity of pore water solution—a decisive parameter of rebar corrosion and repair methods. *Construction and Building Materials* 10(5):381-389.

Hunkeler, F. (2005). Corrosion in reinforced concrete: processes and mechanisms. In ed. Hans, B., *Corrosion in reinforced concrete structures*, Chapter 1, 1-45. Woodhead publishing limited, Cambridge, England.

Hussain, S.E. (1994). Corrosion resistance performance of fly ash blended cement concrete. *Materials Journal* 91(3):264-272.

Hussain, R.R. & Ishida, T. (2010). Influence of connectivity of concrete pores and associated diffusion of oxygen on corrosion of steel under high humidity. *Construction and Building Materials* 24(6):1014-1019.

Hussain, R.R. (2011). Effect of moisture variation on oxygen consumption rate of corroding steel in chloride contaminated concrete. *Cement and Concrete Composites* 33(1):154-161.

Hussain, R.R., Ishida, T. & Wasim, M. (2012). Oxygen Transport and Corrosion of Steel in Concrete under Varying Concrete Cover, w/c, and Moisture. *Materials Journal* 109(1):3-10.

Islam, M.M. & Islam, M.S. (2013). Strength and durability characteristics of concrete made with fly-ash blended cement. *Australian Journal of Structural Engineering* 14(3):303-319.

Ji, Y., Zhao, W., Zhou, M., Ma, H. & Zeng, P. (2013). Corrosion current distribution of macrocell and microcell of steel bar in concrete exposed to chloride environments. *Construction and Building Materials* 47(2013):104-110.

Ji, Y., Wu, M., Tan, Z., Gao, F. & Liu, F. (2014). Process control of reinforcement corrosion in concrete. Part 2: Time-dependent dominating factors under different environmental conditions. *Construction and Building Materials* 73(2014):214-221.

Ji, Y., Zhan, G., Tan, Z., Hu, Y. & Gao, F. (2015). Process control of reinforcement corrosion in concrete. Part 1: Effect of corrosion products. *Construction and Building Materials* 79(2015):214-222.

Jones, S., Martys, N., Lu, Y. & Bentz, D. (2015). Simulation studies of methods to delay corrosion and increase service life for cracked concrete exposed to chlorides. *Cement and Concrete Composites* 58(2015):59-69.

Juenger, M.C.G., Winnefeld, F., Provis, J.L. & Ideker, J.H. (2011). Advances in alternative cementitious binders. *Cement and concrete research* 41(12):1232-1243.

Juenger, M.C., Snellings, R. & Bernal, S.A. (2019). Supplementary cementitious materials: New sources, characterization, and performance insights. *Cement and Concrete Research* 122(2019)257-273.

Kanjee, J.P. (2015). Assessing the influence of crack width on the durability potential of cracked concrete using the durability index approach. MSc thesis, Department of Civil Engineering, University of Cape Town, Cape Town, South Africa.

Kellerman, J. & Croswell, S. (2009). Properties of fresh concrete. In ed. Owens, G., *Fulton's Concrete Technology*, Chapter 6, 83 - 96. Cement & Concrete Institute, Midrand, South Africa.

Kessy, J.G., Alexander, M.G. & Beushausen, H. (2015). Concrete durability standards: International trends and the South African context. *Journal of the South African Institution of Civil Engineering* 57(1):47-58.

Khan, M.I. & Lynsdale, C.J. (2002). Strength, permeability, and carbonation of high-performance concrete. *Cement and Concrete Research*, *32*(1):123-131.

Kim, J., McCarter, W.J., Suryanto, B., Nanukuttan, S., Basheer, P.A.M. & Chrisp, T.M. (2016). Chloride ingress into marine exposed concrete: A comparison of empirical- and physically- based models. *Cement and Concrete Composites* 72(2016):133-145.

Kosior-Kazberuk, M. & Lelusz, M. (2007). Strength development of concrete with fly ash addition. *Journal of Civil Engineering and Management* 13(2):115-122.

Kwon, S.J., Lee, H.S., Karthick, S., Saraswathy, V. & Yang, M.H. (2017). Long-term performance of blended cement concrete in the marine environment – A real time study. *Construction and Building Material* 154(November):349-360.

Layssi, H., Ghods, P., Alizadeh, A.R. & Salehi, M. (2015). Electrical resistivity of concrete. *Concrete International* 37(5):41-46.

Liu, J. Tang, K., Qiu, Q., Pan, D., Lei, Z. & Xing, F. (2014). Experimental investigation on pore structure characterization of concrete exposed to water and chlorides. *Materials* 7(2014):6646-6659.

Liu, J., Xing, F., Dong, B., Ma, H. & Pan, D. (2014). Study on water sorptivity of the surface layer of concrete. *Materials and structures* 47(11):1941-1951.

Lopez-Calvo, H.Z., Montes-García, P., Jimenez-Quero, V.G., Gomez-Barranco, H., Bremner, T.W. & Thomas, M.D.A. (2018). Influence of crack width, cover depth and concrete quality on corrosion of steel in HPC containing corrosion inhibiting admixtures and fly ash. *Cement and Concrete Composites* 88(2018):200-210.

Lothenbach, B., Scrivener, K. & Hooton, R.D. (2011). Supplementary cementitious materials. *Cement and concrete research* 41(12):1244-1256.

Luping, T. (2002). A study of the polarisation techniques for corrosion rate measurement in a steel-concrete system, *9th International Conference on the Durability of Building Materials and Components,* 17-20. Brisbane, Australien.

Luping, T. & Lofgren, I. (2016). *Evaluation of Durability of Concrete with Mineral Additions with regard to Chloride- Induced Corrosion*. Report No. 2016-4. Chalmers University of Technology, Gothenburg, Sweden.

Mackechnie, J.R. (2001). *Predictions of reinforced concrete durability in the marine environment*. Research Monograph No. 1, Department of Civil Engineering, University of Cape Town and University of Witwatersrand.

Madhavi, T.C. & Annamalai, S. (2016). Electrical conductivity of concrete. *ARPN J.Eng.Appl.Sci* 11(9):5979-5982.

Malumbela, G., Moyo, P. & Alexander, M. (2012). A step towards standardising accelerated corrosion tests on laboratory reinforced concrete specimens. *Journal of the South African Institution of Civil Engineering* 54(2):78-85.

Mangat, P.S., Khatib, J.M. & Molloy, B.T. (1994). Microstructure, chloride diffusion and reinforcement corrosion in blended cement paste and concrete. *Cement and Concrete Composites* 16(2):73-81.

Mangat, P.S. & Elgarf, M.S. (1999). Flexural strength of concrete beams with corroding reinforcement. *ACI Structural Journal*. 96(1):149–158.

Marinescu, M.V.A. & Brouwers, H.J.H. (2010). June. Free and bound chloride contents in cementitious materials. In *8th fib PhD Symposium in Kgs,* 20-23 June 2010, Lyngby, Denmark.

Maslehuddin, M., Saricimen, H. & Al-Mana, A.I. (1987). Effect of fly ash addition on the corrosion resisting characteristics of concrete. *ACI Materials Journal* 84(1):42-50.

McCarter, W.J., Linfoot, B.T., Chrisp, T.M. & Starrs, G. (2008). Performance of concrete in XS1, XS2 and XS3 environments. *Magazine of Concrete Research* 60(4):261-270.

McNally, C. & Sheils, E. (2012). Probability-based assessment of the durability characteristics of concretes manufactured using CEM II and GGBS binders. *Construction and Building Materials* 30(2012):22-29.

Mehta, P.K. (1991). Concrete in the Marine Environment. Elsevier Applied Science, New York, United States of America.

Mehta, P.K. (1983). Pozzolanic and cemetitious products as mineral admixtures for concrete: A critical view. In: eds. Montebello, V.M., *Proceedings of the first International Conference on the use of fly ash, silica fume, slag and other mineral by-products in concrete*, 1-46. American Concrete Institute, Detroit, United States of America.

Meira, G.R., Andrade, C., Vilar, E.O. & Nery, K.D. (2014). Analysis of chloride threshold from laboratory and field experiments in marine atmosphere zone. *Construction and Building Materials* 55(2014):289-298.

Menadi, B., Kenai, S., Khatib, J. & Ait-Mokhtar, A. 2009. Strength and durability of concrete incorporating crushed limestone sand. *Construction and Building Materials 23*(2):625-633.

Miyazato, S. & Otsuki, N. (2010). Steel corrosion-induced by chloride or carbonation in mortar with bending cracks or joints. *Journal of Advanced Concrete Technology* 8(2):135-144.

Moore, A. (2019). Effect of oxygen availability on the corrosion rate of reinforced concrete in marine exposure zones: inference from site and lab studies. MSc thesis, Department of Civil Engineering, University of Cape Town, Cape Town, South Africa.

Moore, A.J., Bakera, A.T. & Alexander, M.G. (2021). A critical review of the Water Sorptivity Index (WSI) parameter for potential durability assessment: Can

WSI be considered in isolation of porosity?. *Journal of the South African Institution of Civil Engineering*, 63(2):27-34.

Moradllo, M.K., Sadati, S. & Shekarchi, M. (2018). Quantifying maximum phenomenon in chloride ion profiles and its influence on service-life prediction of concrete structures exposed to seawater tidal zone - A field oriented study. *Construction and Building Materials* 180(2018):109-116.

Morris, W., Moreno, E.I. & Sagues, A.A. (1996). Practical evaluation of resistivity of concrete in test cylinders using a Wenner array probe. *Cement and Concrete Research,* 26(12):1779-1787.

Neville, A. (1999). Concrete cover to reinforcement – or cover-up. *Concrete Beton* 95(1999):13-18.

Nganga, G.W., Beushausen, H. & Alexander, M.G. (2017). Practical implications of durability index performance-based specifications: current experience. *Concrete Beton* 150(2017):18-22.

Otieno, M. (2008). Corrosion propagation in cracked and un-cracked concrete, MSc thesis, Department of Civil Engineering, University of Cape Town, Cape Town, South Africa.

Otieno, M., Alexander, M. & Beushausen, H. (2010). Transport Mechanisms, Corrosion of steel (initiation, propagation and factors affecting) and Corrosion Assessment in Concrete. University of Cape Town, Cape Town, South Africa.

Otieno, M.B., Beushausen, H.D. & Alexander, M.G. (2011). Modelling corrosion propagation in reinforced concrete structures – A critical review. *Cement and Concrete Composites* 33(February):240-245.

Otieno, M. (2014). The development of Empirical Chloride-induced corrosion rate prediction model for cracked and un-cracked steel reinforced concrete structures in the marine tidal zone. PhD thesis, Department of Civil Engineering, University of Cape Town, Cape Town, South Africa.

Otieno, M., Beushausen, H. & Alexander, M. (2016). Chloride-induced corrosion of steel in cracked concrete - Part I: Experimental studies under accelerated and natural marine environments. *Cement and Concrete Research* 79(2016):373-385.

Otieno, M., Golden, G., Alexander, M.G. & Beushausen, H. (2019). Acceleration of steel corrosion in concrete by cyclic wetting and drying: effect of drying duration and concrete quality. *Materials and Structures* 52(2):50.

Otieno, M. (2020). Techniques for accelerating chloride-induced corrosion of steel in concrete: A review and general guidelines. *Journal of the South African Institution of Civil Engineering* 28(6):28-34.

Otsuki, N., Madlangbayan, M.S., Nishida, T., Saito, T. & Baccay, M.A. (2009). Temperature Dependency of Chloride Induced Corrosion in Concrete. *Journal of Advanced Concrete Technology* 7(1):41-50.

Ozkul, H., Dogan, U.A., Saglam, A.R. & Parlak, N. (2008). Corrosion resistance of GGBS concrete, *11th International Conference on Durability of Building Materials and Components*, 11-14 May 2008, Istanbul, Turkey.

Perrie, B. (2009). Strength of hardened concrete. In ed. Owens, G., *Fulton's Concrete Technology*, Chapter 7, 97-110. Cement & Concrete Institute, Midrand, South Africa.

Polder, R., Andrade, C., Elsener, B., Vennesland, O., Gulikers, J., Weidert, R. & Raupach, M. (2000). RILEM TC 154-EMC: electrochemical techniques for measuring metallic corrosion. *Materials and Structures* 33(10):603-611.

Polder, R.B & de Rooij, M.R. (2005). Durability of marine concrete structures – field investigations and modelling *Heron*. 50(3):133-153.

Poursaee, A. & Hansson, C.M. (2009). Potential pitfalls in assessing chloride-induced corrosion of steel in concrete. *Cement and Concrete Research* 39(2009):391-400.

Poursaee, A. (2010). Corrosion of steel bars in saturated $Ca(OH)_2$ and concrete pore solution, *Concrete Research Letters* 1(3):90-97.

Presuel-Moreno, F., Liu, Y. & Wu, Y. (2013). Numerical modeling of the effects of rebar presence and/or multilayered concrete resistivity on the apparent resistivity measured via the Wenner method. *Construction and Building Materials* 48(2013):16-25.

Raupach, M. (1996). Chloride-induced macrocell corrosion of steel in concrete-theoretical background and practical consequences. *Construction and building materials* 10(5):329-338.

Real, S. & Bogas, J.A. (2017). Oxygen permeability of structural lightweight aggregate concrete. *Construction and Building Materials* 137(2017):21-34.

Rodrigues, R., Gaboreau, S., Gance, J., Ignatiadis, I. & Betelu, S. (2021). Reinforced concrete structures: A review of corrosion mechanisms and

advances in electrical methods for corrosion monitoring. *Construction and Building Materials* 269(2021):121240.

Ryu, D., Ko, J. & Noguchi, T. (2011). Effects of simulated environmental conditions on the internal relative humidity and relative moisture content distribution of exposed concrete. *Cement and Concrete Composites* 33(1)142-153.

Safehian, M. & Ramezanianpour, A.A. (2013). Assessment of service life models for determination of chloride penetration into silica fume concrete in the severe marine environmental condition. *Construction and Building Materials* 48(2013):287-287.

Sanjuan, M.A., Andrade, C., Mora, P. & Zaragoza, A. (2020). Carbon dioxide uptake by mortars and concretes made with Portuguese cements. *Applied Sciences* 10(2):646-661.

Sakata, K. (1983). A study on moisture diffusion in drying and drying shrinkage of concrete. *Cement and Concrete Research* 13(2):216-224.

Samad, S. & Shah, A. (2017). Role of binary cement including Supplementary Cementitious Material (SCM), in production of environmentally sustainable concrete: A critical review. *International journal of Sustainable built environment* 6(2):663-674.

Samad, S., Shah, A. & Limbachiya, M.C. (2017). Strength development characteristics of concrete produced with blended cement using ground granulated blast furnace slag (GGBS) under various curing conditions. *Sadhana* 42(7):1203-1213.

SANS 5863. (2006). Concrete tests – Compressive strength of hardened concrete. SABS, Pretoria, South Africa.

SANS 10100-2. (2013). The Structural Use of Concrete – Part 2: Materials and Execution of work. SABS, Pretoria, South Africa.

SANS 50197-1. (2013). Cement – Part 1: Composition, specifications and conformity criteria for common cements. SABS, Pretoria, South Africa.

SANS 3001-CO3-1. (2015). Concrete durability index testing – Part 1: Preparation of test specimens. SABS, Pretoria, South Africa.

SANS 3001-CO3-2. (2015). Concrete durability index testing – Part 2: Oxygen permeability test. SABS, Pretoria, South Africa.

SANS 3001-CO3-3. (2015). Concrete durability index testing – Part 3: Chloride conductivity test. SABS, Pretoria, South Africa.

Scott, A.N. (2004). The influence of binder type and cracking on reinforcing steel corrosion in concrete. PhD thesis, Department of Civil Engineering, University of Cape Town, Cape Town, South Africa.

Scott, A. & Alexander, M.G. (2007). The influence of binder type, cracking and cover on corrosion rates of steel in chloride contaminated concrete. *Magazine of Concrete research* 59(7):495-505.

Shi, X., Xie, N., Fortune, K. & Gong, J. (2012). Durability of steel reinforced concrete in chloride environments: An overview. *Construction and Building Materials* 30(2012):125-138.

Simcic, T., Pejovnik, S., De Schutter, G. & Bosiljkov, V.B. (2015). Chloride ion penetration into fly ash modified concrete during wetting–drying cycles. *Construction and Building Materials* 93(2015):1216-1223.

Snellings, R., Mertens, G. & Elsen, J. (2012). Supplementary cementitious materials. *Reviews in Mineralogy and Geochemistry* 74(1):211-278.

Stern, M. & Geary, A.L. (1957). Electrochemical polarization: I. A theoretical analysis of the shape of polarization curves. *Journal of the Electrochemical Society* 104(1):56.

Streicher, P.E. & Alexander, M.G. (1995). A chloride conduction test for concrete. *Cement and Concrete Research*, 25(6):1284-1294.

Sun, C., Yuan, L., Zhai, X., Qu, F., Li, Y. & Hou, B. (2018) Numerical and experimental study of moisture and chloride transport in unsaturated concrete. *Construction and Building* Materials 189(2018):1067-1075.

Tadayon, M.H., Shekarchi, M. & Tadayon, M. (2016). Long-term field study of chloride ingress in concretes containing pozzolans exposed to severe marine tidal zone. *Construction and Building Materials* 123(2016):611-616.

Tang, F., Chen, G. & Brow, R.K. (2016). Chloride-induced corrosion mechanism and rate of enamel-and epoxy-coated deformed steel bars embedded in mortar. *Cement and Concrete Research* 82(2016):58-73.

Thomas, M.D.A. & Bamforth, P.B. (1999). Modelling chloride diffusion in concrete: Effect of fly ash and slag. *Cement and Concrete* Research 29(4):487-495.

Thomas, M.D.A. & Matthews, J.D. (2004). Performance of pfa concrete in a marine environment – 10-year results. *Cement and Concrete Composites* 26(1):5-20.

Thomas, M. (2013). Durability of Concrete. *Supplementary Cementing Materials in Concrete*, Chapter 9, 103-160. CRC Press, Taylor & Francis Group, Boca Raton, FL, USA.

Thomas, M.D.A. & Moffatt, E.G. (2018). The Performance of Concrete in a Marine Environment, *6th International Conference on Durability of Concrete Structures*, 18-20 July 2018, Leeds, United Kingdom.

Tuutti, K. (1982). *Corrosion of Steel in Concrete*. Report No. 4. Swedish Cement and Concrete Research Institute, Stockholm, Sweden.

Van der Wegen, G., Polder, R.B. & van Breugel, K. (2012). Guideline for service life design of structural concrete - A performance based approach with regard to chloride induced corrosion. *Heron* 57(3):153-168.

Vidal, T., Castel, A. & Francois, R. (2007). Corrosion process and structural performance of a 17 year old reinforced concrete beam stored in chloride environment. *Cement and Concrete Research* 37(2007):1551-1561.

Valipour, M., Pargar, F., Shekarchi, M., Khani, S. & Moradian, M. (2013). In situ study of chloride ingress in concretes containing natural zeolite, metakaolin and silica fume exposed to various exposure conditions in a harsh marine environment. *Construction and Building Materials* 46(2013):63-70.

Valipour, M., Shekarchi, M. & Ghods, P. (2014). Comparative studies of experimental and numerical techniques in measurement of corrosion rate and time-to-corrosion-initiation of rebar in concrete in marine environments. *Cement and Concrete Composites* 48(2014):98-107.

Vedalakshmi, R., Rajagopal, K. & Palaniswamy, N. (2008). Long-term corrosion performance of rebar embedded in blended cement concrete under macro cell corrosion condition. *Construction and Building Materials* 22(3):186-199.

Vollpracht, A., Lothenbach, B., Snellings, R. & Haufe, J. (2016). The pore solution of blended cements: a review. *Materials and Structures.* 49(2016):3341-3367.

Vollpracht, A., Soutsos, M. & Kanavaris, F. (2018). Strength development of GGBS and fly ash concretes and applicability of fib model code's maturity function–A critical review. *Construction and Building Materials* 162(2018):830-846.

Walsh, M.T. (2015). Corrosion of steel in submerged concrete structures. PhD thesis. Department of Civil and Environmental Engineering, College of Engineering, University of South Florida, Florida.

Walsh, M.T. & Sagues, A.A. (2016). Steel corrosion in submerged concrete structures - Part 1: field observations and corrosion distribution modelling. *Corrosion Science Section* 72(4):518-533.

Wang, Y., Gong, X. & Wu, L. (2019). Prediction model of chloride diffusion in concrete considering the coupling effects of coarse aggregate and steel reinforcement exposed to marine tidal environment. *Construction and Building Materials* 216(2019)40-57.

Wang, Y., Oleiwi, H., Wang, C., Xiang, N. & Geng, J. (2020). The characterization of chloride effect on concrete water sorption and its application in the modelling of concrete conditions in tidal zones. *Construction and Building Materials* 253:119074.

Wang, Y., Jia, J., Cao, Q. & Gao, X. (2022). Effect of calcium formate on the compressive strength, and hydration process of cement composite containing fly ash and slag. Journal of Building Engineering, 50(2022):104133.

Wei, J., Wang, C.G., Wei, X., Mu, X., He, X.Y., Dong, J.H. & Ke, W. (2019). Corrosion evolution of steel reinforced concrete under simulated tidal and immersion zones of marine environment. *Acta Metallurgica Sinica* (English Letters), 32(7):900-912.

Wu, L., Li, W. & Yu, X. (2017). Time-dependent chloride penetration in concrete in marine environments. *Construction and Building Materials* 152(2017):406-413.

Wu, K., Long, J., Xu, L. & De Schutter, G. (2019). A study on the chloride diffusion behaviour of blended cement concrete in relation to aggregate and ITZ. *Construction and Building Material* 223(October):1063-1073.

Xu, H., Chen, Z., Xu, B. & Ma, D. (2012). Impact of low calcium fly ash on steel corrosion rate and concrete-steel interface. *The Open Civil Engineering Journal* 6(2012):1-7.

Xu, P., Zhao, M., Fu, X. & Zhao, C. (2022). Effect of chloride ions on the corrosion behavior of carbon steel in an iron bacteria system. *RSC Advances* 12(24):15158-15166.

Yahia, A., Tanimura, M. & Shimoyama, Y. (2005). Rheological properties of highly flowable mortar containing limestone filler-effect of powder content and W/C ratio. *Cement and concrete Research* 35(3):532-539.

Yang, C., Li, L. & Li, J. (2020). Service life of reinforced concrete seawalls suffering from chloride attack: Theoretical modelling and analysis. *Construction and Building Materials* 263(2020):120172.

Yang, Z., Fischer, H. & Polder, R. (2013). Modified hydrotalcites as a new emerging class of smart additive of reinforced concrete for anticorrosion applications: A literature review. *Materials and Corrosion* 64(12) 1066-1074.

Yi, Y., Zhu, D., Guo, S., Zhang, Z. & Shi, C. (2020). A review on the deterioration and approaches to enhance the durability of concrete in the marine environment. *Cement and Concrete Composites* 113(2020):103695.

Yuan, Q., Shi, C., De Schutter, G. & Audenaert, K. (2009). Effect of temperature on transport of chloride ions in concrete. In *2nd International Conference on Concrete Repair, Rehabilitation and Retrofitting (ICCRRR)*, 345-351. CRC Press/Balkema, Cape Town, South Africa.

Yu, A., Naqvi, MW., Hu, L. & Zhao, Y. (2020). An experimental study of corrosion damage distribution of steel bars in reinforced concrete using acoustic emission technique. *Construction and Building Materials* 254(2020):119256.

Yu, L., Francois, R., Dang, V.H., L'Hostis, V. & Gagne, R. (2015). Development of chloride-induced corrosion in pre-cracked RC beams under sustained loading: Effect of load-induced cracks, concrete cover, and exposure conditions. *Cement and Concrete Research* 67(2015): 246-258.

Zhang, Y.M. Sun, W. Yan, H.D. (2000). Hydration of high-volume fly ash cement pastes. *Cement and Concrete Composite* 22(6):445-452.

Zhang, J., Shi, C., Zhang, Z. & Ou, Z. (2017). Durability of alkali-activated materials in aggressive environments: a review of recent studies. *Construction and Building Material* 152(October):598-613.

Zivica, V. (2003). Influence of w/c ratio on rate of chloride induced corrosion of steel reinforcement and its dependence on ambient temperature. *Bulletin of Materials Science* 26(5):471-475.

Zuquan, J., Xia, Z., Tiejun, Z. & Jianqing, L. (2018). Chloride ions transportation behaviour and binding capacity of concrete exposed to different marine corrosion zones. *Construction and Building Material* 177(July):170-183.

Appendix A: Detailed Compressive Strength

Table A-1: 28-day compressive strength

Mix Label	Cube	w/b	Mass (kg)	Density (kg/m^3)	Loading Failure (N)	Strength (MPa)
PC-45	1	0.45	2.45	2450	606000	60.6
	2		2.47	2470	618000	61.8
	3		2.53	2530	598000	59.8
Average			**2.48**	**2483**	**607333**	**61.0**
FA-45	1		2.46	2460	480000	48.0
	2		2.40	2400	508000	50.8
	3		2.42	2420	434000	43.4
Average			**2.43**	**2427**	**474000**	**47.0**
SL-45	1		2.44	2440	450000	45.0
	2		2.48	2480	440000	44.0
	3		2.43	2430	416000	41.6
Average			**2.45**	**2450**	**435333**	**44.0**
PC-65	1	0.65	2.47	2470	362000	36.2
	2		2.44	2440	272000	27.2
	3		2.42	2420	362000	36.2
Average			**2.44**	**2443**	**332000**	**33.0**
FA-65	1		2.46	2460	278000	27.8
	2		2.42	2420	254000	25.4
	3		2.45	2450	246000	24.6
Average			**2.44**	**2443**	**259333**	**26.0**
SL-65	1		2.45	2450	340000	34.0
	2		2.50	2500	286000	28.6
	3		2.48	2480	282000	28.2
Average			**2.48**	**2477**	**302667**	**30.0**

Table A-2: 90-day compressive strength

Mix Label	Cube	w/b	Mass (kg)	Density (kg/m^3)	Loading Failure (N)	Strength (MPa)
PC-45	1	0.45	2.51	2510	608000	60.8
	2		2.53	2530	716000	71.6
	3		2.50	2500	700000	70.0
Average			**2.51**	**2513**	**674667**	**67.0**
FA-45	1		2.42	2420	652000	65.2
	2		2.45	2450	580000	58.0
	3		2.44	2440	650000	65.0
Average			**2.44**	**2437**	**627333**	**63.0**
SL-45	1		2.48	2480	644000	64.4
	2		2.48	2480	540000	54.0
	3		2.45	2450	592000	59.2
Average			**2.47**	**2470**	**592000**	**59.0**
PC-65	1	0.65	2.48	2480	458000	45.8
	2		2.45	2450	446000	44.6
	3		2.50	2500	426000	42.6
Average			**2.48**	**2477**	**443333**	**44.0**
FA-65	1		2.38	2380	428000	42.8
	2		2.48	2480	412000	41.2
	3		2.41	2410	406000	40.6
Average			**2.42**	**2423**	**415333**	**42.0**
SL-65	1		2.41	2410	390000	39.0
	2		2.50	2500	410000	41.0
	3		2.48	2480	378000	37.8
Average			**2.46**	**2463**	**392667**	**39.0**

Appendix B: Detailed Durability Index Test Results

Table B-1: 28-day oxygen permeability test results

Mix Label	Cube	w/b	Diameter (mm)	Thickness (mm)	k (m/s)	r^2	OPI
PC-45	1	0.45	68.72	29.93	1.493E-11	0.9936	10.83
	2		69.37	30.14	8.208E-11	0.9990	10.09
	3		70.00	28.96	1.557E-11	0.9976	10.81
	4		69.51	28.99	7.825E-11	0.9985	10.11
Average			**69.40**	**29.51**	**4.771E-11**	**0.997**	**10.46**
FA-45	1		69.70	29.38	3.097E-10	0.9968	9.51
	2		69.75	31.03	3.151E-10	0.9992	9.50
	3		69.46	29.85	2.931E-10	0.9999	9.53
	4		69.73	29.90	3.621E-10	0.9909	9.44
Average			**69.66**	**30.04**	**3.200E-10**	**0.997**	**9.50**
SL-45	1		69.65	28.80	1.316E-11	0.9930	10.88
	2		69.43	32.39	1.004E-10	0.9984	10.00
	3		69.82	29.59	1.561E-11	0.9965	10.81
	4		69.62	30.88	1.327E-10	0.9978	9.88
Average			**69.63**	**30.42**	**6.545E-11**	**0.996**	**10.39**
PC-65	1	0.65	69.75	27.80	2.761E-11	0.9959	10.56
	2		69.88	27.84	8.479E-11	0.9997	10.07
	3		69.88	28.30	3.062E-11	0.9998	10.51
	4		69.75	27.50	8.924E-11	0.9969	10.05
Average			**69.82**	**27.86**	**5.806E-11**	**0.998**	**10.30**
FA-65	1		59.65	29.68	4.483E-10	0.9997	9.35
	2		69.81	29.61	4.278E-10	0.990	9.37
	3		69.82	30.02	3.155E-10	0.990	9.50
	4		69.79	28.78	2.539E-10	0.990	9.60
Average			**67.27**	**29.52**	**3.614E-10**	**0.992**	**9.45**
SL-65	1		69.63	29.79	7.147E-11	0.9987	10.15
	2		69.84	29.30	1.017E-10	0.9984	9.99
	3		69.78	30.56	2.349E-11	0.9999	10.63
	4		69.40	28.71	1.052E-10	0.9928	9.98
Average			**69.66**	**29.59**	**7.548E-11**	**0.997**	**10.19**

Table B-2: 90-day oxygen permeability test results

Mix Label	Cube	w/b	Diameter (mm)	Thickness (mm)	k (m/s)	r^2	OPI
PC-45	1	0.45	69.32	32.18	7.107E-11	0.9963	10.15
	2		69.43	30.48	6.013E-11	0.9971	10.22
	3		69.52	29.64	5.840E-11	0.9954	10.23
	4		70.01	30.27	5.260E-11	0.9996	10.28
Average			**69.57**	**30.64**	6.055E-11	**0.997**	**10.22**
FA-45	1		69.50	30.52	3.636E-10	0.9972	9.44
	2		69.52	30.66	5.855E-11	0.9939	10.23
	3		69.38	31.35	2.879E-10	0.9962	9.54
	4		69.38	30.49	6.032E-11	0.9900	10.22
Average			**69.45**	**30.76**	**1.926E-10**	**0.994**	**9.86**
SL-45	1		69.43	29.85	3.969E-11	0.9901	10.40
	2		69.47	30.90	3.997E-11	0.9998	10.40
	3		69.73	31.35	2.961E-11	0.9954	10.53
	4		69.33	30.68	3.208E-11	0.9945	10.49
Average			**69.49**	**30.70**	**3.534E-11**	**0.995**	**10.46**
PC-65	1	0.65	69.40	29.58	3.687E-11	0.9901	10.43
	2		69.74	31.39	5.823E-11	0.9996	10.23
	3		69.50	28.83	2.985E-11	0.9987	10.53
	4		69.26	28.83	8.078E-11	0.9995	10.09
Average			**69.48**	**29.66**	**5.143E-11**	**0.997**	**10.32**
FA-65	1		69.50	30.34	1.628E-11	0.9913	10.79
	2		69.37	31.73	2.971E-11	0.9915	10.53
	3		69.48	30.60	2.907E-11	0.9998	10.54
	4		69.52	30.60	2.959E-11	0.9997	10.53
Average			**69.47**	**30.82**	**2.616E-11**	**0.996**	**10.60**
SL-65	1		69.19	30.42	3.540E-11	0.9940	10.45
	2		69.56	29.79	1.924E-11	0.9983	10.72
	3		69.41	30.13	2.151E-11	0.9994	10.67
	4		69.87	31.94	1.406E-11	0.9994	10.85
Average			**69.51**	**30.57**	**2.255E-11**	**0.998**	**10.67**

Table B-3: 28-day water sorptivity test results

Mix Label	Cube	w/b	Diameter (mm)	Thickness (mm)	R^2	Sorptivity ($mm/hr^{0.5}$)	Porosity (%)
PC-45	1	0.45	68.72	29.93	0.9850	10.40	9.48
	2		69.37	30.14	0.9921	13.32	8.91
	3		70.00	28.96	0.9898	9.07	8.19
	4		69.51	28.99	0.9887	8.91	6.95
Average			**69.40**	**29.51**	**0.989**	**10.33**	**8.38**
FA-45	1		69.70	29.38	0.9827	15.76	13.16
	2		69.75	31.03	0.9940	13.97	12.31
	3		69.46	29.85	0.9896	8.13	10.26
	4		69.73	29.90	0.9931	9.15	11.03
Average			**69.66**	**30.04**	**0.990**	**11.75**	**11.69**
SL-45	1		69.65	28.80	0.9879	5.20	8.33
	2		69.43	32.39	0.9964	5.99	8.00
	3		69.82	29.59	0.9890	5.95	7.72
	4		69.62	30.88	0.9808	5.86	7.90
Average			**69.63**	**30.42**	**0.989**	**5.75**	**7.99**
PC-65	1	0.65	69.75	27.80	0.9844	10.06	11.85
	2		69.88	27.84	0.9811	10.89	11.68
	3		69.88	28.30	0.9855	9.64	11.18
	4		69.75	27.50	0.9816	10.16	11.96
Average			**69.82**	**27.86**	**0.983**	**10.16**	**11.67**
FA-65	1		59.65	29.68	0.9855	9.59	16.67
	2		69.81	29.61	0.9879	9.02	12.89
	3		69.82	30.02	0.9855	8.89	13.04
	4		69.79	28.78	0.9814	7.13	14.35
Average			**67.27**	**29.52**	**0.985**	**8.66**	**14.24**
SL-65	1		69.63	29.79	0.9891	7.98	11.46
	2		69.84	29.30	0.9921	7.65	11.82
	3		69.78	30.56	0.9849	7.65	10.23
	4		69.40	28.71	0.9863	7.14	11.73
Average			**69.66**	**29.59**	**0.988**	**7.61**	**11.31**

Table B-4: 90-day water sorptivity test results

Mix Label	Cube	w/b	Diameter (mm)	Thickness (mm)	R^2	Sorptivity ($mm/hr^{0.5}$)	Porosity (%)
PC-45	1	0.45	69.32	32.18	0.9940	5.62	7.22
	2		69.43	30.48	0.9945	5.47	6.86
	3		69.52	29.64	0.9953	5.76	6.93
	4		70.01	30.27	0.9984	5.13	7.03
Average			**69.57**	**30.64**	**0.996**	**5.50**	**7.01**
FA-45	1		69.50	30.52	0.9988	4.38	5.01
	2		69.52	30.66	0.9970	3.45	5.01
	3		69.38	31.35	0.9913	5.13	7.92
	4		69.38	30.49	0.9948	4.92	8.03
Average			**69.45**	**30.76**	**0.995**	**4.47**	**6.49**
SL-45	1		69.43	29.85	0.9998	6.26	11.19
	2		69.47	30.90	0.9994	6.43	11.27
	3		69.73	31.35	0.9977	4.90	4.82
	4		69.33	30.68	0.9983	4.22	4.76
Average			**69.49**	**30.70**	**0.999**	**5.45**	**8.01**
PC-65	1	0.65	69.40	29.58	0.9939	5.84	11.11
	2		69.74	31.39	0.9972	6.49	10.64
	3		69.50	28.83	0.9998	8.01	11.46
	4		69.26	28.83	0.9996	8.00	10.76
Average			**69.48**	**29.66**	**0.998**	**7.09**	**10.99**
FA-65	1		69.50	30.34	0.9881	6.48	6.46
	2		69.37	31.73	0.9926	6.85	5.74
	3		69.48	30.60	0.9970	5.93	12.10
	4		69.52	30.60	0.9961	5.98	12.30
Average			**69.47**	**30.82**	**0.993**	**6.31**	**9.15**
SL-65	1		69.19	30.42	0.9908	5.89	6.98
	2		69.56	29.79	0.9937	5.99	6.99
	3		69.41	30.13	0.9943	5.79	7.48
	4		69.87	31.94	0.9813	5.17	7.74
Average			**69.51**	**30.57**	**0.990**	**5.71**	**7.30**

Table B-5: 28-day chloride conductivity test results

Mix Label	Cube	w/b	Oven dry mass (g)	Saturated mass (g)	Voltage (V)	Current (mA)	Conductivity (mS/cm)
PC-45	1	0.45	277.75	289.09	10.57	90.0	0.69
	2		289.59	300.84	10.26	101.0	0.81
	3		256.47	264.67	10.03	55.0	0.40
	4		291.40	301.08	10.07	54.0	0.43
Average			**278.80**	**288.92**	**10.23**	**75.00**	**0.58**
FA-45	1		256.08	270.31	10.55	217.0	1.54
	2		268.28	282.73	10.26	183.0	1.39
	3		279.36	293.72	10.08	115.0	0.92
	4		271.37	285.66	10.06	119.0	0.93
Average			**268.77**	**283.11**	**10.24**	**158.50**	**1.20**
SL-45	1		277.29	285.52	10.86	35.0	0.26
	2		252.51	260.29	10.80	32.0	0.22
	3		291.01	299.52	10.05	23.0	0.19
	4		286.95	295.40	10.05	21.0	0.17
Average			**276.94**	**285.18**	**10.44**	**27.75**	**0.21**
PC-65	1	0.65	271.09	283.01	10.64	85.0	0.63
	2		269.90	282.99	10.75	89.0	0.65
	3		280.11	293.00	10.04	155.0	1.22
	4		289.69	304.40	10.03	166.0	1.36
Average			**277.70**	**290.85**	**10.37**	**123.75**	**0.96**
FA-65	1		266.96	282.14	10.57	263.0	1.94
	2		261.06	276.46	10.83	258.0	1.77
	3		279.36	293.72	10.08	115.0	0.92
	4		271.37	285.66	10.06	119.0	0.93
Average			**269.69**	**284.50**	**10.39**	**188.75**	**1.39**
SL-65	1		267.27	280.59	10.39	63.0	0.48
	2		274.22	287.62	10.95	88.0	0.64
	3		261.82	273.59	10.06	48.0	0.36
	4		306.61	320.35	10.04	44.0	0.36
Average			**277.48**	**290.54**	**10.36**	**60.75**	**0.46**

Table B-6: 90-day chloride conductivity test results

Mix Label	Cube	w/b	Oven dry mass (g)	Saturated mass (g)	Voltage (V)	Current (mA)	Conductivity (mS/cm)
PC-45	1	0.45	292.92	301.04	10.16	29.0	0.24
	2		275.22	282.72	10.76	36.0	0.26
	3		287.22	295.33	10.66	46.0	0.35
	4		261.67	270.87	10.19	60.0	0.46
Average			**279.26**	**287.49**	**10.44**	**42.75**	**0.33**
FA-45	1		258.74	271.20	10.31	82.0	0.59
	2		275.13	288.80	10.07	72.0	0.56
	3		289.83	300.44	10.33	33.0	0.27
	4		282.47	293.49	10.64	36.0	0.28
Average			**276.54**	**288.48**	**10.34**	**55.75**	**0.43**
SL-45	1		284.22	289.49	10.35	9.0	0.07
	2		279.46	288.41	10.69	19.0	0.14
	3		296.22	302.17	10.18	12.0	0.10
	4		274.69	280.71	10.56	13.0	0.10
Average			**283.65**	**290.20**	**10.45**	**13.25**	**0.10**
PC-65	1	0.65	268.57	276.86	10.44	21.0	0.15
	2		277.52	284.51	10.34	14.0	0.11
	3		292.61	306.02	10.74	198.0	1.52
	4		272.11	284.45	10.37	179.0	1.35
Average			**277.70**	**287.96**	**10.47**	**103.00**	**0.78**
FA-65	1		283.03	297.19	10.00	135.0	1.48
	2		285.23	300.51	10.59	136.0	1.05
	3		283.16	297.99	10.19	91.0	0.73
	4		275.79	291.00	10.41	90.0	0.71
Average			**281.80**	**296.67**	**10.30**	**113.00**	**0.99**
SL-65	1		279.73	288.02	10.14	17.0	0.13
	2		288.38	293.67	10.08	7.0	0.06
	3		307.73	316.98	10.73	22.0	0.17
	4		312.73	322.32	10.19	21.0	0.17
Average			**297.14**	**305.25**	**10.29**	**16.75**	**0.13**

Appendix C: Concrete Resistivity Results

Table B-1: Resistivity values for w/b 0.45 for 20 mm cover depth

Number of Weeks	Resistivity Values		
	w/b 0.45 @ cover 20 mm		
	PC-45	**FA-45**	**GGBS-45**
1	8.6	5.3	21
2	4.2	3.5	6.6
3	2.2	2.9	2.5
4	14.6	14.3	12.9
5	30	29.9	36.7
6	28.1	31.2	24.8
7	35.5	55.5	41.7
8	43.8	64.8	62.5
9	38.1	41.9	65.2
10	39.3	47.3	65.3
11	38.5	42.8	54.1
12	35.7	34.2	49.1
13	45.6	60.2	101.4
Average resistivity values	**364.2**	**433.8**	**543.8**

Table B-2: Resistivity values for w/b 0.65 for 20 mm cover depth

Number of Weeks	Resistivity Values		
	w/b 0.65 @ cover 20 mm		
	PC-65	FA-65	GGBS-65
1	5	5.3	13.2
2	3	3.3	6.8
3	2.3	2.7	2.5
4	13.8	13	17.4
5	33.6	24.5	30.1
6	23.7	25.1	29.5
7	26.1	19.6	35
8	30.7	40.2	53.4
9	31.4	32.5	49.9
10	39.8	32.9	44.4
11	27.9	40.7	39.5
12	24.1	33	43.9
13	28.8	53.4	56.2
Average resistivity values	**290.2**	**326.2**	**421.8**

Table B-3: Resistivity values for w/b 0.45 for 40 mm cover depth

Number of Weeks	Resistivity Values		
	w/b 0.45 @ cover 40 mm		
	PC-45	FA-45	GGBS-45
1	7.2	5.8	13.9
2	4.1	3.6	7.1
3	2	2.8	2.2
4	14.7	16	12.2
5	35.8	33.4	26.7
6	31.5	29.4	24.9
7	43.6	51	32.7
8	53.8	40.2	67.7
9	43.3	44.1	64.4
10	61.4	58.7	76.75
11	39.8	42	43.4
12	41.3	56.5	58.1
13	117.65	105	119.4
Average resistivity values	**496.15**	**488.5**	**549.45**

Table B-4: Resistivity values for w/b 0.65 for 40 mm cover depth

Number of Weeks	Resistivity Values		
	w/b 0.65 @ cover 40 mm		
	PC-65	**FA-65**	**GGBS-65**
1	5.6	5.2	10.9
2	3.1	3.5	6.5
3	2.5	2.7	2.5
4	13.6	12.6	17.6
5	30.4	24.5	25.2
6	35.9	26.3	29.2
7	40.4	29.1	27.5
8	60.2	51.4	45.1
9	39.9	35.1	40.4
10	52.7	37.3	50
11	38.4	42.6	38.9
12	40.2	35.9	35.6
13	65.8	68.4	49.1
Average resistivity values	**374.6**	**378.5**	**428.7**